Reconstructing past atmospheric CO$_2$ levels from the stable carbon isotopic composition of general algal biomarkers

Caitlyn R Witkowski

Members of the reading committee:

Katherine H. Freeman
Jack Middelburg
Francien Peterse
Appy Sluijs
Heather Stoll

Reconstructing past atmospheric CO₂ levels from the stable carbon isotopic composition of general algal biomarkers

Reconstructie van vroegere CO₂ concentraties op basis van de stabiele koolstofisotoopsamenstelling van algemeen voorkomende chemische fossielen van algen

(met een samenvatting in het Nederlands)

Proefschrift

door

Caitlyn Rose Witkowski

geboren op 31 januari 1989
te New York, Verenigde Staten van Amerika

Promotoren:

Prof. dr. J.S. Sinninghe Damsté
Prof. dr. S. Schouten

Copromotor:

Dr. M.T.J. van der Meer

Contents

Samenvatting

Koolstofdioxide speelt een belangrijke rol in de bio- en geosfeer en in de regulatie van het wereldwijde klimaat. Uit directe metingen aan luchtbelletjes in ijs, afgezet in de laatste miljoen jaar, blijkt dat de concentratie van atmosferisch koolstofdioxide (PCO_2) een opvallend verband met de temperatuur op Aarde vertoond. Omdat PCO_2 hoogstwaarschijnlijk zal blijven stijgen met de toenemende energiebehoefte van de groeiende wereldbevolking, is het voor de toekomst essentieel om de precieze relatie tussen PCO_2 en klimaat (de klimaatgevoeligheid) te begrijpen. Daartoe wordt de relatie tussen PCO_2 en temperatuur in het verleden bestudeerd. Het reconstrueren van PCO_2 in het aardse verleden is echter een grote uitdaging. Afgezien van het ijskernarchief dat een miljoen jaar beslaat, worden grootschalige PCO_2-reconstructies gedaan aan de hand van zogenaamde proxies, bepaalde gegevens opgeslagen in fysiek geconserveerd materiaal die een milieuparameter reflecteren. Hoewel hiermee in de afgelopen decennia enorme vooruitgang is geboekt, blijft het moeilijk om PCO_2 accuraat te reconstrueren.

Dit proefschrift heeft als doel PCO_2 reconstructies te verbeteren door een nieuwe proxy te ontwikkelen. Hiervoor wordt een nieuwe benadering van een bekend concept gebruikt, namelijk de reconstructie van PCO_2 op basis van de stabiele isotoopsamenstelling van koolstof ($\delta^{13}C$) van door algen geproduceerde karakteristieke organische verbindingen die bewaard kunnen blijven in sedimenten (zgn. chemische fossielen of biomarkers), waarin hun $\delta^{13}C$ waarde (de proxy) indirect gerelateerd is aan PCO_2. Eerdere studies die dit concept toepasten maakten vrijwel uitsluitend gebruik van soort-specifieke verbindingen, voornamelijk alkenonen, geproduceerd door slechts een beperkt aantal algensoorten. Deze alkenoon-gebaseerde reconstructies van PCO_2 zijn gelimiteerd tot tijden wanneer de alkenoon-producerende algen leefden, namelijk ongeveer de laatste 45 miljoen jaar. In dit proefschrift zijn de PCO_2 reconstructies gebaseerd op minder specifieke chemische fossielen van algen: dit zijn verbindingen die worden geproduceerd door een veelheid van algensoorten en dus alomtegenwoordig zijn, zowel geografisch (locatie) als geologisch (tijd). Dit proefschrift is opgebouwd uit twee delen, namelijk onderzoek naar de toepasbaarheid van een aantal algemene chemische fossielen van algen als PCO_2 proxy en vervolgens de toepassing ervan voor verbeterde PCO_2 reconstructies in het aardse verleden.

Het eerste deel van dit proefschrift beschrijft onderzoek aan algenbiomarkers als potentiële PCO_2-proxies door hun $\delta^{13}C$ waarden te analyseren over een transect met

een grote PCO_2 gradiënt, gecreëerd door vulkanisch CO_2 afkomstig van een onderwaterbron. Dit werd onderzocht bij CO_2 bronnen voor de kust van het eiland Shikine, Japan en het eiland Vulcano, Italië. De transecten zijn in twee seizoenen bemonsterd (laat in de lente en vroeg in de herfst) om seizoensgebonden effecten te bestuderen. Drie algemene algenbiomarkers konden op alle bemonsterde locaties, in alle soorten monsters en in beide seizoenen worden geanalyseerd: loliolide afkomstig van de algengroep diatomeeën, fytol afkomstig van al het fytoplankton en cholesterol afkomstig van eukaryoten. Omdat alle andere milieuomstandigheden op de locaties constant waren (i.e. temperatuur, zoutgehalte, beschikbaarheid van voedingsstoffen, licht) suggereert de sterke verlaging in de $\delta^{13}C$ waarden van deze drie biomarkers dichterbij de CO_2 bron dat verhoogde CO_2 concentraties een sterke invloed hebben op de isotoopfractionering die plaatsvindt bij de vastlegging van CO_2 door fytoplankton. In Japan onderschatten de op basis van de biomarkers gereconstrueerde opgeloste CO_2 waarden echter de gemeten opgeloste CO_2 waarden, waarschijnlijk vanwege de extreme weersomstandigheden in deze regio, zoals waargenomen op het moment van bemonstering. Op het eiland Vulcano in Italië vertoonde fytol de meest consistente verandering in haar $\delta^{13}C$ waarden tussen hoge en lage CO_2 concentraties en werd fytol dus gebruikt om de opgeloste CO_2 concentraties en, vervolgens via de wet van Henry, PCO_2 te schatten. De op fytol gebaseerde opgeloste CO_2 reconstructies waren opmerkelijk vergelijkbaar met gemeten waarden voor opgelost CO_2, hetgeen suggereert dat deze proxy inderdaad nuttig kan zijn voor het reconstrueren van PCO_2, en schommelingen daarin, in het aardse verleden.

In het tweede deel van dit proefschrift is de mogelijke toepassing van de $\delta^{13}C$ waarde van fytol als proxy voor de reconstructie van PCO_2 geëvalueerd en toegepast op verschillende geologische perioden waarin PCO_2 varieerde: van glaciale-interglaciale cycli in de afgelopen 200 duizend jaar, van het midden Mioceen Klimaat Optimum naar het heden over de afgelopen 16 miljoen jaar en van het Phanerozoïcum over de afgelopen 500 miljoen jaar. Allereerst werden de glaciale-interglaciale cycli gebruikt om de robuustheid van de fytol $\delta^{13}C$ proxy te testen door deze reconstructies te vergelijken met directe PCO_2 metingen aan de luchtbellen in ijskernen. Tijdens de vorming van organisch rijke lagen (sapropelen) in het oostelijke Middellandse Zeegebied in het late Pleistoceen zijn de $\delta^{13}C$ waarden van de algemene algenbiomarker fytol en de meer specifieke alkenonen zeer vergelijkbaar en beide geven redelijke schattingen voor PCO_2 gedurende deze periode. De trends in de PCO_2 reconstructies komen echter niet overeen met die in ijskernen, mogelijk als gevolg van koolstofconcentratiemechanismen in sommige algen of een variabele groeisnelheid. Op basis van deze bevindingen lijkt de proxy

gebaseerd op de $\delta^{13}C$ fytol moeite te hebben met het reconstrueren van PCO_2 veranderingen in een "lage CO_2 wereld".

Als tweede zijn de algemene algenbiomarkers toegepast in een geologisch tijdvak waarin PCO_2 veel meer varieerde: het midden Mioceen Klimaat Optimum (17-15 Ma) tot het heden. Het Mioceen Klimaat Optimum is belangrijk voor het begrijpen van klimaatgevoeligheid omdat het een periode is die qua PCO_2 een mogelijk analoog is voor onze nabije toekomst, maar ook een periode met zeer variabele en betwiste PCO_2 schattingen. De $\delta^{13}C$ waarden van verschillende steranen (5α-cholestaan, 24-ethyl-5α-cholestaan, 24-methyl-5α-cholestaan; de eerste een diageneseproduct van cholesterol), fytaan (een diageneseproduct van phytol) en alkenonen, in sedimenten verkregen in het Deep Sea Drilling Project, locatie 467, voor de kust van Californië zijn gebruikt om PCO_2 te reconstrueren. Reconstructies op basis van de $\delta^{13}C$ waarden van steranen en fytaan vertoonden allemaal een gestaag dalende trend in PCO_2, anders dan de meerderheid van de gepubliceerde PCO_2 reconstructies voor die periode die stabiele waardes laten zien. Deze gestage afname weerspiegelt, echter, de wereldwijde temperatuurreconstructies voor deze periode, hetgeen overeenkomt met de verwachting dat veranderingen in PCO_2 en temperatuur gekoppeld zijn. Deze studie laat daarom zien dat de $\delta^{13}C$-waarden van algemene algenbiomarkers veelbelovend zijn voor PCO_2 reconstructies op lange termijn.

Tenslotte werd PCO_2 gedurende het gehele Phanerozoïcum (de laatste 500 miljoen jaar) gereconstrueerd met behulp van de $\delta^{13}C$ waarde van fytaan, een reconstructie die een langere tijdsperiode beslaat dan de tot nu toe beschikbare PCO_2 reconstructies. Deze reconstructies zijn voornamelijk op basis van $\delta^{13}C$ van carbonaat in paleosolen (fossiele bodems) en de dichtheid van huidmondjes van fossiele bladeren en deze reconstructies worden meer onbetrouwbaar met toenemende ouderdom. Proxies met de kleinste mate van onzekerheid, zoals de boorisotoopverhouding ($\delta^{11}B$) van foraminiferen en de $\delta^{13}C$ waarde van alkenonen, zijn beperkt tot ruwweg de laatste 50 miljoen jaar. Deze PCO_2 reconstructie op basis van de $\delta^{13}C$ waarden van fytaan vertoont opmerkelijk vergelijkbare waarden met die van de vijf meest robuuste proxies uit eerdere studies. Naast de zeer redelijke schattingen over het gehele Phanerozoïcum, met meer consistente waarden per tijdsperiode, gaan de op fytaan gebaseerde reconstructies verder terug in de tijd dan de andere PCO_2 proxies en kan de proxy potentieel nog verder terug in de tijd gebruikt worden.

In het algemeen laten de bevindingen in dit proefschrift zien dat de $\delta^{13}C$ waarde van algemene algenbiomarkers veel potentie heeft voor het reconstrueren van PCO_2 voor

een groot deel van de geologische geschiedenis van de Aarde. De toepassing van fytaan gaat het verst terug in de tijd en lijkt algemeen toepasbaar voor de reconstructie van PCO$_2$. Deze proxy werkt het beste in afzettingen van een goed gemengde, open oceaan, waardoor de gebruikte verbindingen voornamelijk afkomstig zijn van fytoplankton. De proxy moet voorzichtig worden toegepast tijdens recentere perioden met lage PCO$_2$ omdat de methode ongevoelig lijkt voor relatief kleine veranderingen in PCO$_2$. Ondanks dat er nog veel te leren valt, zijn PCO$_2$ schattingen op basis van de δ^{13}C waarde van fytaan robuust en consistent, en een nuttige toevoeging aan de bestaande collectie van PCO$_2$ proxies.

Summary

Carbon dioxide plays a critical role in the biosphere and geosphere, as well as global climate. Direct measurements of air bubbles trapped in ice, deposited in the last one million years, show that the concentration of atmospheric carbon dioxide (PCO_2) has a striking relationship with temperature on Earth. Because PCO_2 will likely continue to rise with increasing energy needs from a growing world population, it is essential for the future to understand the precise relationship between PCO_2 and climate (i.e. climate sensitivity). To this end, the relationship between PCO_2 and temperature in the past has t been studied. However, reconstructing PCO_2 in past Earth remains a challenge. PCO_2 reconstructions beyond the one-million-year ice core record are made on the basis of proxies, i.e. physically preserved material which reflect an environmental parameter. Although tremendous strides have been made over the past several decades, it remains difficult to accurately reconstruct PCO_2.

This thesis aims to improve PCO_2 reconstructions by developing a new proxy. This is achieved through taking new approaches to the PCO_2 proxy based on the stable carbon isotopic composition ($\delta^{13}C$) of characteristic organic compounds produced by algae and can stored in sediments (known as molecular fossils or biomarkers). Previous studies that have applied this concept almost exclusively used species-specific compounds i.e. alkenones, produced by only a limited number of species. These alkenone-based reconstructions of PCO_2 are limited to times when these alkenone-producers live, namely about the last 45 million years. In this thesis, the PCO_2 reconstructions are based on less specific compounds produced by algae; so-called general algal biomarkers, which are produced by a multitude of species and are thus ubiquitously found, both geographically (location) and geologically (time). This thesis is divided in two parts, namely the applicability of general algal biomarkers as a PCO_2 proxy and subsequently their application towards improved PCO_2 reconstructions in earth history.

The first part of this thesis describes research on algal biomarkers as potential PCO_2 proxies by analyzing their $\delta^{13}C$ values over a transect with a large PCO_2 gradient created by marine volcanic CO_2 seeps. This was investigated at the CO_2 sources off the coast of Shikine Island, Japan and Vulcano Island, Italy. The transects have been sampled in two seasons (late spring and early autumn) to study seasonal effects. Three general algal biomarkers could be analysed at all sampled locations, all sample matrices, and both seasons: loliolide from the algal group of diatoms, phytol from phytoplankton, and cholesterol from eukaryotes. Because all other environmental

conditions at the locations were constant (e.g. temperature, salinity, nutrient availability, light), the sharp reduction in the $\delta^{13}C$ of these three biomarkers closer to the CO_2 source suggests that increased CO_2 concentrations in the seawater have a strong influence on the isotopic fractionation that takes place during the capture of CO_2 by phytoplankton. In Japan, however, the dissolved CO_2 values reconstructed from each biomarker underestimated the actual PCO_2 measured at each site. Although proxy limitations are considered, the most likely reason is extreme weather conditions, as observed at the time of sampling. In Italy, this was not observed. Here, phytol showed the most consistent change between high to low CO_2 concentrations and was thus used to estimate dissolved CO_2 and, subsequently via Henry's law, PCO_2. The phytol-based dissolved CO_2 reconstructions had remarkably close values to the measured dissolved CO_2, suggesting that this proxy can indeed be useful for reconstructing PCO_2 in the geologic past.

In the second part of this thesis, the possible application of the $\delta^{13}C$ of phytol for reconstructing PCO_2 was evaluated by applying this proxy to different geologic periods in which PCO_2 varied: from glacial-interglacial cycles in the past 200 thousand years, the mid-Miocene Climatic Optimum towards today over the past 16 million years, and the Phanerozoic over the past 500 million years. First, glacial-interglacial cycles were used to test the robustness of the $\delta^{13}C$ of phytol proxy against direct PCO_2 measurements from ice core air bubbles in a low PCO_2 world. In late Pleistocene sapropels in the Eastern Mediterranean Sea, both the $\delta^{13}C$ values of the newly developed general algal biomarker (phytol) and the more species-specific compounds (alkenones) closely reflected one another and showed reasonable estimates for PCO_2 during the period of sapropel deposition. However, the individual reconstructions did not correlate with the fluctuations of the individual ice core data, possibly due the implementation of carbon concentrating mechanisms in some algae or due to a variable growth rate factor. Based on these findings, this proxy should be used with caution in "low CO_2 worlds".

Second, general algal biomarkers were applied in a geologic period in which PCO_2 varied much more: the mid-Miocene Climatic Optimum (17-15 Ma) to present. The mid-Miocene Climatic Optimum is particularly important for understanding climate sensitivity; in terms of PCO, this period is a possible analogue for our near-future but is also a period with highly variable and disputed PCO_2 estimations. The $\delta^{13}C$ of several steranes (5α-cholestane, 24-ethyl-5α-cholestane, 24-methyl-5α-cholestane, the diagenetic products of sterols), phytane (a diagenetic product of phytol), and alkenones in sediments at Deep Sea Drilling Project Site 467 off the coast of California were used to reconstruct PCO_2. Reconstructions based on the $\delta^{13}C$ values

of these biomarkers all showed a steady declining trend in PCO_2, differing from the stable values estimated in the majority of published PCO_2 records. This steady decline, however, does reflect the global temperature reconstructions for this period, which corresponds with the expectation that PCO_2 and temperature were in fact linked. This study therefore shows that the $\delta^{13}C$ of general algal biomarkers are promising for PCO_2 reconstructions over long timescales.

Finally, PCO_2 was reconstructed over the entire Phanerozoic (ca. 500 Ma) using $\delta^{13}C$ of phytane, a reconstruction that covers a longer period of time than the PCO_2 reconstructions currently available. These latter reconstructions are mainly based on the $\delta^{13}C$ of carbonate in paleosols (fossil soils) and the density of stomata on fossil leaves which become more unreliable with increasing age. Proxies with the least degree of uncertainty, such as the boron isotope ratio ($\delta^{11}B$) of foraminifera and the $\delta^{13}C$ of alkenones, are limited to approximately the past 50 Ma. This PCO_2 reconstruction based on the $\delta^{13}C$ of phytane shows remarkably similar values to those of the five most robust proxies in the earlier studies. In addition to the very reasonable estimations over the Phanerozoic, with more internally consistent values per time period, the phytane-based reconstructions span further than the other PCO_2 proxy records and has the potential to span even further back in time.

Overall, the findings of this thesis show that $\delta^{13}C$ of general algal biomarkers has great potential for reconstructing PCO_2 for much of Earth's geologic history. Of these general algal biomarkers, the use of phytane goes furthest back in time and seems to be generally applicable for the reconstruction of PCO_2. This proxy works best in well-mixed, open oceans where the source of the general compounds can be better constrained, i.e. originating from phytoplankton. The proxy should be used with caution during periods of PCO_2 stress when the proxy is less sensitive to CO2 changes. Despite that much remains to be understood, PCO_2 estimates based on the $\delta^{13}C$ of general algal biomarkers are robust and consistent, and a useful addition to the existing collection of PCO_2 proxies.

Chapter 1

Introduction

1.1 Carbon Dioxide

Carbon dioxide (CO_2) plays a key role in earth system dynamics. Weaving throughout the fabric of life, CO_2 is inhaled and exhaled throughout the biosphere, providing the bases of the global food web where CO_2 is taken up by plants and algae and released again through respiration and decomposition (Fig. 1.1). Beyond life itself, CO_2 is involved in the sea, land, and atmosphere, roiling through hydrology, geology, and climate. Notably, CO_2 turns the knobs on climate as a greenhouse gas, trapping incoming energy from the sun for the earth, without which our planet would be much colder -18ºC instead of the current 15ºC (Ma and Tipping, 1998).
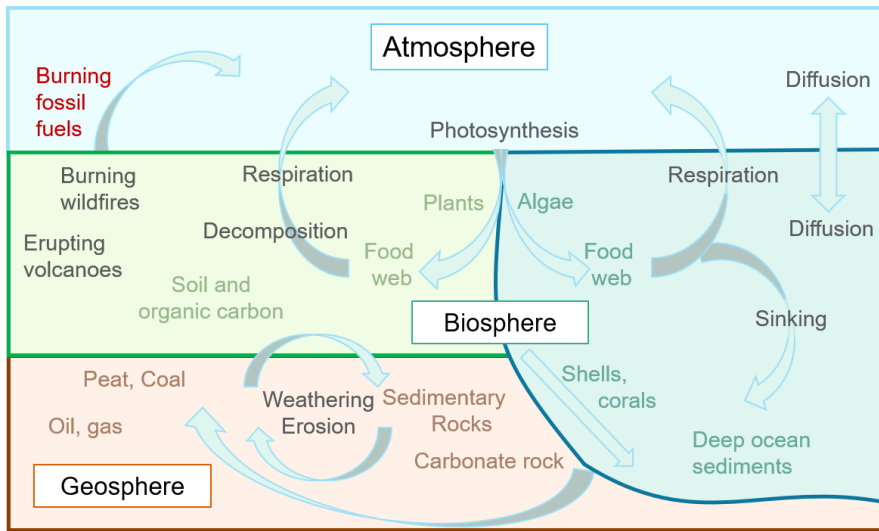
Fig. 1.1. Simplified carbon cycle. Carbon cycle shows major processes (dark gray text and arrows) throughout the atmosphere, biosphere, and geosphere (green text).

The atmospheric concentration of CO_2 (PCO_2, expressed in μatm) has varied over geological time by natural causes. The oldest direct measurements of PCO_2 are collected from gas bubbles trapped in 990 thousand year (ka) old ice (Higgins et al., 2015). These show that PCO_2 has oscillated between ca. 180 to 280 μatm every ca. 100 ka in glacial-interglacial cycles as seen in Fig. 1.2 (Lüthi et al., 2008; Monnin et al., 2001; Petit et al., 1999; Siegenthaler et al., 2005). During this period, temperature shows a nearly identical pattern as PCO_2 (Fig. 1.2). This strongly suggests that the two climate parameters are linked, in accordance with our understanding of the greenhouse gas effect of CO_2 on Earth's surface temperatures. This regular cyclic pattern holds true for the entire record, with the exception of only very recently, since

the Industrial Revolution. In just the past fifty years alone, continuous direct measurements of PCO_2 have risen drastically, from 315 μatm in 1958 to 410 μatm in 2019 (Keeling et al., 2010). The rates of PCO_2 increase seen during this time period are unprecedented for at least the last one million years and possibly for the history of the Earth.
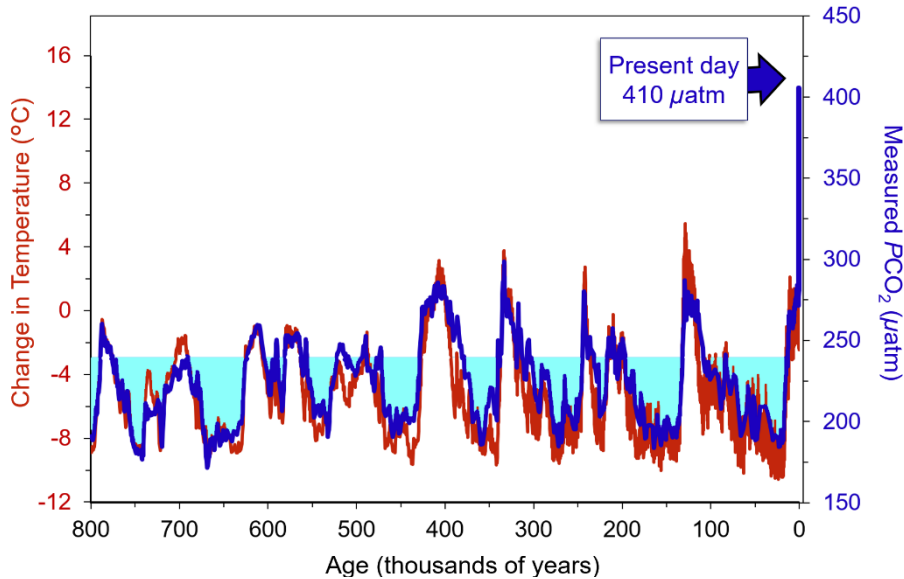
Fig. 1.2. Trends in temperature and PCO_2 over the past 800 ka. Ice-core measurements of temperature (red; Jouzel et al., 2007) and PCO_2 (blue; compiled from Petit et al., 1999; Monnin et al., 2001; Siegenthaler et al., 2005; and Luthi et al., 2009).

Understanding earth equilibrium states, especially climate sensitivity of temperature as a function of PCO_2, has become increasingly more relevant for developing possible future scenarios based on this recent rapid rise of PCO_2. Context for temperature and PCO_2 are thus explored on long timescales, achieved through the use of proxies, i.e. physically preserved material which reflect an environmental parameter. Currently, temperature can be reconstructed fairly well from a number of different proxies, including estimates based on the chemical composition incorporated into hard fossils at the time of their formation, e.g. the $\delta^{18}O$ of calcareous foraminifera (Erez and Luz, 1983), and estimates based on the formation of certain molecular fossil biomarkers in response to the local temperature, e.g. the degree of cyclization membrane lipids produced by *Thaumarchaeota* (Schouten et al., 2002)or the degree of unsaturation of long-chain alkenones produced by haptophyte algae (Brassell et al., 1986). Reconstructing PCO_2, on the other hand, has proven to be more difficult to constrain, as will be discussed below.

1.2 Reconstructing $P\mathrm{CO}_2$

$P\mathrm{CO}_2$ proxies can be based on a number of archived materials – some on minerals, others on organic material, some from land, others from the sea – and can span as far back as 420 million years (Ma). The four most well-studied $P\mathrm{CO}_2$ proxies are the $\delta^{13}\mathrm{C}$ of paleosols, leaf stomata, the $\delta^{11}\mathrm{B}$ of marine carbonates, and the $\delta^{13}\mathrm{C}$ of alkenones (Table 1.1; Fig. 1.3).

The first proxy listed here is derived from paleosols, or ancient carbonate-free bedrock soils. Based on the distinct isotopic mass balance between the two primary sources of carbon in soils, the stable carbon isotopic composition ($\delta^{13}\mathrm{C}$) of pedogenic carbonate and the $^{13}\mathrm{C}$ content of atmospheric CO_2 can be used to estimate $P\mathrm{CO}_2$. Additional constraining parameters like the concentration and $\delta^{13}\mathrm{C}$ of soil-derived CO_2 from respiration further constrain this proxy (Cerling, 1991). This proxy has provided one of the farthest spanning and richest records for secular trends in $P\mathrm{CO}_2$ (Foster et al., 2017). However, it also has large uncertainties (ca. ± 100%) due to the difficulties in constraining soil respiration (Breecker et al., 2010; Cotton and Sheldon, 2012), via complications such as the isotopic fractionation during microbial decomposition (Bowen and Beerling, 2004), carbonate diagenesis (Quast et al., 2006), and other local and regional influences on carbon cycles in these terrestrial settings.

Table 1.1. Proxies used for $P\mathrm{CO}_2$ reconstructions. The name of the proxy along with their approximate timespan, uncertainty in estimation, and primary limitation.

Proxy	Span	Error	Main Limitation
$\delta^{13}\mathrm{C}$ of carbonate in paleosols	420 Ma	100%	Soil respiration
Leaf stomata	400 Ma	30%	Hydrology
$\delta^{11}\mathrm{B}$ carbonates	50 Ma	17%	Seawater composition
$\delta^{13}\mathrm{C}$ alkenones of sediments	40 Ma	20%	Growth rate

The second proxy listed here is based on stomata of leaf surfaces of higher plants, the pores that facilitate the exchange of CO_2, O_2, and water between the plant and the atmosphere. The density of stomata negatively correlates with $P\mathrm{CO}_2$ (Woodward, 1987), and is further refined as a proxy via stomatal indices and considerations to the specific plant species (Royer, 2014). However, the density of stomata lose sensitivity under moderately high $P\mathrm{CO}_2$ conditions (i.e. above ca. 500-1000 μatm), possibly making the upper limits unbounded (e.g. (Royer et al., 2001; Smith et al., 2010). Mechanistic leaf gas-exchange models reduce the otherwise unbounded uncertainty

to ca. -25% to +35% (Franks et al., 2014) by using leaf assimilation rates (and associated relationships) based on the $\delta^{13}C$ of the leaf, stomatal size, and density (Konrad et al., 2008). Regardless of the constraints this model enables, many modern experiments do not show the expected trends (Bernacchi and VanLoocke, 2015; DaMatta et al., 2016; Haworth et al., 2013; Ward et al., 2013), suggesting that this may be a general but not universal response due to some unexpected effects, e.g. ecological systems, species, and development stage (Xu et al., 2016). This thus makes relating extinct fossils to modern species a persistent challenge. However, these stomata-based proxies do offer estimates (at the least, semi-quantitative) that span ca. 400 Myr (Fig. 1.3).

The third proxy explored is based on the boron isotopic composition ($\delta^{11}B$) of marine carbonates, i.e. calcareous shells of foraminifera. This concept is based on the relative proportions of two isotope-distinct boron species in marine seawater: boric acid and borate (Hemming and Hanson, 1992); their relative proportions vary with pH, from which PCO_2 can be then estimated given another seawater carbonate parameter, e.g. total alkalinity or dissolved inorganic carbon (Honisch and Hemming, 2005). Estimates from marine boron isotopes have been largely successful in laboratory cultures and in reconstructing shorter timescales (ca. 800 ka), with some of the smallest uncertainty among PCO_2 proxies (ca. ± 17%). However, uncertainty increases depending on the constraints of e.g. vital effects in extinct species (Honisch et al., 2003), the $\delta^{11}B$ of the seawater (e.g. (Lemarchand et al., 2002), and the carbonate system, making it more difficult to constrain on longer timescales. Although the $\delta^{11}B$ of marine carbonates can be one of the most accurate proxies, it is short-lived (as compared with the other proxies discussed here), spanning the past ca. 50 Myr (Fig. 1.3).

The final main proxy for PCO_2 reconstruction is based on the $\delta^{13}C$ of alkenones, the long-chain unsaturated methyl and ethyl n-ketones produced by several Haptophytes (de Leeuw et al., 1980; Volkman et al., 1980). The $\delta^{13}C$ of algal biomass and its composites, e.g. alkenones, has a negative correlation with PCO_2 due to via the stable carbon isotopic fractionation that occurs during CO_2-fixation (ε_p) (Farquhar et al., 1982; Hayes et al., 1990), a concept that will be explored in depth in Section 3. Alkenones are by far the most common method to estimate the $\delta^{13}C$ of phototrophic biomass in these calculations. Through rigorous testing, PCO_2 estimations from alkenones also have some of the smallest uncertainty (ca. 20%). These uncertainties notably increase depending on how well parameters are constrained, e.g. temperature and growth rate. Furthermore, alkenones are essentially limited to ca. 45 Ma (Fig. 3), the evolutionary history of their producers (Brassell, 2014).
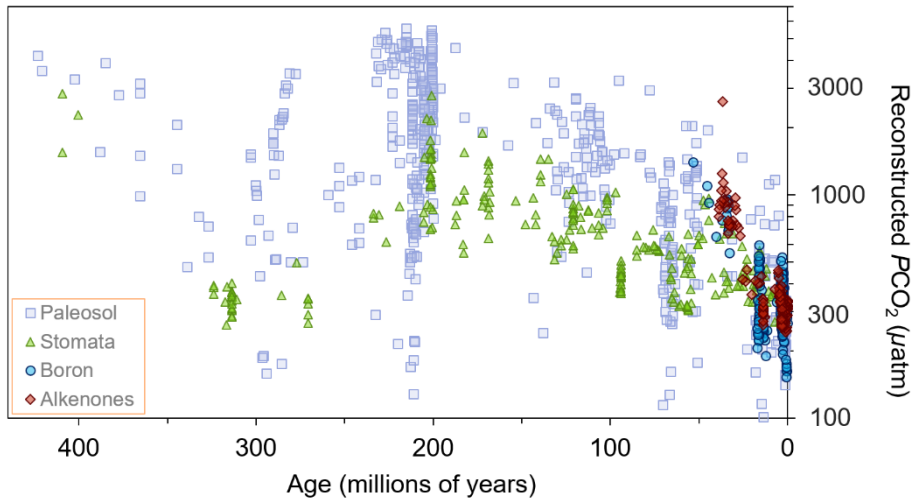
Fig. 1.3. PCO$_2$ estimations reconstructed from proxies. Proxies that span over the past 420 Ma (Foster et al., 2017) include paleosols (squares), stomata (triangles), boron isotopes (circles), and alkenones (diamonds). Note the logarithmic scale for reconstructed PCO$_2$. Beyond the Cenozoic, there are fewer data and with increasingly large scatter among estimations, thus the need for a new method to reconstruct PCO$_2$.

Although these proxies all provide insights into the past, they still leave much to be desired. Our understanding of secular PCO$_2$ trends relies on the compilation of these many proxies, each with different timespans and uncertainties and often with conflicting estimations where they overlap (see Fig. 1.3 from a compilation in Foster et al., 2017). Having a single proxy that can span these long timescales could complement the current compilation of PCO$_2$ proxies, possibly illuminating older periods where there is less data and greater uncertainty. In order to provide longer and more ubiquitous records of PCO$_2$ from a single proxy, this thesis explores and expands the concept behind the δ^{13}C of alkenones to more general marine algal biomarkers.

1.3 Carbon Isotopic Fractionation

Kinetic carbon isotopic fractionation occurs in photoautotrophs as their CO$_2$-fixing enzyme Rubisco (ribulose 1,5-biphosphate carboxylase oxygenase) more readily reacts with ^{12}C over ^{13}C, which can be quantified in ϵ_p, the isotopic fractionation between CO$_2$ and photosynthetic biomass (Farquhar et al., 1982). Isotopic fractionation consequently causes photoautotrophic biomass to become isotopically

lighter than their inorganic carbon substrate, CO_2. The abundance of CO_2 affects the ratio of these two isotopes; under lower PCO_2 conditions, photoautotrophic biomass incorporates more ^{13}C, and vice versa (Fig. 1.4).
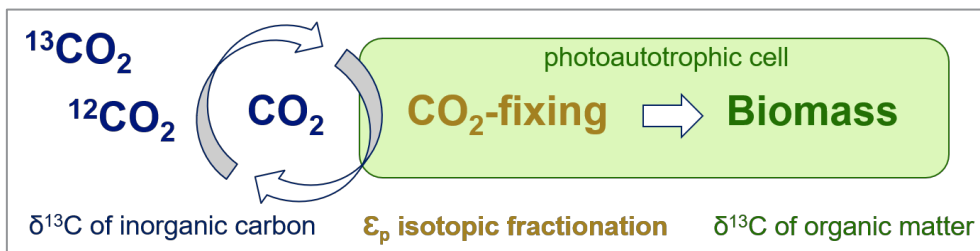

Fig. 1.4. Conceptual model of passive CO_2 diffusion. $^{12}CO_2$ reacts more readily with the CO_2-fixing enzyme Rubisco than $^{13}CO_2$, which consequently results in the stable carbon isotopic fractionation associated with CO_2-fixation (ε_p). The magnitude of ε_p is positively related to the availability of PCO_2.

ε_p is calculated from the $\delta^{13}C$ of photosynthetic biomass (δ_p), or a proxy for this (e.g. the $\delta^{13}C$ of alkenones), and the $\delta^{13}C$ of inorganic carbon (δ_d), or a proxy for this (e.g. the $\delta^{13}C$ of the carbonate shell of planktonic foraminifera), considering other factors such as temperature-dependent carbon isotopic fractionation of $CO_{2[aq]}$ with respect to HCO_3^- (Mook, 1974), as shown by the relationship:

$$\varepsilon_p = 1000 \cdot [\ (\delta_d+1000) \ / \ (\delta_p+1000) - 1] \qquad [1]$$

Based on laboratory cultures, environmental samples, and paleo-applications, ε_p ranges between a low value of ca. 4‰ up to a high of 25-28‰, in which the maximum fractionation associated with Rubisco-based CO_2-fixation (ε_f) is full-expressed (Goericke et al., 1994). In this concept, the underlying assumption is that the primary source of carbon is dissolved CO_2 passively diffusing into the cell, in which case ε_p positively correlates with PCO_2. However, it should be noted that this assumption may be falsified under low PCO_2 conditions where algae may actively uptake bicarbonate (Badger et al., 2019; Stoll et al., 2019), an inorganic carbon source with a significantly heavier $\delta^{13}C$ compared to dissolved CO_2 (Badger et al., 1998; Mook, 1974).

PCO_2 has been related to ε_p using the revised higher plant model (Farquhar et al., 1989) for algae (Bidigare et al., 1997; Popp et al., 1989):

$$PCO_2 = [\ b \ / \ (\varepsilon_f - \varepsilon_p) \ ] \ / \ K_0 \qquad [2]$$

where K_0 represents the constant of Henry's Law to convert dissolved CO_2 to atmospheric CO_2 concentrations (Weiss, 1974). The elusive catchall term "*b*" expresses influences on ε_p other than CO_2, e.g. growth rate (Laws et al., 1995) and cell size (Popp et al., 1998b), as well as seasonality, light, and temperature. This makes "*b*" intrinsically difficult to constrain.

ε_p-based PCO_2 reconstructions have been applied to a number of proxies for $\delta^{13}C$ of biomass, including bulk OM (Hayes et al., 1999), alkenones (Jasper and Hayes, 1990), and general phytoplankton biomarkers (Freeman and Hayes, 1992; Popp et al., 1989). Bulk OM offers widely available data over at least 800 Ma, easily doubling any other currently used proxy. However, concerns regarding lack of an identifiable source, isotopic heterogeneity due to differences in biosynthetic pathways (Hayes, 1993), mixing of terrestrial and marine OM, and diagenetic changes (e.g. (Sinninghe Damsté et al., 1998a) has shifted the preference to compound-specific isotope analysis, in particular alkenones. As a species-specific biomarker, alkenones are well suited for understanding independent species constraints for *b*, such as cell geometry and physiology (Henderiks and Pagani, 2007). However, the effect of changes in fossilized species including extinct species may be more pronounced when limiting the organic matter source to only a small group of species and the evolutionary history of alkenone-producers is limited to the most recent 45 Myr (Brassell, 2014), limiting its applicability.

An alternative which has been rarely applied is based on general phytoplankton biomarkers. The stable carbon isotopic composition of different diagenetic products of chlorophyll, for example, have been applied as a PCO_2 proxy for periods spanning beyond the evolutionary-limit of the alkenone proxy, such as the first studies to apply marine-based ε_p as a PCO_2 proxy (Freeman and Hayes, 1992; Popp et al., 1989), as well as several Cretaceous reconstructions (Bice et al., 2006; Naafs et al., 2016; Sinninghe Damsté et al., 2008). However, these studies are limited, and none have thoroughly investigated the utility or limitations of general algal biomarkers as a PCO_2 proxy.

1.4 Scope and Framework of this Thesis

This thesis aims to develop and apply the stable carbon isotopic composition of general phytoplankton biomarkers as a proxy for PCO_2. In **Chapters 2 and 3**, this approach is validated by testing a suite of general phytoplankton biomarkers in

contemporary settings. In **Chapters 4, 5, and 6**, this concept is applied to phytol, phytane, and steranes to reconstruct PCO_2 over the geologic record.

To test PCO_2 proxies in contemporary settings, in **Chapters 2 and 3**, naturally high-CO_2 environments were used in order to have natural phytoplankton communities and ecological conditions under high CO_2 conditions, as opposed to previous studies which have focused on manipulated systems such as laboratory cultures and mesocosms. CO_2 vents, formed near plate boundaries where pockets of gases build, continually stream CO_2 gas into the environment, creating a natural gradient of CO_2 away from the vent. At these sites, all factors of the environment are relatively constant with the exception of the CO_2 gradient away from the vent, offering an excellent testing ground for the effects of CO_2 on the stable carbon isotopic composition of algal biomarkers.

In **Chapter 2**, we measured ε_p near a CO_2 vent off the coast of Shikine Island (Japan) for three general phytoplankton biomarkers: the diatom biomarker loliolide, the photoautotroph biomarker phytol, and the eukaryote biomarker cholesterol. These biomarkers were tested over two seasons in different matrices, including surface sediments, seawater and plankton net filters, macro-algae affixed to the rocks, and floating microbial mats. Among the matrices and seasons, the $\delta^{13}C$ of all three biomarkers became more depleted closer to the vent, confirming CO_2-dependent isotopic fractionation. In surface sediments collected in June, PCO_2 estimates based on the isotopic composition of these biomarkers were nearly identical to the actual PCO_2 observed in the bay. Surface sediments collected in September, however, yielded PCO_2 estimates which highly underestimated actual values, likely attributed to extreme weather events in this region, i.e. typhoons, that may have transported sediment around the bay where ambient values may mix into the higher PCO_2 sites. These results provide strong evidence that general phytoplankton biomarkers can be used as a PCO_2 proxies and the CO_2 vents may provide excellent testing grounds for PCO_2 proxies.

In **Chapter 3**, ε_p was measured in surface sediments near another CO_2 vent in a higher resolution transect along the CO_2 gradient off the coast of Vulcano Island, Italy, a site with presumably more mild climatic conditions. Following the study in Chapter 2, we tested the $\delta^{13}C$ of the general phytoplankton biomarkers loliolide, phytol, and cholesterol. Again, all three biomarkers exhibited enhanced ε_p values with decreasing distance to the CO_2 vent. Across this higher resolution transect (16 sites as opposed to three sites used in Chapter 2), loliolide-based ε_p values had some fluctuations in values closer to the vent, possibly due to the changing diatom

communities, as observed by light microscopy. Cholesterol-based ε_p values showed a consistent increasing trend towards the vent, but to a lesser degree than phytol, possibly due to the fluctuations in the mobile heterotrophic contributors to the cholesterol pool. Phytol-based ε_p reconstructions of PCO_2 came closest to the measured PCO_2 values, suggesting that it is a strong candidate for reconstructing PCO_2.

Chapters 4, 5, and 6 apply the stable carbon isotopic composition of phytol and its diagenetic product phytane for PCO_2 reconstructions on different timescales: the past 200 thousand years, the past 16 million years, and the past 500 million years, respectively. In **Chapter 4**, the $\delta^{13}C$ of phytol was tested as a tool for PCO_2 reconstructions over the past several glacial and interglacial cycles as recorded in sapropels, organic rich layers deposited in the Mediterranean Sea. Comparison with PCO_2 from ice core records shows overestimated reconstructions (by ca. 100 μatm), which tracks with the ca. 100 μatm disequilibrium the present-day Mediterranean Sea has with modern global average for PCO_2, due to its relatively high alkalinity. This suggests ε_p-based PCO_2 yields robust estimates. However, the ε_p-based PCO_2 estimates do not correlate with the ice core data. This is possibly due to the variable growth rate factor (b) but as there are currently no ways to estimate growth rate over long timescales, such as over the Phanerozoic, we do not suggest using a variable *b*. An alternative explanation is the proposed decreased sensitivity of ε_p to PCO_2 under CO_2 stress, in which some species have been shown to implement carbon concentrating mechanisms. Thus, this proxy may need to be used with caution under low PCO_2 conditions.

In **Chapter 5**, the period of 16.4 to 0.1 million years ago is examined at Deep Sea Drilling Project Site 467 off the coast of California. This time period starts with the Mid-Miocene Climatic Optimum (MMCO), considered a potential analogue for modern trends in PCO_2. Here, a suite of general phytoplankton biomarkers (5α-cholestane, 24-methyl-5α-cholestane, 24-ethyl-5α-cholestane, and phytane) yield comparable reconstructed PCO_2 values to one another, which continually decline, i.e. from ca. 650 μatm at 16.4 Ma to ca. 280 μatm at 0.1 Ma. This steady decline differs from other published proxy records, which suggest a near-constant 300 μatm over the past 16 Ma. However, the generated PCO_2 record closely follows the same declining trend observed for reconstructed sea surface temperatures for the same period, suggesting that these two climate parameters are indeed linked over this time period, as they are over the past 990 ka (Fig. 1.2).

Finally, in **Chapter 6**, we apply phytane-based ε_p to reconstruct secular trends in $P\text{CO}_2$ over the Phanerozoic (ca. 500 Ma). In this record, new and published data of the general phytoplankton biomarker phytane were compiled. This spatially and temporally abundant compound enables $P\text{CO}_2$ reconstructions which span farther back in time than any other currently known proxy for $P\text{CO}_2$ and offers estimates from a single proxy. The reconstructed $P\text{CO}_2$ trends show internally consistent estimations for the same time periods, with estimates ranging from ca. 280 to 1800 μatm over the studied geologic record. Phytane-estimated $P\text{CO}_2$ estimates also show remarkably similar trends as compared with a compilation of all previously reported $P\text{CO}_2$ estimates. The only notable exceptions are during the Cretaceous and the Paleo-Eocene periods where our estimates are substantially higher (ca. 1500 μatm instead of 1000 μatm). These higher estimates match well with the high temperatures which have been reconstructed for these time periods.

The results presented in this thesis show that the ε_p derived from general algal biomarkers strongly relates to $P\text{CO}_2$. This was seen in modern environments via transects from natural CO_2 vents, which illuminated the strengths and limitations of several general biomarkers. When then applied to past environments, ε_p derived from general phytoplankton biomarkers yielded $P\text{CO}_2$ estimates in agreement with other $P\text{CO}_2$ proxies and mirrored trends in sea surface temperature over the past 16 Ma. The $\delta^{13}\text{C}$ of algal biomarkers show great promise for the reconstruction of $P\text{CO}_2$ over long timescales and thus requires further investigation and application.

Chapter 2

Validation of carbon isotope fractionation in algal lipids as a PCO$_2$ proxy using a natural CO$_2$ seep (Shikine Island, Japan)

Caitlyn R Witkowski[1], Sylvain Agostini[2], Ben P Harvey[2], Marcel TJ van der Meer[1], Jaap S Sinninghe Damsté[1,3], Stefan Schouten[1,3]

[1] Department of Marine Microbiology and Biogeochemistry, Royal Netherlands Institute for Sea Research, and Utrecht University, The Netherlands
[2] Shimoda Marine Research Center, University of Tsukuba, Japan
[3] Department of Geosciences, Utrecht University, The Netherlands

Abstract

Carbon dioxide concentrations in the atmosphere play an integral role in many earth system dynamics, including its influence on global temperature. The past can provide insights into these dynamics, but unfortunately reconstructing long-term trends of atmospheric carbon dioxide (expressed in partial pressure; PCO$_2$) remains a challenge in paleoclimatology. One promising approach for reconstructing past PCO$_2$ utilizes the isotopic fractionation associated with CO$_2$-fixation during photosynthesis into organic matter (ε_p). Previous studies have focused primarily on testing estimates of ε_p derived from the δ^{13}C of species-specific alkenone compounds in laboratory cultures and mesocosm experiments. Here, we analyze ε_p derived from the δ^{13}C of more general algal biomarkers, i.e. compounds derived from a multitude of species, from sites near a CO$_2$ seep off the coast of Shikine Island (Japan), a natural environment with CO$_2$ concentrations ranging from ambient (ca. 310 μatm) to elevated (ca. 770 μatm) PCO$_2$. We observed strong, consistent δ^{13}C shifts in several algal biomarkers from a variety of sample matrices over the steep CO$_2$ gradient. Of the three general algal biomarkers explored here, namely loliolide, phytol, and cholesterol, ε_p positively correlates with PCO$_2$, in agreement with ε_p theory and previous culture studies. PCO$_2$ reconstructed from the ε_p of general algal biomarkers show the same trends throughout, as well as the correct control values, but with lower absolute reconstructed values than the measured values at the elevated PCO$_2$ sites. Our results show that naturally occurring CO$_2$ seeps may provide useful testing grounds for PCO$_2$ proxies and that general algal biomarkers show promise for reconstructing past PCO$_2$.

2.1 Introduction

The current increase in the atmospheric concentration of carbon dioxide (expressed in partial pressure, PCO$_2$) plays a leading role in climate change (Forster et al., 2007). PCO$_2$ is significantly higher now than it has been in the past 800 ka (Lüthi et al., 2008) and although long-term changes in PCO$_2$ are not uncommon over millions of years (Foster et al., 2017), this current spike in PCO$_2$ has occurred within only the past two centuries (IPCC, 2013). Uncertainties remain on the exact magnitude to which PCO$_2$ influences climate, as well as the exact response of the environment to these climate changes. Long-term PCO$_2$ trends help us better understand the context for these changes and are reconstructed via indirect means, i.e. environmental proxies. Two proxies can span timescales over 100 Ma (Foster et al., 2017), e.g. the

terrestrial proxies paleosols and leaf stomata. The paleosol proxy has large uncertainties due to the difficulties in constraining soil respiration (Breecker et al., 2010; Cotton and Sheldon, 2012) due to carbon isotopic fractionation during microbial decomposition (Bowen and Beerling, 2004), carbonate diagenesis (Quast et al., 2006), and other local and regional influences on carbon cycles in these terrestrial settings. Although the leaf stomata proxy is often better constrained than paleosols, some experiments do not show the expected trends (Ellsworth et al., 2011; Ward et al., 2013; DaMatta et al., 2016), suggesting that factors other than PCO_2, e.g. ecological systems, species, and development stage, also impact the leaf stomata proxy (Xu et al., 2016). The development of new proxies for PCO_2 may help us better constrain past long-term trends, particularly marine-based proxies which tend to have more homogenized signals but are currently relatively limited in time.

A proxy that has been explored with mixed success over the past several decades is the stable carbon isotopic fractionation associated with photosynthetic inorganic carbon fixations (ε_p), which has been shown to positively correlate with PCO_2 (Bidigare et al., 1997; Jasper and Hayes, 1990; Zhang et al., 2013). ε_p occurs as the CO_2-fixing enzyme in photoautotrophs, Rubisco (ribulose 1,5-biphosphate carboxylase oxygenase), favors ^{12}C which consequently results in photosynthates isotopically more depleted in ^{13}C than the original carbon source. A greater abundance of CO_2 increases Rubisco-based isotopic discrimination, resulting in an even lower $^{13}C/^{12}C$ ratio ($\delta^{13}C$) in photoautotroph biomass (Farquhar et al., 1989; Farquhar et al., 1982; Francois et al., 1993; Popp et al., 1989). When this phototrophic biomass is preserved in the geologic record, the $\delta^{13}C$ of sedimentary organic matter can be used to reconstruct PCO_2 (Hayes et al., 1999). The largely mixed contributions and diagenetic processes on bulk organic matter can, however, mask this signal (Hayes, 1993; Hayes et al., 1999). Thus, isotope analysis of specific biomarker lipids is preferred in order to better define the source of the $\delta^{13}C$ signal (Jasper and Hayes, 1990; Pagani, 2002).

The most studied biomarkers for calculating ε_p are alkenones, i.e. long-chain unsaturated methyl and ethyl ketones produced by select Haptophytes (de Leeuw et al., 1980; Volkman et al., 1980). The stable carbon isotopic fractionation of alkenones has been studied using cultures and mesocosms with controlled environments (Benthien et al., 2007; Laws et al., 1995), but conditions do not always mimic natural environments and the natural variation in carbonate chemistry that occurs on a daily to seasonal time scales. Furthermore, these experiments are also time-consuming given that they must have delicately balanced water chemistry

including CO$_{2[aq]}$ concentrations, pH, and alkalinity, as well as nutrients such as nitrate and phosphate (Bidigare et al., 1997; Laws et al., 1995; Popp et al., 1998b), along with the additional challenge of maintaining a constant $\delta^{13}C$ of the CO$_{2[aq]}$ while photoautotrophs continually enrich the growth water as they fix CO$_2$. Water column studies (Bidigare et al., 1997) and surface sediments (Pagani, 2002) have been applied but rarely reach elevated PCO$_2$ levels such as those encountered in the past.

Here we use an alternative approach by analyzing algal lipids near natural CO$_2$ seep systems. In tectonically active zones, volcanically induced seeps consistently bubble high PCO$_2$ concentrations into the surrounding water, substantially increasing the local CO$_2$ concentrations in the water and providing an environment referent to past and future high-CO$_2$ worlds. CO$_2$ seeps were previously overlooked for biological studies due to the typically high sulfide (H$_2$S) concentrations associated with volcanic degassing that make these environments largely uninhabitable (Dando et al., 1999). However, certain CO$_2$ seep systems have been found to have low H$_2$S concentrations making them suitable for ocean acidification experiments (Hall-Spencer et al., 2008), prompting further research in e.g. the Mediterranean (Boatta et al., 2013), in Japan (Agostini et al., 2015), Papua-New-Guinea (Fabricius et al., 2011), and New Zealand (Brinkman and Smith, 2015). These sites may provide an ideal testing ground for the impact of isotopic fractionation on algal lipids where environmental conditions are at naturally balanced levels with the exception of the large gradient of CO$_2$ concentrations.

In our study, we explore the relationship between ϵ_p and CO$_{2[aq]}$ across several pre-established sites with different (temporally consistent) levels of PCO$_2$ at the warm-temperate CO$_2$ seep at Mikama Bay off the shore of Shikine Island, Japan. We test this relationship using general algal biomarkers, i.e. compounds derived from a multitude of species and which have rarely been used for ϵ_p-based PCO$_2$ reconstructions despite their potential utility (Freeman and Hayes, 1992; Popp et al., 1989; Witkowski et al., 2018).

2

2.2 Materials and Methods

2.2.1 Sample site

The site is briefly described here. For further details, we refer to Agostini et al. (2018). Mikama Bay is located on the south-southwest corner of Shikine Island off the Izu Peninsula, Japan bay (34.320865 N, 139.204868 E) with several venting locations in the north of the bay (Fig. 2.1). The gas emitted from the seep contains 98% CO_2 and the bay has a spatially and temporally constant total alkalinity averaging at 2265 $\pm$ 10 μmol kg^{-1}. Samples were collected from three preestablished PCO_2 sites (Agostini et al., 2015), "Control PCO_2" site in an adjacent bay outside the influence of the CO_2 seep (PCO_2 309 $\pm$ 46μatm), a "Mid PCO_2" site (PCO_2 ca. 460 $\pm$ 40 μatm), and a "High PCO_2" site (PCO_2 769 $\pm$ 225) (Fig. 2.1). PCO_2 estimates are based on the carbonate chemistry parameters (pH$_{NBS}$, temperature, salinity, and total alkalinity) of water in the bay and calculated using the program CO2sys (Agostini et al., 2018; Harvey et al., 2018). Temperature (annual range ca. 14 to 28ºC) and salinity (ca. 34‰) are relatively homogenous throughout the bay and do not differ between the elevated PCO_2 sites and control PCO_2 sites (Agostini et al. 2018). Currents and wind were measured in October 2014 and April 2015 (Agostini et al., 2015). October 2014 measurements showed moderate turbulent winds (ranging from 0.6-11.5 m s^{-1}, average 4.5 m s^{-1}) associated with current velocities (ranging from 0 to 1.6 knots, average 0.4 knots) at 5 m in the surface water, whereas April 2015 measurements showed moderate north-northeast winds (1.5-8.6 m s^{-1}, average 5.1 m s^{-1}) associated with low current velocities (0-0.2 knots, average 0.04 knots). Monthly surveys in the bays over the past five years show that these sites have similar annual mean values for temperature, salinity, and currents. Weather station data shows that the severity of seasonal extreme weather event (e.g. typhoons) varies on an annual basis (Japan Meteorological Agency, https://www.jma.go.jp/en/typh/).

2.2.2 Materials

Samples were collected in June and September of 2016 (indicated in Fig. 2.1). All samples were collected in at least triplicate for each site ("Control PCO_2", "Mid PCO_2" and "High PCO_2" site). Additional control sites (at ca. 1.8 km and 2.4 km away from the CO_2 seep) around the island were taken to ensure the fidelity of the Control site closest to the seep. June sampling included surface waters for dissolved inorganic carbon (DIC) measurements, surface sediments, and benthic diatoms attached to surface sediment through extracellular polymeric substance production.

In September, macroalgae and plankton tows were collected, in addition to surfaced water DIC and surface sediments, taken in triplicate at each site on four separate days.

Water for the δ^{13}C of DIC analysis was collected by overfilling glass vials with sea surface water and adding mercury chloride (0.5%) before closing with a septa cap and sealing with electrical tape. Surface sediments were collected by divers using geochemical sample bags. Macroalgae and benthic diatoms were scraped off submerged rocks at each respective site. . A 25 μm mesh plankton net ("small plankton net", Rigo, Saitama, Japan) was towed 50 m three times per site and filtered using a portable hand aspirator on the boat over a single 0.7 μm GF/F (glass fiber filters; combusted prior to sampling for 4 h at 450°C).. All samples were immediately frozen; once back in the lab, these were freeze-dried and kept in a refrigerator.

2

2.2.3 Methods

Each seawater sample was measured for the δ^{13}C of DIC in duplicate on a Thermo Scientific Gas Bench II coupled to a Thermo Scientific Delta V mass spectrometer. Prior to running samples, 12 ml vials were prepared with 100 μL of 85% H$_3$PO$_4$ and flushed with He. 500 μL of seawater was added and left to react for at least 1 h prior to measuring the headspace. Standards were run at the start, end, and every six runs of a sequence. Standards were prepared with 0.3 mg of Na$_2$CO$_3$ and 0.4 mg of Ca$_2$CO$_3$ (all calibrated against NBS-19) flushed with He, injected with 500 μL of 85% H$_3$PO$_4$, and reacted for 1 h. The headspace was measured and average values and standard deviation errors reported are based on six measurements for June (three at the High PCO$_2$ site and three at the Control) and thirty-six measurements for September (three each at the High PCO$_2$ site, Mid PCO$_2$ site, and Control collected on four separate days).

Freeze-dried sediments, benthic diatoms, and macroalgae were homogenized using mortar and pestle and extracted using a Dionex 250 accelerated solvent extractor at 100°C, 7.6x106 Pa using dichloromethane (DCM): MeOH (9:1 v/v). GFFs containing plankton net material were cut into 1 mm x 1 mm squares and extracted using ultrasonication (5x) with 2 ml dichloromethane (DCM): MeOH (9:1 v/v). All total lipid extracts (TLEs) were hydrolyzed by refluxing the TLE with 1N of KOH in MeOH for one hour and neutralized to pH 5 using 2 N of HCl in MeOH. Bi-distilled water (2 ml) and DCM (2 ml) were added (5x) to the hydrolyzed centrifuge
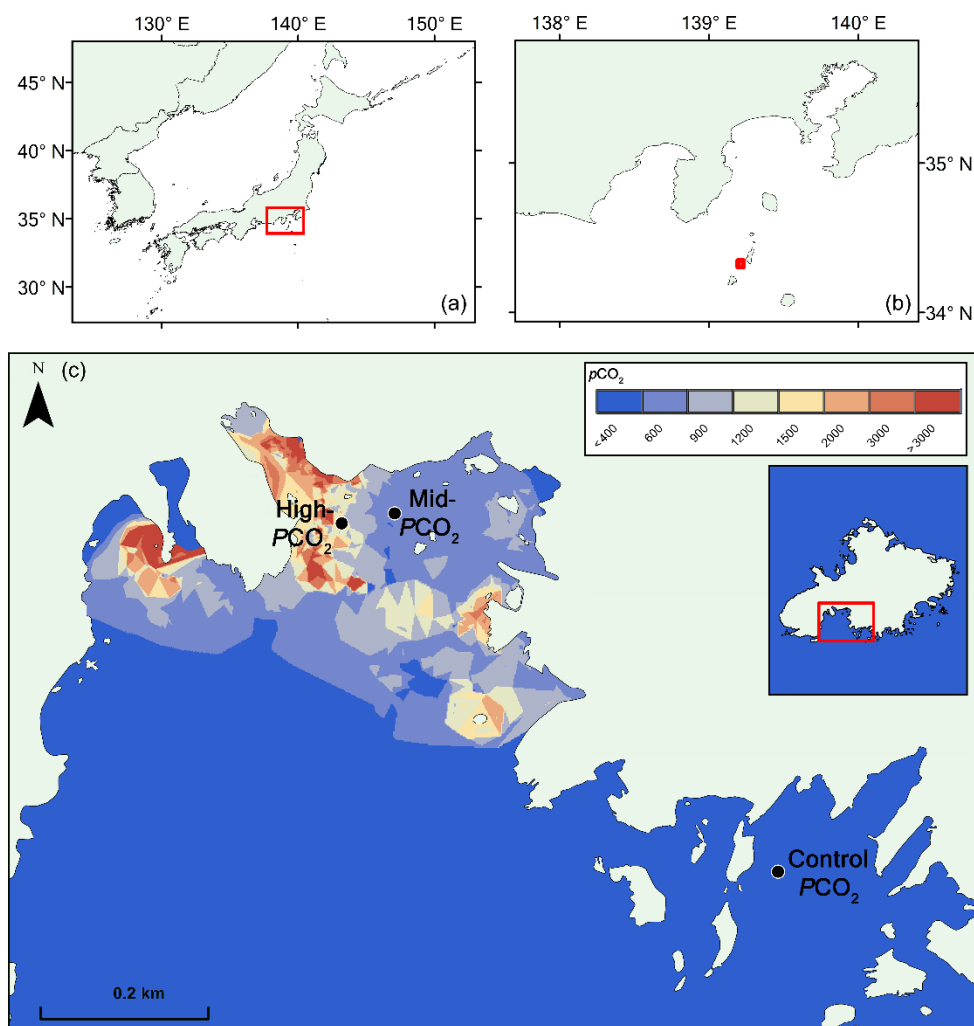
Fig. 2.1. Map of PCO$_2$ in the study region at Shikine Island (Japan). Top panel shows geographical context. Lower panel shows the bay on Shikine Island, with spatial variability in PCO$_2$ (Agostini et al., 2018), computed using the nearest neighbor algorithm in ArcGIS 10.2 software.

tubes and the organic matter in the DCM layers were pooled and dried over Na$_2$SO$_4$. The resulting hydrolyzed TLEs were eluted over an alumina packed column and separated into apolar (hexane: DCM, 9:1 v/v), ketone (DCM), and polar (DCM: MeOH, 1:1 v/v) fractions. Polar fractions were silylated using pyridine: N,O-Bis(trimethylsilyl)trifluoroacetamide (BSTFA) (1:1 v/v) and heated at 60°C for 1 h prior to analyses on the gas chromatography-flame ionization detector (GC-FID),

gas chromatography-mass spectrometry (GC-MS), and gas chromatography isotope-ratio mass spectrometry (GC-IRMS).

Silylated polar fractions were analyzed by GC-FID for quantification. Based on the quantities, fractions were diluted with ethyl acetate and ca. 1 ug of polar fraction was injected on-column for GC-MS to identify compounds and for GC-IRMS to measure the isotopic composition of specific compounds. Each instrument is equipped with the same CP-Sil 5 column (25 m x 0.32 mm; df 0.12 μm) and He is used as carrier gas. GC oven was programmed from 70ºC to 130ºC at 20ºC/min and then to 320ºC at 4ºC/min which was held for 10 min. All three instruments use the same in-house mixture of n-alkanes and fatty acids to check chromatography performance at the start of each day (GC-standard). For compound specific stable carbon isotope analysis using GC-IRMS, additional standards with known isotopic values (-32.7 and -27.0‰) of per deuterated (99.1%) n-alkanes (C$_{20}$ and C$_{24}$, respectively), were co-injected with the GC-standard. Samples were also co-injected with the same GC-IRMS standards to monitor instrument performance. Every day, the Isolink II combustion reactor of the GC-IRMS was oxidized for at least 10 min, backflushed with He for 10 min, and purged for 5 min; a shorter version of this sequence is conducted in post-sample seed oxidation which includes 2 min oxidation, 2 min He backflush, and 2 min purge conditioning line. Longer oxidations were run weekly. Each derivatized compound was corrected for the δ^{13}C of the BSTFA used in silylation (-32.2‰).

2.3   Results

Samples from the different matrices were collected at several Control PCO$_2$ sites (309 ± 46, at a "Mid PCO$_2$" site (ca. 100 m from the venting area; 460 ± 40 μatm), and near the venting area ("High PCO$_2$" site; 769 ± 225 μatm) during June and September 2016 (Fig. 2.1), which included June-collected surface waters (for DIC), surface sediments, and benthic diatoms, and September-collected surface waters (for DIC), surface sediments, plankton net tows, and macroalgae. The δ^{13}C of DIC demonstrated minimal change over the gradient of CO$_2$ and minimal change between the two seasons (Fig. S1). The June δ^{13}C of DIC was 0.2 ± 0.2 ‰ (± SD; N=3) at the Control site and 0.5 ± 0.04 ‰ (N=3) at the High PCO$_2$ site. The September δ^{13}C of DIC was -0.4 ± 0.2 ‰ (N=8) at the Control site, -0.1 ± 0.1 ‰ (N=8) at the Mid PCO$_2$ site, and 0.2 ± 0.4 ‰ (N=8) at the High PCO$_2$ site.
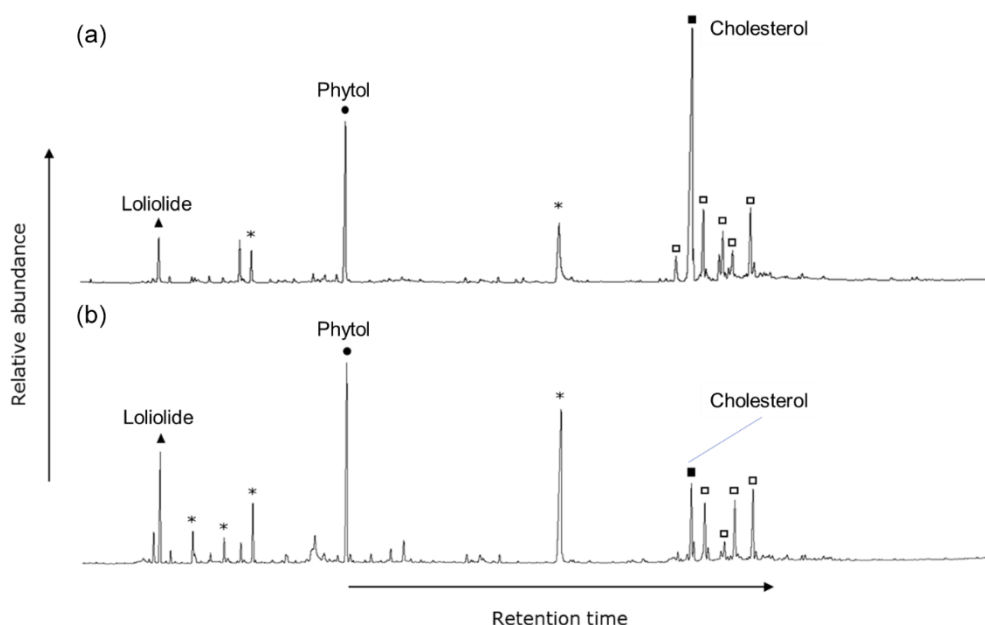
Fig. 2.2. GC-FID trace of silylated polar fraction. June sediment collected at the A) Control site and B) CO_2 vent, showing saturated fatty alcohols (asterisk) and sterols (square), and the representative compounds found among all sample matrices, seasons, and CO_2 concentrations: loliolide, phytol, and cholesterol.

The polar fractions of the extracts of the surface sediments, plankton, macroalgae, and benthic diatoms showed a similar suite of compounds, observed across all sites and during both seasons. The most prominent compounds were loliolide, phytol, C_{14}-C_{16} alkanols, and sterols such as cholesta-5,22E-dien-3β-ol, cholesterol, 23-methylcholesta-5,22dienol, campesterol, stigmasterol, and β-sitosterol (e.g. Fig. 2.2). Terrestrial biomarkers such as long chain alcohols and triterpenoids were not detected. Loliolide, phytol, and cholesterol were targeted for stable carbon isotope analysis as the most abundant algal biomarkers and with relatively good separation in the GC. Biological sources of these compounds will be discussed in Section 4.1.

Among the sample matrices, the $\delta^{13}C$ of loliolide ranges from -19.8 to -22.0 ‰ at the Control sites, from -20.5 to -22.9 ‰ at the Mid PCO$_2$ site, and from -23.1 to -29.0 ‰ at the High PCO$_2$ site (Fig. 2.3A; Table S1). The $\delta^{13}C$ of loliolide from June surface sediments shows the strongest change from the Control site to the High PCO$_2$ site (-21.2 to -29.0 ‰), followed by the $\delta^{13}C$ of loliolide from September macroalgae (-21.3 to -25.7 ‰). A lesser $\delta^{13}C$ shift is observed in the September surface sediment-derived loliolide (-19.8 to -23.1 ‰). The $\delta^{13}C$ of the benthic diatom-derived loliolide

(-20.2 to 23.6 ‰) and the plankton tow-derived loliolide show the smallest shifts from the Control to High PCO$_2$ site (-22.0 to -23.6 ‰).

Similar to the results of the δ^{13}C of loliolide, the δ^{13}C of phytol also consistently shows higher δ^{13}C values in the Control sites and lower δ^{13}C values in the elevated PCO$_2$ sites among all samples types collected in both seasons (Fig. 2.3B; Table S1). For the whole sample set, the δ^{13}C of phytol ranges from -18.9 to -22.6 ‰ at the Control site, from -19.4 to -22.4 ‰ at the Mid PCO$_2$ site, and from -22.6 to -27.8 ‰ at the High PCO$_2$ site (Fig 3B), similar ranges as observed for loliolide. A similar shift in δ^{13}C values of phytol is observed with increasing PCO$_2$ in the June surface sediments (-22.6 to -27.8 ‰), the June benthic diatoms (-18.9 to -24.4 ‰), and the September macroalgae (-21.5 to -26.9 ‰). Smaller changes in the δ^{13}C of phytol are observed for September plankton (-21.7 to -24.4 ‰) and September sediment (-20.5 to -22.6 ‰).
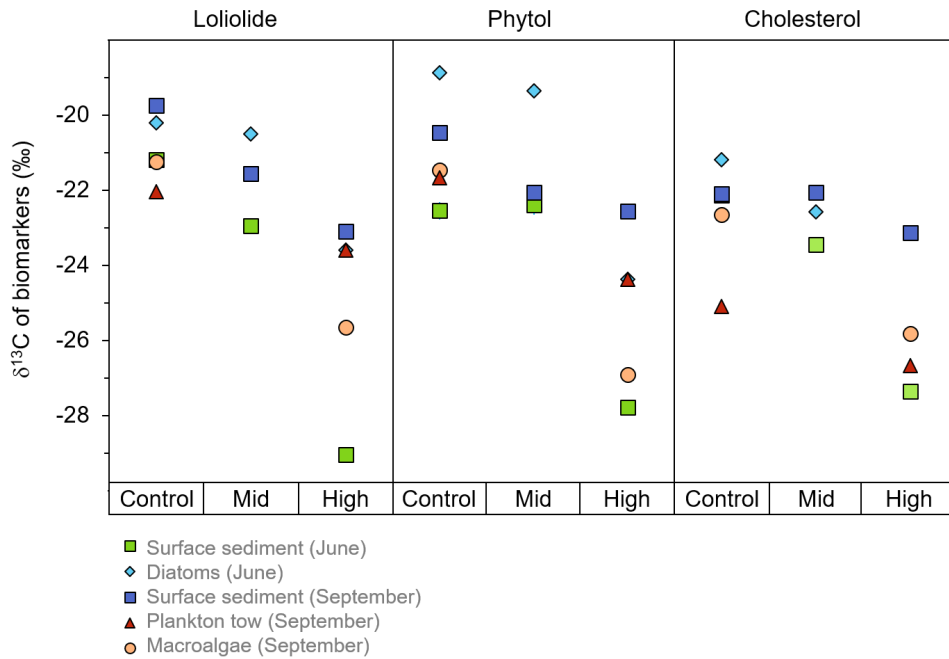

Fig. 2.3. The δ^{13}C of general algal biomarkers in sediments: A) loliolide, B) phytol, and C) cholesterol from the Control, Mid, and High PCO$_2$ sites during June and September from different sample matrices, including surface sediment (square), benthic diatoms (diamond), plankton tow (triangle), and macroalgae (circle).

The $\delta^{13}C$ of cholesterol likewise shows a similar trend to the other two biomarkers but with a smaller shift in the $\delta^{13}C$ values from the Control PCO$_2$ sites to the elevated PCO$_2$ sites. Among the different sample matrices, the $\delta^{13}C$ of cholesterol ranges from -21.2 ‰ to -25.1 ‰ at the Control site, -22.1 to -23.4 ‰ at the Mid PCO$_2$ site and -23.1 to -27.4 ‰ at the High PCO$_2$ site (Fig. 2.3C; Table S1). The strongest change in the $\delta^{13}C$ of cholesterol with increase PCO$_2$ occurs in the June surface sediments from -22.6 ‰ in the Control to -27.8 ‰ at the High PCO$_2$ site. The June benthic diatoms also have a large isotopic shift in the $\delta^{13}C$ of cholesterol (-21.2 to -25.8 ‰), as does the September macroalgae (-22.7 to -25.8 ‰). The September surface sediments (-22.2 to -23.1 ‰) and plankton tow-derived cholesterol (-25.1 to -26.7 ‰), however, have a smaller shift from the control to the elevated PCO$_2$ sites.

2.4 Discussion

2.4.1 The $\delta^{13}C$ differences in biomarkers among matrices and seasons

All three biomarkers, phytol, loliolide and cholesterol, show a negative shift in $\delta^{13}C$ values with increasing PCO$_2$ in each matrix and each season (Fig. 2.3), agreeing with the theory that higher PCO$_2$ conditions result in lower $\delta^{13}C$ values in biomass (Farquhar et al., 1982). However, despite all having algal sources, the absolute isotope values vary for 1) each compound, 2) each matrix, and 3) both seasons, which we will now discuss.

First, the absolute values of $\delta^{13}C$ values vary among the three compounds. This may be expected given the different biosynthetic pathways leading to formation of each compound (Schouten et al., 1998), as well as the different contributors to each compound. Loliolide, considered a diatom biomarker in paleoreconstructions (e.g. Castaneda et al., 2009), is a diagenetic product of fucoxanthin (Klok et al., 1984; Repeta, 1989), a xanthophyll which contributes to approximately 10% of all carotenoids found in nature (Liaaen-Jensen, 1978). Phytol, considered a photoautotroph biomarker in paleoreconstructions (Hayes et al., 1990), is the side-chain of the vital and omnipresent pigment chlorophyll a that directly transfers sunlight energy into the photosynthetic pathway in nearly all photosynthetic organisms. Sterols, considered a general eukaryotic biomarker in paleoreconstructions, are the eukaryotic tetracyclic triterpenoid lipids used for critical regulatory roles of cellular functions e.g. maintaining membrane fluidity (Nes et al., 1993). Although sterols are virtually restricted to eukaryotes, some exceptions have been found in bacteria (Wei et al., 2016). Here we only examine

cholesterol, which is universally absent in prokaryotes and composes of up to 20-40% of eukaryotic plasma membranes (Mouritsen and Zuckermann, 2004). Phytol and cholesterol may also have terrestrial sources given that they are derived from all photoautotrophs and all eukaryotes, respectively. However, these samples were taken off the coast of a small island in open ocean and the absence of characteristic terrestrial biomarkers indicates that terrestrial contributions can be considered to be minimal. The close resemblance of the isotopic composition among all three compounds, including the primarily diatom-limited compound loliolide, suggests that these compounds share relatively similar source organisms. Cholesterol shows a lessened isotopic shift than the other two compounds from the ambient to elevated PCO$_2$ sites. Although we cannot fully exclude that this is due to terrestrial input, it is more likely due to the mobile eukaryotic zooplankton in the water column which also contribute to the cholesterol signal.

Within the same biomarker and same season, some differences among matrices were observed. This difference may be due to the mobility of the matrix, as well as the algal assemblages. The plankton tow which captured free-floating surface water algae from that specific growth season is more readily transported by wind than the surface sediment, which likely reflects the culmination of multiple growth seasons throughout the water column. This is seen, for example, in the δ^{13}C of cholesterol collected in September from the same Control site where surface sediments are -22.2 ‰ and plankton tows are -25.1 ‰, where the latter has possibly been transported from sites with elevated PCO$_2$ levels. Similar differences among matrices are also observed in phytol and loliolide. The hypothesis of transportation affecting the isotopic signal in certain matrices is supported by the results from the macroalgae. The macroalgae, in contrast to the algae collected by plankton tows, were unaffected by transportation due to being fixed to the nearby rocks at each site. Thus, the isotopic composition of compounds of the macroalgae was similar to that of the long-accumulated surface sediments, e.g. -22.7 ‰ for the δ^{13}C of cholesterol at the September Control site.

Finally, there is a difference in the δ^{13}C values for biomarkers between seasons. The June-collected surface sediments and algae yielded a larger difference in δ^{13}C values along the CO$_2$ gradient than the September-collected surface sediments and algae. This seasonal difference may be due to extreme weather conditions experienced between the two sampling campaigns. Although typhoons are common in this region, in the weeks preceding the fieldwork in September, Shikine Island experienced an unusually high quantity of storms. The storms were also of unusual strength for this region of the Pacific, including Typhoons Mindulle and Kompasu, the severe tropic

storms Omais and Chanthu, and the long-lived, erratic Lionrock typhoon. This atypical abundance and severity of storms observably ripped corals out of the rocks around Shikine Island and thus likely resuspended and transported some sediment around the bay. This would explain the reduced $\delta^{13}C$ difference between the Control and High PCO$_2$ site in the surface sediments collected in September, as well as the readily transportable algae collected by the plankton tow, and would explain why the rock-affixed macroalgae, also collected in September, maintained a strong $\delta^{13}C$ change across the transect.

2.4.2 The $\mathcal{E}_p$ among general algal biomarkers

To further validate the impact of PCO$_2$, we calculated the isotopic fractionation of algal biomass based on the $\delta^{13}C$ of the three biomarkers. Here we focus on surface sediments as they are a close analogue to the geological sediment records. Although the macroalgae and benthic diatoms also show strong isotopic fractionation, they represent a limited number of species and a single growth season. Furthermore, we calculated the $\mathcal{E}_p$ from the June-collected surface sediments, which appear to be the least affected by typhoon activity and represent fractionation over multiple seasons.

To calculate $\mathcal{E}_p$ in the June-collected surface sediments, we correct the $\delta^{13}C$ of the organic matter (δ_p) for the $\delta^{13}C$ of the inorganic carbon source for the producers of these compounds (δ_d) in Eq. (1):

$$\mathcal{E}_p = 1000 \cdot [(\delta_d+1000) / (\delta_p+1000) - 1] , \qquad\qquad [1]$$

δ_p is calculated by correcting the $\delta^{13}C$ for each individual biomarker for the offset with photosynthetic biomass caused by isotopic fractionation during biosynthesis. The isotopic offset between phytol and biomass is 3.5 ± 1.3 ‰ based on the average of twenty-three species compiled in Witkowski et al. (2018) and the isotopic offset between sterols and biomass is 4.5 ± 3.0 ‰ based on the average of eight algal species (Schouten et al., 1998). The isotopic offset for loliolide from biomass, however, has not been determined. Because isoprenoids are formed from the same biosynthetic pathway, we here average the offset of the other two isoprenoids here (4.0 ‰) to estimate a value for the difference between loliolide and biomass.

δ_d is calculated by correcting the measured $\delta^{13}C$ of DIC for temperature (Mook, 1974) and pH (Madigan et al., 1989), which considers the relative contribution of different inorganic carbon species to the measured DIC. Based on the equations of Mook et al. (1974), we correct for the temperature-dependent carbon isotopic fractionation of

dissolved CO$_2$ with respect to HCO$_3^-$ using the annual mean sea surface temperature for Shikine Island of 20.4ºC (Agostini et al., 2018). Based on the equations of Madigan et al. (1989), we corrected for the δ^{13}C of HCO$_3^-$ and δ^{13}C of CO$_{2[aq]}$ mass balance calculation that accounts for the relative abundance of these inorganic carbon species based on pH (Lewis and Wallace, 1998) at the High PCO$_2$ site (7.81 pH$_T$) and Mid PCO$_2$ site (7.99 pH$_T$) relative to the ambient Control (8.14 pH$_T$). The corrected δ$_d$ values yield -10.1 ‰ at the Control site, -10.0 ‰ at the Mid PCO$_2$ site, and -9.5 ‰ at the High PCO$_2$ site (Table S2).
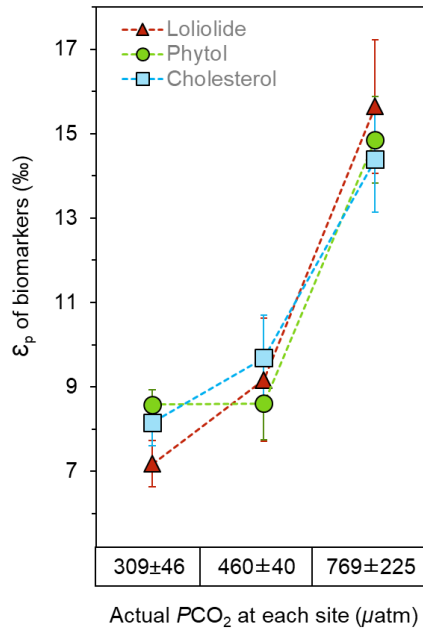

Fig. 2.4. The ε$_p$ of general algal biomarkers in sediments. Loliolide (triangle), phytol (circle), and cholesterol (square) from the Control, Mid and High PCO$_2$ sites during June sediment collection.

ε$_p$ values consistently yield much higher values at the elevated PCO$_2$ sites than the ambient Control sites for all three biomarkers, which share similar trends and absolute values (Fig. 2.4; Table S3). ε$_p$ derived from loliolide averages 7.2 ± 1.6 ‰ at the Control, 9.2 ± 1.6 ‰ at the Mid PCO$_2$ site, and 15.9 ± 1.6 ‰ at the High PCO$_2$ site, ε$_p$ derived from phytol at 8.6 ± 0.4 ‰, 8.6 ± 0.9 ‰, and 14.9 ± 1.0 ‰, respectively, and ε$_p$ derived from cholesterol at 7.6 ± 3.0 ‰, 9.2 ± 3.1 ‰, to 13.7 ± 3.1 ‰, respectively, where errors represent the standard deviation of the triplicate samples taken at each site. These results show that CO$_2$ has a profound impact on ε$_p$

as it is the only variable with a large gradient in the bay. Given that maximum fractionation for algae species is ca. 25 to 28 ‰ in laboratory cultures (Goericke and Fry, 1994), the CO_2 seep values suggests strong, but does not approach maximum fractionation (ε_f) at the high CO_2 site. This may be due to presence of carbon concentrating mechanism in phytoplankton which utilize ^{13}C-enriched bicarbonate or possible due to the presence of Rubisco types with different ε_f values than previously assumed (Thomas et al., 2018).

2.4.3 $P\text{CO}_2$ reconstructed from general algal biomarkers

We estimate $P\text{CO}_2$ from the ε_p values, a relationship first derived for higher plants (Farquhar et al., 1989; Farquhar et al., 1982) and later adapted for algae (Jasper et al., 1994; Rau et al., 1996) in Eq. (2):

$$P\text{CO}_2 = [\ b\ /\ (\varepsilon_f - \varepsilon_p)\ ]\ /\ K_0 \qquad\qquad [2]$$

where ε_f reflects the maximum Rubisco-based isotopic fractionation, b reflects species carbon demand per supply such as growth rate and cell-size (Jasper et al., 1994), and K_0 reflects a constant to convert $CO_{2[aq]}$ to $P\text{CO}_2$ based on temperature and salinity (Weiss, 1974). ε_f for algal species range from 25 to 28 ‰ in laboratory cultures (Goericke and Fry, 1994); we use an average 26.5 ‰ with an uncertainty of 1.5 ‰ uniformly distributed for these general algal biomarkers (Witkowski et al., 2018). The b value is difficult to estimate as it is a catchall for factors other than $P\text{CO}_2$ that affect fractionation and is particularly difficult to estimate for general algal biomarkers because they are derived from a multitude of species. Previous studies using phytol's diagenetic product phytane as a $P\text{CO}_2$ proxy (Bice et al., 2006; Sinninghe Damsté et al., 2008; van Bentum et al., 2012) have used a mean value of 170 ‰ kg μM^{-1}, similar to the mean of alkenone-producers. This is supported by a compilation of the $\delta^{13}C$ values of modern surface sediment organic matter mean average of 168 ± 43 ‰ kg μM^{-1} (Witkowski et al., 2018) and a single study on phytol in the equatorial Pacific Ocean (Bidigare et al., 1997). We apply this average, rounded to 170 ± 50 ‰ kg μM^{-1} to all three general algal biomarkers.

The resulting reconstructed $P\text{CO}_2$ estimations show the expected values in the Control sites and much higher values in the elevated CO_2 sites among all three biomarkers (Fig. 2.5; Table S3). Loliolide shows the biggest shift, from 239 +50/-49 μatm at the Control, 266 +57/-54 μatm at Mid $P\text{CO}_2$ site, and 437 +113/96 μatm at the High $P\text{CO}_2$ site. Phytol has similar but a slightly smaller shift in $P\text{CO}_2$ estimates to loliolide, with estimations of 264 +55/-54 μatm, 291 +56/-53 μatm, and 444 +98/-

87 μatm at the Control, Mid PCO$_2$ site, and High PCO$_2$ site, respectively. Cholesterol shifts similarly to the other two biomarkers with 244 +67/-54 μatm, 266 +77/-61 μatm, and 358 +136/-90 μatm, respectively. These reconstructed values closely match each other and trend in the same direction as the actual values.

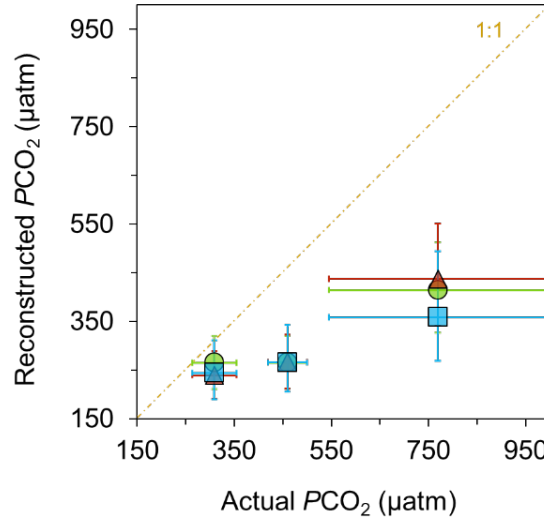**Fig. 2.5.** Reconstructed PCO$_2$ from general algal biomarkers. PCO$_2$ reconstructed from the δ^{13}C of loliolide (triangle), phytol (circle), and cholesterol (square) in June-collected sediments versus the actual PCO$_2$ measured at each location (Agostini et al., 2018; Harvey et al. 2018).

The reconstructed PCO$_2$ values derived from the δ^{13}C of general algal biomarkers closely match the actual measured PCO$_2$ values of the Control (Fig. 2.5), i.e. 309 $\pm$ 46 μatm (Agostini et al., 2018; Harvey et al., 2018), when considering the uncertainty in the reconstructed estimations. However, the proxies underestimate the absolute values measured at the elevated PCO$_2$ sites (Fig. 2.5; Table S3), i.e. 460 $\pm$ 40 μatm at the Mid PCO$_2$ site and 769 $\pm$ 225 μatm at the High PCO$_2$ site (Agostini et al., 2018; Harvey et al., 2018). There are several possible explanations to why there is an underestimation. As discussed above, carbonate concentration mechanisms may be operating in a large number of phytoplankton, such that they become relatively enriched in ^{13}C and thus lead to lower reconstructed PCO$_2$ values (Badger et al., 2019; Stoll et al., 2019). There is also a large uncertainty in the b value applied, which may be much lower than the value assumed here. However, if so, then PCO$_2$ values reconstructed for past times may be much higher, leading to considerable discrepancies with other PCO$_2$ proxies (c.f. Witkowski et al., 2018). A simple explanation for this underestimation may be some site limitations. The high

variability of PCO_2 at these sites could have impacted the reconstructed values, as these algae could have been exposed to much different, and perhaps lower, levels than those observed during the times that PCO_2 values were measured. Furthermore, there is a strong possibility of allochthonous marine input of sediment at the Mid and High PCO_2 site, i.e. input from sediment outside of the bay area. This allochthonous input seems likely given the intense weather conditions that occur annually in this small bay in which lateral transport of sediment could bring algal material grown in ambient PCO_2 conditions into the bay and dampen the overall PCO_2 signal picked up in the biomarkers. Future research conducted at another CO_2 seep settings with different weather and current conditions could illuminate this.

2.5 Conclusion

We analyzed the $\delta^{13}C$ of general algal biomarkers in surface sediments, plankton, benthic diatoms, and macroalgae collected in a transect from a CO_2 vent during two seasons. The strong $\delta^{13}C$ change between the Control and elevated PCO_2 sites suggest that the increased CO_2 concentrations in the seawater does indeed influence fractionation of photoautotrophic biomass and validates previous PCO_2 reconstructions which have considered utilizing general algal biomarkers for this purpose. Reconstructions correctly estimate control values, though reconstructions at the elevated PCO_2 sites show underestimations of the actual PCO_2, possibly due to the allochthonous input from nearby marine sediments deposited under normal PCO_2 levels caused by the intense annual typhoon activity in this region. Our results show that CO_2 seeps may offer testing grounds for exploring new PCO_2 proxies under natural conditions at high PCO_2 levels such as those encountered in the geological past.

Acknowledgements

2

Supplementary material

Table S1. The δ^{13}C of biomarkers from different matrices. The δ^{13}C of general biomarkers loliolide, phytol, and cholesterol measured during two seasons from sea surface sediments, diatom mats, plankton net tows, and macroalgae.

Table S2. The δ^{13}C of CO$_2$. All parameters used to calculate the δ^{13}C of CO$_2$ (represented in the equations as δ$_d$), including corrections for sea surface temperature and pH.

Table S3. The δ^{13}C of algal biomarkers and all parameters used to estimate PCO$_2$. All parameters used to calculate PCO$_2$ from the δ^{13}C of general algal biomarkers: loliolide, phytol, and cholesterol.

Chapter 3

Testing algal-based PCO_2 proxies at a modern CO_2 seep (Vulcano, Italy)

Caitlyn R Witkowski[1], Marcel TJ van der Meer[1], Nadine T Smit[1], Jaap S Sinninghe Damsté[1,2], Stefan Schouten[1,2]

[1] Department of Marine Microbiology and Biogeochemistry, Royal Netherlands Institute for Sea Research, and Utrecht University, The Netherlands
[2] Department of Geosciences, Utrecht University, The Netherlands

Abstract

Understanding long-term trends in atmospheric concentrations of carbon dioxide (PCO$_2$) has become increasingly relevant as modern concentrations surpass recent historic trends. One method for estimating past PCO$_2$, the stable carbon isotopic fractionation associated with photosynthesis (ε_p) based on specific biomarker lipids, particularly alkenones, has shown promise over the past several decades. Recently, the ε_p of more general biomarker lipids, i.e. organic compounds derived from a multitude of species, have been applied to generate longer-spanning, more ubiquitous records but the sensitivity of this proxy to changes in PCO$_2$ has not been constrained in modern settings. Here, we test ε_p using a variety of general biomarkers along a transect taken from a naturally occurring marine CO$_2$ seep in Levante Bay of the Aeolian island of Vulcano in Italy. The studied general biomarkers, loliolide, cholesterol, and phytol, all show increasing depletion in ^{13}C over the transect from the control site towards the seep, suggesting that CO$_2$ exerts a strong control on isotopic fractionation in natural phytoplankton communities. The strongest shift in fractionation was seen in phytol, and PCO$_2$ estimates derived from phytol confirm the utility of this biomarker as a proxy for PCO$_2$ reconstruction.

3.1   Introduction

The concentration of atmospheric carbon dioxide (PCO$_2$, expressed in partial pressure µatm), as directly measured from air trapped in ice cores, has had a major influence on climate over the past 800 ka (Caillon et al., 2003). During this period, PCO$_2$ and temperature oscillated together between stable bounds every 100 ka (Petit et al., 1999). In the past two centuries, the rise of PCO$_2$ has broken those bounds from the pre-industrial values, previously only ranging between ca. 180 to 280 µatm, to the 410 µatm of today (Betts et al., 2016). This rapid rise in PCO$_2$ causes concern that climate, i.e. temperature, will accordingly change. To better understand how changes may occur, reconstructing longer trends in PCO$_2$ over the geologic record could offer context for evaluating the direction and magnitude of climate change.

Many proxies have been developed for reconstructing past PCO$_2$ and applied with mixed success over the past several decades (Hollis et al., 2019). One method for studying past PCO$_2$ makes use of the stable carbon isotopic fractionation due to CO$_2$-fixation (ε_p), where biomass of photoautotrophs becomes increasingly depleted in ^{13}C as PCO$_2$ increases due to kinetic discrimination by the CO$_2$-fixing enzyme Rubisco (Farquhar et al., 1982; Hayes et al., 1990; Popp et al., 1989). ε_p can be

derived from the $\delta^{13}C$ of photoautotrophic biomass, recorded in sedimentary organic matter, and the $\delta^{13}C$ of CO_2 derived from e.g. planktonic foraminifera (Jasper et al., 1994).

Although PCO_2 has been shown to be one of the dominant physiological control on the $\delta^{13}C$ of photoautotrophic biomass (Young et al., 2012), studies on ε_p in algae have shown that other factors may influence this value, primarily growth rate (Laws et al., 1998) and cell geometry (Popp et al., 1998b), as well as minor influences such as light, and temperature (Degens et al., 1968; Francois et al., 1993; Laws et al., 1995; Nimer and Merrett, 1993). These additional influencing factors on ε_p are considered in PCO_2 reconstructions via the catchall term b (Rau et al., 1997), described in the equation (Bidigare et al., 1997) as:

$$CO_{2[aq]} = b \, / \, (\varepsilon_f - \varepsilon_p) \qquad\qquad [1]$$

where ε_f is the maximum isotopic fractionation due to CO_2-fixation via the enzyme Rubisco, which has shown to range from 25 to 28‰ (Bidigare et al., 1997; Goericke et al., 1994; Wilkes et al., 2017). Several other studies have expanded on Eq. 1 for specific consideration, particularly in calculating b, e.g. instantaneous cell growth rate accounting for differences in photoperiod (Rau et al., 1996; Stoll et al., 2019) and CO_2 fixation rate (Holtz et al., 2015).

Using the knowledge obtain from culture studies (Laws et al., 2001; Popp et al., 2006), the measurement of ε_p in specific algal biomarkers preserved in the geologic record can be used to reconstruct past PCO_2, the primary focus of which has been alkenones, long-chain unsaturated methyl and ethyl n-ketones produced by haptophytes (Jasper and Hayes, 1990; Jasper et al., 1994; Pagani et al., 1999a). Although this proxy has generated a large number of PCO_2 records (Badger et al., 2013; Pagani et al., 2005; Zhang et al., 2013), there are several limitations, such as the exceptionally low ε_f recorded for the alkenone-producer *Emiliania huxleyi* of 11‰ (Boller et al., 2011), a potential insensitivity of this proxy at low CO_2 levels (Badger et al., 2019; Stoll et al., 2019), and difficulties in constraining the b factor over time (Zhang et al., 2019).

One other limitation is the fact that alkenones first commonly appeared in the geologic record ca. 45 Ma ago (Brassell, 2014), prohibiting PCO_2 reconstructions prior to this time. As an alternative, the isotopic fractionation of general phytoplankton biomarkers, compounds that are produced by a multitude of species, have been used. For example, phytane, a diagenetic product of omnipresent chlorophyll-a, has been used in periods extending beyond the alkenone record, i.e.

the Cretaceous (Bice et al., 2006; Naafs et al., 2016; Sinninghe Damsté et al., 2008), and in a Phanerozoic compilation (Witkowski et al., 2018). However, this general biomarker approach has not been extensively tested in laboratory cultures or present-day environments. For this, naturally-occurring phytoplankton communities are necessary to mimic the widespread contributors to general phytoplankton biomarkers, as opposed to the typical single-species approach of laboratory cultures. Mesocosm experiments may offer more natural environmental conditions and communities, though none have been conducted on general phytoplankton biomarkers for PCO$_2$ reconstructions. Alkenones and particulate organic carbon (POC) have been explored in one mesocosm experiment using natural communities, i.e. under three PCO$_2$ conditions in a contained area for ca. 21 days (Benthien et al., 2007). These authors suggested the minor changes they observed in δ^{13}C values for alkenones and POC indicate that fractionation is not primarily controlled by CO$_2$ concentrations but instead by algal growth rate and carbon-uptake mechanisms.

We use a different approach by testing the response of isotopic fractionation in general phytoplankton biomarkers across a CO$_2$ gradient at a naturally occurring CO$_2$ seep. CO$_2$ seeps, which consistently bubbles CO$_2$ into the surrounding environment, were not previously explored for biological studies due to the assumed high sulfide concentrations, toxic to many organisms, typically associated with volcanic degassing (Dando et al., 1999). However, Hall-Spencer et al. (2008) successfully used these environments for ocean acidification experiments, which lead to studies at other seep sites, i.e. Italy (Johnson et al., 2011a), Papua-New-Guinea (Fabricius et al., 2011), New Zealand (Brinkman and Smith, 2015), and Japan (Agostini et al., 2015). An initial test of a marine CO$_2$ seep site on Shikine Island, Japan showed promise (Witkowski et al., 2019), though the imprint of CO$_2$ on $\mathcal{E}_p$ measured in general biomarkers of surface sediment was masked by extreme weather events that caused sediment transport.

Here, we explore a different marine CO$_2$ seep system approximately 30 m into Levante Bay at Vulcano Island, Italy, where we collected surface sediments in a transect from high CO$_2$ towards ambient CO$_2$ values. This CO$_2$ seep system has been previously explored for abundance patterns of passive versus active carbon-uptake mechanisms in different macroalgae were assessed at high CO$_2$, mid CO$_2$, and control sites and showed notable differences in isotopic fractionations between physiological groups (Cornwall et al., 2017). Here, we analyzed the $\mathcal{E}_p$ of several general phytoplankton biomarkers deposited in surface sediments and tested their response to the CO$_2$ gradient at sixteen sites throughout the bay.

3

3.2 Materials and Methods

3.2.1 Sample site

Levante Bay (Fig. 3.1) is on the northeast of Vulcano Island, an Aeolian Island north of Sicily. Volcanic activity on the island started in the upper Pliocene (Frazzetta et al., 1984), where the cooling of magmatic and hydrothermal fluid mixing into the crater fumeroles created the pocket of CO_2 that outgasses into the bay (Chiodini et al., 1993). Located 1 m depth at 38.41694°N 14.96°E, the main underwater venting gas field outputs ca. 3.6 tons of gas per day (Inguaggiato et al., 2012). This gas is composed of 97-98% CO_2 and ca. 2% H_2S (Boatta et al., 2013). The sea water temperature (Boatta et al., 2013) of ca. 19.7°C and salinity (Johnson et al., 2011b) of ca. 38‰ is homogenous throughout the small bay. Currents are mostly wind-driven, with minimal tidal range (<40 cm). The input of CO_2 gas intensely influences the geochemical composition of the bay's waters, as seen by the strong pH gradient starting at the seep to across the bay from pH 5.5 to 8.2 in April and from pH 6 to 8 in September. For more details on the geochemistry, see Boatta et al. (2013).

Fig. 3.1. Map of sites in Levante Bay. Sampling sites along the transect from the CO_2 seep (star, Site 1) to the ambient control (Site 16) on Vulcano Island, Italy (Google Maps). White symbols indicate the additional sampling sites in May 2017.

3.2.2 Materials

Samples were collected in May and October of 2017. A preliminary study was conducted in May using one site with a high CO$_2$ concentration, two sites with a middle CO$_2$ concentration, and one control site (i.e. not affected by the CO$_2$ seep) as defined in Johnson et al. (2011), where seawater was collected for the δ^{13}C of dissolved inorganic carbon (DIC) and surface sediments were collected for the δ^{13}C of biomarker lipids. Seawater for DIC analysis was collected by overfilling glass vials and adding mercury chloride (0.5%) before sealing the vials closed with Apiezon M grease and securing the stopper with rubber bands. Surface sediments were collected by diving, scooped into geochemical bags, and immediately frozen; once back in the lab, these sediments were freeze-dried and kept refrigerated. All surface sediments were collected in triplicate at each site within a square of 2 by 2 m. The same sediment sampling method was used again in October, when a higher-resolution transect of sixteen sites was collected (Fig. 3.1). Given that the results of the δ^{13}C of DIC collected in May was homogenous throughout the bay (see Table S1), as also revealed by another study in this region (Horwitz et al., 2015a), seawater samples were not collected in October.

3.2.3 Methods

 The δ^{13}C of DIC of seawater collected in May was measured on a gas bench coupled to an isotope ratio mass spectrometer (IRMS) in duplicate. Samples were prepared using 100 µL of 85% H$_3$PO$_4$ then flushed with He. Seawater (500 µL) was injected to each vial, left to react for 1 h, and then the headspace was measured. Standards prepared with 0.3 mg of Na$_2$CO$_3$ and 0.4 mg of Ca$_2$CO$_3$ were flushed with He, injected with 100 µL of 85% H$_3$PO$_4$, and reacted for 1 h. The standards were run at the start and end of each sequence, as well as every six runs.

Sediments were freeze-dried and homogenized using a mortar and pestle. Sediments were then extracted using a Dionex 250 accelerated solvent extractor at 7.6 x 106 Pa at 100°C using dichloromethane (DCM): MeOH (9:1 v/v). Extracts were transferred to centrifuge tubes to be refluxed with 1N KOH in MeOH and the resulting base hydrolyzed extracts were neutralized to pH 5 using 2N HCl in MeOH. The hydrolyzed extract was separated into apolar (hexane: DCM, 9:1 v/v), ketone (DCM), and polar (DCM: MeOH, 1:1 v/v) fractions, respectively, over an alumina column. Polar fractions were silylated with pyridine: N,O-Bis(trimethylsilyl) trifluoroacetamide (1:1 v/v) and heated for 1 h at 60°C. The δ^{13}C values of loliolide,

cholesterol, and phytol were corrected for the addition of three C atoms in the trimethylsilyl group using the known $\delta^{13}C$ value of BSTFA (-32.2‰).

Silylated polar fractions were then injected on gas chromatography-flame ionization detector (GC-FID) to determine concentrations and general quality of chromatography before analyzing it on a gas chromatography-mass spectrometer (GC-MS) to identify compounds and on gas chromatography-isotope ratio-mass spectrometer (GC-IRMS) to measure the isotopic composition of specific compounds. GC-FID, GC-MS, and IRMS instrumentation all had starting oven temperatures of 70ºC ramped at 20ºC/min to 130ºC and then ramped at 4ºC/min to 320ºC for 10 min. Separation was accomplished using a CP-Sil 5 column (25 m x 0.32 mm; df 0.12 μm) with He carrier gas. System performance on all three instruments was conducted daily using the same in-house mixture of n-alkanes and fatty acids. Additional standards were run on the IRMS using perdeuterated n-alkanes (C_{20} and C_{24}) with known $\delta^{13}C$ values (-32.7 and -27.0‰, respectively) and were limited to uncertainty within the standard of $\pm$ 0.5‰; if outside this range, the machine was conditioned until it was within this limit. The IRMS was also oxidized regularly, with a daily oxidation of 10 min, backflushed with He for 10 min, and purged for 5 min; a shorter version of this sequence was conducted in post-sample seed oxidation, which includes 2 min oxidation, 2 min He backflush, and 2 min purge conditioning line and a longer version of this sequence was conducted at the end of each week with 1 h oxidation, 1 h He backflush, and 10 min purge conditioning line.

3.2   Results

For this study, we collected surface sediments in May and October close to the seep site (ca. 3 m distance) to a control site unaffected by the seep (Urbarova et al., 2019) (Fig. 3.1). The $\delta^{13}C$ of DIC measured in seawater collected in May from the bay does not express notable change over the gradient of CO_2 (Table S1), which affirms that lack of change noted in the literature (Horwitz et al., 2015b). For this reason, we averaged the $\delta^{13}C$ of DIC measured in our study with that of Cornwall et al. (2017) across all sites (0.7‰ $\pm$ 0.4‰ s.d.) and assumed this to be representative for the bay region.

Analysis of the polar fractions of the lipid extracts obtained from the surface sediments showed the same biomarker lipids throughout the transect from the CO_2 seep to the control sites, though in different relative abundances (e.g. Fig. 3.2). These include: loliolide, phytol, even carbon numbered C_{10}-C_{16} fatty alcohols, C_{30} alkane-

1,15-diol, C$_{32}$-17β(H),21β-hopanol, and sterols, such as cholesta-5,22E-dien-3β-ol, cholesterol, 23-methylcholesta-5,22dienol, campesterol, stigmasterol, and β-sitosterol (Fig. 3.2). Consistently the most abundant among these compounds were loliolide, cholesterol, and phytol, as were also observed at the CO$_2$ seep site in Japan (Witkowski et al., 2019). Loliolide is derived from the major xanthophyll fucoxanthin and is considered a biomarker for diatoms, especially in the absence of haptophyte algae (Castaneda et al., 2009; Klok et al., 1984). Cholesterol is produced by eukaryotes such as phytoplankton or by heterotrophs, which modify ingested sterols (Martin-Creuzburg and von Elert, 2009; Volkman, 2003). Finally, phytol is derived from the omnipresent pigment chlorophyll-a responsible for photosynthesis and is thus found in all photoautotrophs (Mccarthy and Calvin, 1967). Thus, these biomarker lipids represent broad phytoplankton groups.

All three general phytoplankton biomarkers show a steady increase in δ^{13}C values over the transect from the CO$_2$ seep towards the control site (Fig. 3.3; Table S2). The exceptions are the more depleted δ^{13}C values at Site 2 and Site 9, where we observed
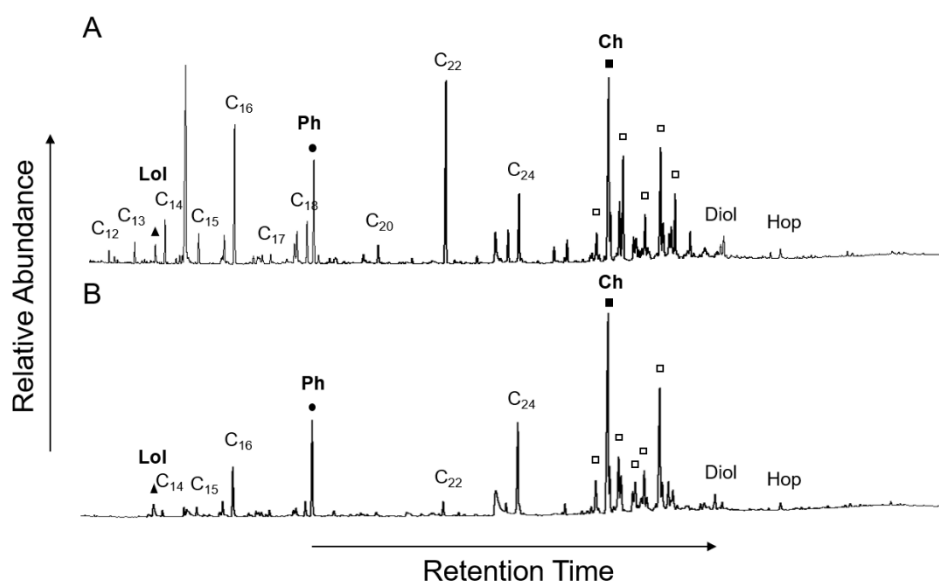
3

Fig. 3.2. Chromatogram of silylated polar fraction of extract of surface sediments with A) control site with ambient CO$_2$ concentrations and B) Site 5 near CO$_2$ vent. Major compounds are loliolide (Lol, closed triangle), phytol (Ph, closed circle), cholesterol (Ch, closed square), as well as fatty alcohols (chain-lengths shown), C$_{30}$ alkane-1,15-diol (Diol), C32-17β(H),21β-hopanol (Hop), and sterols (squares).
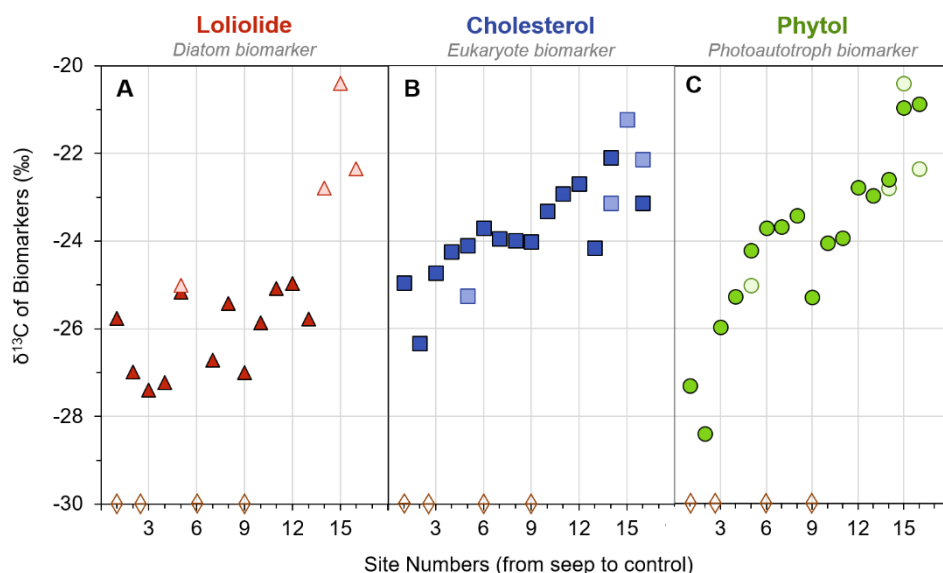
Fig. 3.3. The δ^{13}C of general phytoplankton biomarkers in surface sediments from Levante Bay, Italy. Loliolide (red triangle), cholesterol (blue square), and phytol (green circle) from CO_2 seep (Site 1) to control site (Site 16) sediment collected in May (light colors) and October (darker colors). Diamonds mark sites where there was minor additional bubbling of gas observed.

the δ^{13}C of loliolide ranges from -27.4‰ to -21.6‰ (Fig. 3.3A). From the seep to around Site 10, the δ^{13}C of loliolide fluctuates between ca. -27 and -25‰, followed by a prominent increase from ca. -25 to -22.5‰. For the sites sampled in both May and October, there appears to be consistency between the two seasons, i.e. in Site 5 (-25.2‰ for both seasons) and the control site (-22.3‰ in May and -22.6‰ in October), though Site 14 shows a spread of 2‰ between seasons. The δ^{13}C of cholesterol shows a smaller but more consistent shift over the transect, ranging from -26.3‰ to -21.2‰ with a 1‰ difference between the two seasons (Fig. 3.3B). Phytol shows the largest shift, ranging from -28.4‰ at the seep site to -20.4‰ at the control site (Fig. 3.3C). There is a relatively consistent increase in the δ^{13}C of phytol over the entire transect, except for a small decrease at Site 9, where we observed minor additional gas bubbling in the sediment. The δ^{13}C of phytol shows minor variation between seasons (ca. 0.5%), except for the control site which showed a difference of 1.4‰.

3.3 Discussion

All three general phytoplankton biomarkers become increasingly enriched in ^{13}C over the transect from high CO$_2$ near the seep to the control Mediterranean values. The observed isotopic depletion that occurs with increasing CO$_2$ concentrations matches theory (Farquhar et al., 1989; Farquhar et al., 1982; Hayes et al., 1990). Furthermore, this pattern closely follows the results observed at Shikine Island, i.e. a consistent depletion δ^{13}C of the same biomarkers with increasing proximity to the CO$_2$ seep (Witkowski et al., 2019). Given that CO$_2$ was the major variable over the transect in Italy, as well as Shikine Island, this strongly suggests that CO$_2$ concentrations indeed have a strong impact on isotopic fractionation of general phytoplankton biomarkers, suggesting their potential as a PCO$_2$ proxy.

A more detailed comparison showed a few differences in the magnitude and consistency in isotopic changes. In the Shikine Island study, loliolide showed the largest isotopic shift over the transect (-7.9‰) as compared with phytol (-5.2‰) and cholesterol (-5.2‰). However, in the Vulcano Island surface sediments, phytol had the most pronounced isotopic shift (-8.0‰) as compared with loliolide (-5.8‰) and cholesterol (-5.1‰). Furthermore, the changes in loliolide over the Vulcano Island transect are more variable compared with the consistent trends in isotopic values observed in phytol and cholesterol. Here, we will explore these differences.

The δ^{13}C profile of loliolide at Vulcano Island (Fig. 3.3A) has the least consistent trend among the three biomarkers, fluctuating between -27.4‰ and -25.0‰ from Site 1 (the seep) to Site 13, despite being the most species-specific compound, i.e. derived from diatoms. Light microscopy analysis of selected sediments across the transect showed that Site 2 contains nearly no diatom frustules, Site 5 had abundant centric diatoms as well as some pennate diatoms, while Site 9 had a great diversity especially among pennate diatoms though with relatively low overall abundance, and Site 13 and Site 16 (control site) had both high abundance and high diversity of both centric and pennate diatoms (Stoll H. and Mejía Ramírez L. M., personal communications). The different composition of diatoms at each site, in particular between centric and pennate diatoms, may explain why we observe a high δ^{13}C variability in loliolide. Different species may have slightly different isotopic fractionation due to e.g. different cell geometry and morphologies (Popp et al., 1998b) or different bicarbonate pumping strategies that has been observed in diatom species (Burkhardt et al., 2001; Pancost et al., 1997). This concept may be further supported by the stronger increase in δ^{13}C values observed between sites 13 and 16, where the higher diversity of species may yield a more robust overall δ^{13}C signal through

3

averaging biosynthetic differences among species. This complexity in the signal of loliolide may weaken the potential of this biomarker for past $P\text{CO}_2$ reconstructions.

The $\delta^{13}\text{C}$ profile of cholesterol (Fig. 3.3B) showed a more consistent decline over the transect than loliolide, though with a smaller difference in absolute values than phytol and loliolide from the seep towards the control. Because cholesterol is produced by all eukaryotes, terrestrial input, in addition to the algal input, can potentially dilute the autochthonous isotopic signal. However, the lack of terrestrial triterpenoids and long chain ($>\text{C}_{22}$) even carbon number fatty alcohols (Fig. 3.2) suggest minimal input of terrestrial biomarkers in the bay. Another explanation for the smaller isotopic change is that the cholesterol has contributions from heterotrophs, which produce cholesterol by modifying ingested phytoplanktonic sterols. Although this does not yield large isotopic fractionation (Grice et al., 1998), the zooplankton often have greater mobility than their photoautotroph counterparts; they may consume phytoplankton from various locations (and consequently various $\text{CO}_{2[aq]}$ concentrations) throughout the bay. This idea is supported by the notable $\delta^{13}\text{C}$ differences in cholesterol between the two seasons, where the offsets are not consistently in one direction. Based on these observations the $\delta^{13}\text{C}$ of cholesterol must be considered carefully when used in reconstructing past CO_2 concentrations.

The $\delta^{13}\text{C}$ profile of phytol had the most robust trend across the transect (Fig. 3.3C) with an $\delta^{13}\text{C}$ enrichment of ca. 8‰ from the seep to the control. Terrestrial input may affect the signal of phytol but, as discussed above, there is no evidence for this here. Based on these results, phytol shows the greatest sensitivity to the CO_2 gradient, and thus the most promise for reconstructing past $P\text{CO}_2$. The phytol results from Shikine, Japan (Witkowski et al., 2019) likewise show great promise for reconstructing past $P\text{CO}_2$.

To test the validity of using the $\delta^{13}\text{C}$ of the general biomarkers to estimate past $P\text{CO}_2$, we used phytol, the most promising of the various general phytoplankton biomarkers explored here with the most consistent trend and the strongest $\delta^{13}\text{C}$ shift over the gradient. We calculated the stable carbon isotopic photosynthetic fractionation (ε_p) using the $\delta^{13}\text{C}$ of phytoplankton biomass (δ_p) and the $\delta^{13}\text{C}$ of CO_2 (δ_d):

$$\varepsilon_p = 1000 \cdot [\ (\delta_d + 1000) / (\delta_p + 1000) - 1] \qquad\qquad [2]$$

The δ_p is calculated from the offset between phytol and biomass, which is 3.5‰ ± 1.3 standard deviation based on the average of twenty-three species grown in cultures (Witkowski et al., 2018). The δ_d is calculated from the $\delta^{13}\text{C}$ of DIC (0.7‰ ± 0.4‰ s.d.) correcting for temperature and pH (Table S1). The mean annual sea surface

temperature for Vulcano Island (20.2ºC ± 0.5°C s.d.; www.seatemperature.info) was used to calculate the temperature-dependent carbon isotopic fractionation of $CO_{2[aq]}$ with respect to HCO_3^- (Mook et al., 1974). The pH gradient, ranging from 5.5 pH near the vent to 8.2 pH in the control (Boatta et al., 2013), was used to define the relative contribution of different inorganic carbon species to the measured DIC (Madigan et al., 1989) (Table S1). Uncertainty was calculated using Monte Carlo simulations which consider the culmination of each individual parameter with its associated uncertainty, as described by Witkowski et al. (2018), here including δ^{13}C of phytol ± 0.5‰ s.d., offset between biomass and phytol ± 1.3‰ s.d., δ$_d$ ± 0.4‰ s.d., and T°C ± 0.5°C (Table S2).

Phytol-derived Ɛ$_p$ ranges from 22.2‰ to 8.2‰ ± 1.4‰ s.d. (Fig. 3.4A) and shows a consistent decline in fractionation from the seep towards the control site. This includes Site 2 where measured δ^{13}C values are higher than at Site 1, but Ɛ$_p$ now shows the expected trend of more fractionation closer to the vent. This is attributed to the strong shift in pH between these two sites (5.5 pH at the vent and 6.25 pH at Site 2 (Boatta et al., 2013)) which we have here corrected for. The highest Ɛ$_p$ value of 22.2‰ near the seep is approaching maximum isotopic fractionation due to CO_2-fixation (Ɛ$_f$), which has been shown to range between 25 and 28‰ in laboratory cultures (Goericke et al., 1994), but still does not quite reach full expression of Ɛ$_f$. This is somewhat unexpected given the constant bubbling of CO_2 at this site and thus very high CO_2 concentrations, i.e. up to ca. 3x modern $CO_{2[aq]}$ (Johnson et al., 2013).

Several possibilities may explain why the full expression of Ɛ$_f$ has not been reached. For one, given the relatively small area of the bay, it is possible that surface sediment has moved around the bay over time due to tidal actions and bottom water currents, which dampens the overall signal by allochthonous organic matter transported from area's outside of the bay, as also inferred for Shikine Island (Witkowski et al., 2019). Furthermore, algae do not likely grow and deposit in precisely same location and given that the impact of the CO_2 seep noticeably changes over tens of meters (Johnson et al., 2013), this likely leads to some mixed signal among sites, resulting in a suppressed signal. Another possibility for not reaching full expression of Ɛ$_f$ is the phytoplankton community composition, which could be affected by the species preference for carbon concentrating mechanisms (CCM) that actively pump bicarbonate into their cells, as opposed to our passive diffusion model. Cornwall et al. (2017) showed considerable changes in macroalgae species throughout Vulcano Bay in relation to pH as well as a change from species with low affinity CCM near the vent to species with high affinity CCM approaching the control (Cornwall et al., 2017). Thus, despite the high abundances of CO_2, algae do no reach maximum Ɛ$_f$ as

3

they still use some form of carbon concentration mechanisms, which utilizes ^{13}C-enriched bicarbonate. This may also be possible for the microalgae species which we here primarily explore. A final alternative is that the calculated ε_f of the phytoplankton community in Levante Bay may be lower than that inferred from the many culture studies (Hoins et al., 2016; Laws et al., 1997; Wilkes et al., 2017). Indeed, several recent studies show that ε_f of the different Rubisco types may be lower than previously assumed (Thomas et al., 2018).

In order to see how well ε_p of phytol can reconstruct $CO_{2[aq]}$, we estimated $CO_{2[aq]}$ and PCO_2 from the $\delta^{13}C$ of phytol using the equation adapted from the high plant model (Farquhar et al., 1982) for algae (Popp et al., 1989), and described in Eq. 1 (Bidigare et al., 1997), where b reflects species carbon demand per supply (Jasper et al., 1994) and ε_f reflects the maximum isotopic fractionation due to CO_2-fixation. The value of b is a complicated catchall for factors influencing isotopic fractionation such growth rate and cell-size (Popp et al., 1998a), light intensity and membrane leakiness (Hoins et al., 2016; Stoll et al., 2019), further complicated due to the multitude of sources for general phytoplankton biomarkers. Studies have suggested an empirical average 170‰ kg μM^{-1} ± 43 kg μM^{-1} s.d. for b based on a compilation of $\delta^{13}C$ values of bulk organic matter in marine surface sediments, as well as some limited phytol studies (Witkowski et al., 2019; Witkowski et al., 2018). Furthermore, we use an average ε_f for phytoplankton species of 26.5‰ ± 1.5‰ uniform distribution (Witkowski et al., 2018) based on the 25 to 28‰ range observed in laboratory cultures (Goericke and Fry, 1994). As described above, uncertainty was calculated using Monte Carlo simulations, considering each individual parameter with its associated uncertainty, as described by Witkowski et al. (2018). Here, we include the uncertainties associated with ε_p plus the new additional uncertainties associated with b ± 43 kg μM^{-1} s.d., ε_f ± 1.5‰ uniform distribution, T°C ± 0.5°C s.d., and sea surface salinity ± 1‰ s.d.

The resulting phytol-based $CO_{2[aq]}$ values range from 9.3 to 39.4 µM (Fig. 3.4B). The highest value of 39.2 µM (+20.6/-11.0 µM) is near the vent at Site 1, dropping to 23.7 µM (+7.1/-5.2 µM) at Site 2, then to 14.3 µM (+3.0/-2.7 µM) at Site 3, before gently declining to 9.6 µM (± 1.8 µM) at the control Site 16. If we calculate the PCO_2 from $CO_{2[aq]}$ using Henry's Law constant K_0, which considers salinity and temperature (Weiss, 1974), the resulting PCO_2 reconstruction range from 280 to 1182 µatm (Fig. 3.4C). The highest PCO_2 values were reconstructed for the sites closest to the seep, Site 1 at 1200 µatm (+636/-333 µatm) and Site 2 at 728 µatm (+222/-158 µatm), while the remainder of the transect showed fairly ambient values from Site 3 at 438 µatm (+95/-80 µatm) to the Site 16 control at 294 (+56/-50 µatm).
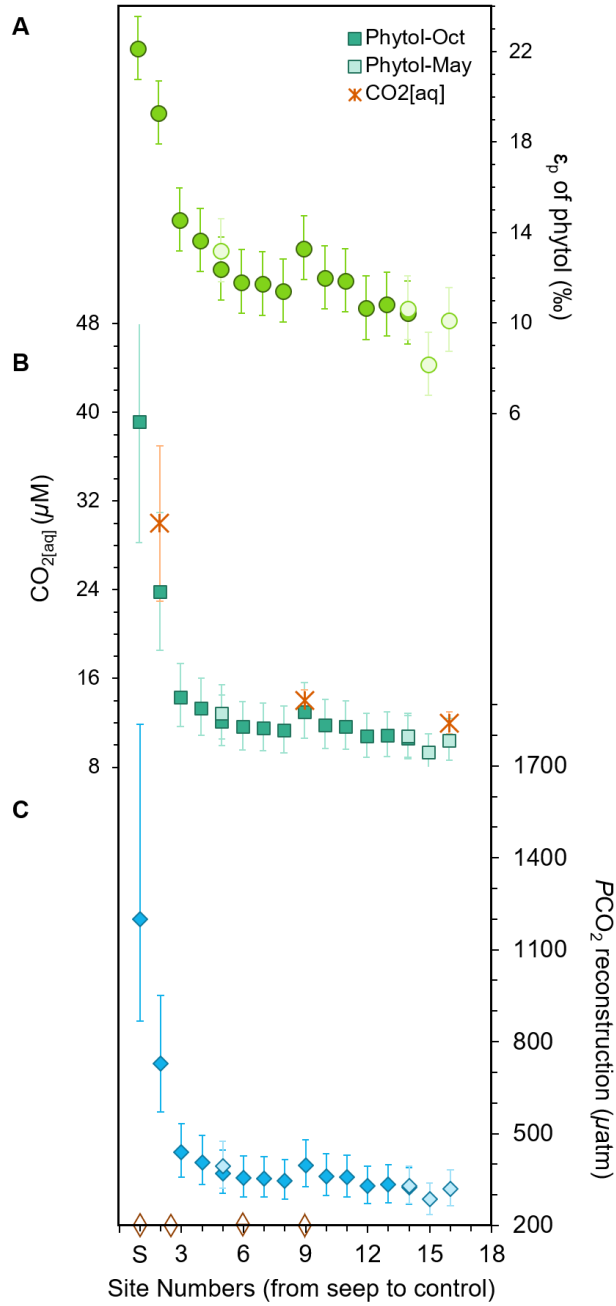
Fig. 3.4. ε_p, CO$_{2[aq]}$, and reconstructed PCO$_2$ from phytol in surface sediments. A) ε_p of phytol, B) CO$_{2[aq]}$ based on ε_p of phytol, and C) PCO$_2$ based on the δ^{13}C of phytol from surface sediments collected in May (light colors) and October (dark colors), ranging from Site 1 (S) to Site 16 (control). Stars indicated CO$_2$ concentrations (Johnson et al., 2011b). Open orange diamonds mark regions where there was minor additional bubbling of gas.

Comparison of $CO_{2[aq]}$ estimates with those reported for sites (Boatta et al., 2013) equivalent of our Site 2, 9, and 16 (30 μM ± 7, 14 μM ± 1, and 12 μM ± 1, respectively; Fig. 3.4B), show that these estimates agree within uncertainty, suggesting that our approach yields reasonable estimates. Only at the control site there is a slight underestimation of CO_2 concentrations. One possible explanation is an incorrect assumption for the b value. However, this seems unlikely given that (i) b values would need to be increased beyond any known b value thus observed to account for this underestimation, and (ii) this would lead to even higher past PCO_2 estimations which are based on b values compiled from laboratory cultures and natural experiments (Witkowski et al., 2018). A more likely explanation is the change in phytoplankton community over the bay, where the control community is dominated by high affinity CCM species as observed for macroalgae (Cornwall et al., 2017). Given that these species actively pump bicarbonate under low CO_2 conditions, this may explain the lessened ε_p, yielding lower CO_2 estimations. This effect has also been observed in the mesocosm experiments with different CO_2 concentrations (Benthien et al., 2007). Recent studies have shown lower sensitivity of ε_p to CO_2 in laboratory cultures and in glacial-interglacial reconstructions caused by the upregulation of phytoplankton CCMs (Badger et al., 2019; Stoll et al., 2019), which suggest using this ε_p based proxy with caution in reconstructing low-CO_2 worlds. In contrast, the proxy seems to do well in estimating PCO_2 concentrations similar to some of the higher concentrations that have been reconstructed over the past 455 Myr (Witkowski et al., 2018), suggesting it may be applicable for past greenhouse worlds.

3.4 Conclusion

We tested three general phytoplankton biomarkers in surface sediments in a transect from a naturally occurring CO_2 seep located in Levante bay, Vulcano Island, Italy, towards the open Tyrrhenian Sea. The $\delta^{13}C$ of the biomarkers showed a distinct increase with increasing distance from the CO_2 seep, in agreement with the idea that CO_2 concentrations have a strong control on isotopic fractionation. In particular, the $\delta^{13}C$ of phytol yielded a strong and consistent trend throughout the transect, and the agreement between estimated and measured CO_2 concentrations demonstrates the promise of this biomarker for paleo PCO_2 reconstructions. Our results show that CO_2 seep environments may prove a useful testing ground for new CO_2 proxies.

Acknowledgements

3

Supplementary Material

Table S1. The δ^{13}C of CO$_2$. All parameters used to calculate the δ^{13}C of CO$_2$ (represented in the equations as δ_d), including corrections for sea surface temperature and pH.

Table S2. Estimating PCO$_2$ from the δ^{13}C phytol. All parameters used to estimate PCO$_2$ starting from the raw δ^{13}C phytol, including estimations in uncertainty for each.

Chapter 4

Stable carbon isotopic fractionation
of algal biomarkers as a proxy for
PCO_2: Constraints from late Quaternary
sapropels in the Eastern Mediterranean

Caitlyn R Witkowski[1*], Marcel TJ van der Meer[1], Brian Blais[2,3], Rick Hennekam[4], Gert-Jan Reichart[4,5], Jaap S Sinninghe Damsté[1,5], Stefan Schouten[1,5]

[1] Department of Marine Microbiology and Biogeochemistry, Royal Netherlands Institute for Sea Research, and Utrecht University, The Netherlands
[2] Department of Science and Technology, Bryant University, USA
[3] Institute for Brain and Neural Systems, Brown University, USA
[4] Department of Ocean Systems, Royal Netherlands Institute for Sea Research, and Utrecht University, The Netherlands
[5] Department of Geosciences, Utrecht University, The Netherlands

Abstract

The concentration of atmospheric carbon dioxide (PCO_2), a predominant greenhouse gas, impacts climate. To understand the influence of PCO_2 on climate dynamics, past PCO_2 levels are estimated via indirect methods, i.e. proxies. Here, we explore the robustness of the PCO_2 proxy based on the stable carbon isotopic fractionation due to photosynthetic CO_2 fixation (ε_p) expressed in organic compounds produced by marine algae. We analyzed the stable carbon isotopic composition ($\delta^{13}C$) of the algal biomarker lipids phytol (derived from phytoplankton) and alkenones (from limited species of haptophytes) deposited during Quaternary sapropel formation (S1, S3, S4, and S5) in the Eastern Mediterranean. The resulting ε_p-based PCO_2 reconstructions are within error of PCO_2 directly measured in ice cores but consistently overestimate by ca. 100 μatm. This offset corresponds with atmospheric disequilibrium of present day $CO_{2[aq]}$ levels in the Mediterranean Sea, equivalent to a PCO_2 offset of ca. 100 μatm from global PCO_2, due to its relatively high alkalinity. Thus, average ε_p-based methods yield reasonable PCO_2 reconstructions. However, relative variability on individual reconstructed estimates are not correlated with the minimal changes observed in the PCO_2 from ice core records. This lack of correlation may be due to the higher variability of local changes in the Mediterranean versus the global average, or possibly due to biases in the proxy, e.g. variable growth rate or carbon concentrating mechanisms that may supplement CO_2 under low PCO_2 levels. These results suggest that application of ε_p for PCO_2 reconstructions may be best suitable for open ocean environments and for larger global changes in PCO_2.

4

4.1 Introduction

The atmospheric concentration of CO_2 (PCO_2, expressed in μatm) has a significant impact on earth system dynamics, including its climate-influencing role as a greenhouse gas. Assessing changes in PCO_2 over geological time scales may help us to better understand current and better predict near-future climate changes. Proxies, indirect methods for reconstructing past conditions, are often required to look beyond the scope of direct measurements and provide secular trends in PCO_2 (Beerling and Royer, 2011). Although there is continual improvement of these proxies (Hollis et al., 2019), their accuracy of remains largely uncertain and discrepancies increase with geologic time (Foster et al., 2017). Terrestrial proxies have been used to reconstruct PCO_2 over the past several hundred million years but often have unconstrained uncertainties, in part due to the different limitations of the proxies and the effects of local carbon cycling that can occur in heterogenous

terrestrial environments (e.g. Hollis et al., 2019). Marine proxies for PCO_2 reconstructions, on the other hand, often have more constrained and more continuous records, but do not span as far in time (Royer, 2014).

A promising marine proxy for reconstructing PCO_2 is the stable carbon isotopic fractionation associated with CO_2-fixation (ε_p), a concept based on the kinetic isotope fractionation that occurs as the CO_2-fixing enzyme Rubisco more rapidly incorporates ^{12}C over ^{13}C into photoautotrophic biomass when algae capture CO_2 for photosynthesis in their environment (Farquhar et al., 1989; Farquhar et al., 1982; Hayes et al., 1990; Popp et al., 1989). This results in a lower ^{13}C content ($\delta^{13}C$) of biomass than the inorganic carbon source fixed during photosynthesis. A positive relationship between PCO_2 and ε_p is often observed, where increasing availability of C leads to increasing fractionation (e.g. Popp et al., 1989; Jasper and Hayes, 1990; Freeman and Hayes, 1992).

Sedimentary bulk organic matter can be used to reconstruct past $\delta^{13}C$ of the algal biomass component (e.g. (Hayes et al., 1999), but often specific algal biomarkers have been the main target (e.g. (Jasper et al., 1994; Pagani, 2002). In the latter case, the $\delta^{13}C$ of each biomarker is corrected for its offset from the $\delta^{13}C$ of biomass (δ_p). δ_p can be used in combination with the $\delta^{13}C$ of dissolved CO_2 in the photic zone (δ_d) estimated via e.g. planktic foraminiferal carbonate, is then used to reconstruct ε_p via:

$$\varepsilon_p = 1000 \cdot [\ (\delta_d+1000) / (\delta_p+1000) - 1] \qquad [1]$$

The relationship between $CO_{2[aq]}$ and ε_p is complex and several models have been applied. The most commonly and simplified equation is based on theory first developed for higher plants (Farquhar et al., 1982), which has been subsequently modified for marine algae (Bidigare et al., 1997; Jasper and Hayes, 1990; Jasper et al., 1994; Popp et al., 1989) to be defined as:

$$PCO_2 = [b\ /\ (\varepsilon_f-\varepsilon_p)]\ /\ K_0 \qquad [2]$$

In this equation, the apparent observed fractionation ε_p is subtracted from the maximum fractionation for CO_2-fixation (ε_f) and related to CO_2 via the catch-all term b, a factor considering influence on fractionation other than CO_2 (Rau et al., 1997) such as e.g. cell geometry (Bolton et al., 2016; Popp et al., 1998b) and growth rate (Krumhardt et al., 2017; Laws et al., 1997). These combined parameters are related to dissolved CO_2, and K_0, representing Henry's Law constant, is then used to relate the concentration of dissolved CO_2 to atmospheric PCO_2 concentrations.

Most studies reconstructing PCO_2 from ε_p have used long-chain alkenones (Pagani, 2002; Zhang et al., 2013), biomarkers produced by a select group of Haptophytes. Due to the selectivity of the biomarkers, the difference between $\delta^{13}C$ of biomarker and $\delta^{13}C$ of biomass can be relatively well constrained based on lab cultures of specific alkenone-producing species (Riebesell et al., 2000). However, due to the fairly recent evolutionary history of alkenone producers, PCO_2 reconstructions are limited to last 45 Myr (Brassell, 2014). The evolutionary development of carbon concentrating mechanisms in alkenone-producers, which actively pump bicarbonate, may limit the use of this proxy during periods of low PCO_2 (Badger et al., 2019; Stoll et al., 2019). This proxy may be further complicated by the nature of the catch-all term b which may vary over time (Zhang et al., 2019), making it difficult to constrain this parameter, and thus PCO_2 reconstructions, over long timescales.

Thus, here the relatively novel application of ε_p to general phytoplankton biomarkers, compounds derived from a multitude of algal species, may have greater spatial and temporal ubiquity in the geologic record. There is minimal research on ε_p from general algal biomarkers, with the exception of some paleo-PCO_2 reconstructions from diagenetic products of chlorophyll, the vital pigment in all photoautotrophs, including the chlorophyll porphyrin head (Freeman and Hayes, 1992; Popp et al., 1989) and the diagenetic product of the chlorophyll phytol side-chain, phytane (Bice et al., 2006; Sinninghe Damsté et al., 2008; van Bentum et al., 2012). A recent reevaluation of phytane has shown the strength of this biomarker for reconstructing PCO_2, offering the longest marine-based PCO_2 record currently available (Witkowski et al., 2018), but this proxy has not been tested on shorter timescales with smaller variability in PCO_2 or compared with the more commonly applied alkenone-based proxy.

Here we compared phytol and alkenone-based PCO_2 reconstructions for the late Pleistocene to Holocene by analyzing organic matter-rich marls (known as sapropels S1, S3, S4, and S5) in the Mediterranean Sea, which were deposited during both glacial-inception (S3 and S4) and interglacial (S1 and S5) conditions. This allows for the ε_p-based PCO_2 reconstructions to be compared for time periods with minimal fluctuations, from the lower PCO_2 in the glacial-inception of ca. 226 μatm (ca. 84 ka for S3) and ca. 234 μatm (ca. 107 ka for S4) and for the slightly higher PCO_2 in the interglacial period of ca. 265 μatm (ca. 10 ka for S1) and ca. 271 μatm (ca. 124 ka for S5). The phytol- and alkenone-derived PCO_2 estimates here are compared with the direct PCO_2 measurements recorded in ice cores. The aim of this study is to shed light on the ability of these PCO_2 proxies to reconstruct PCO_2 in the late Pleistocene to Holocene.

4

4.2   Materials and Methods

A 920.5 cm long piston core (containing sapropels S3 to S5) and accompanying multi-core (containing sapropel S1) were collected at Station 1 (33°18.14898' N, 33°23.71998' E) in the southeast Levantine Sea during the January 2016 R/V Pelagia research cruise 64PE406. Sapropels and their preservation were assessed using Ti, Mn, Br, and Ba intensities derived from X-Ray Fluorescence core-scanning. The age model of the cores was derived by comparison of the Ba profile to sapropel boundaries (Grant et al., 2016), which have been linked to the ages of the well-dated Soreq cave record. The middle of these dark rich-organic layers, which were visually apparent, were measured and sampled.

Sediments were freeze-dried and then ground and homogenized using mortar and pestle. For sapropels S1, S3, and S4, lipids were extracted using a Dionex 250 accelerated solvent extractor at 100°C, 7.6×10^6 Pa using dichloromethane (DCM): methanol (MeOH; 9:1 v/v). For the sapropel S5, lipids were previously extracted using Bligh-Dyer extraction using MeOH: DCM: phosphate buffer (2:1:0.8, v/v/v) (Bale et al., 2015). All extracts were refluxed for 1 h with 1N of KOH in MeOH to hydrolyze the lipids and then neutralized to pH 5 with 2N of HCl in MeOH. Bi-distilled water (2 ml) and DCM (2 ml) were added (5x) to the hydrolyzed centrifuge tubes and the organic matter in the DCM layers were pooled and dried over Na_2SO_4. then eluted over an Al_2O_3 column into apolar (hexane: DCM, 9:1 v/v), ketone (DCM), and polar (DCM: MeOH, 1:1 v/v) fractions, respectively. The polar fractions were silylated with pyridine: N,O-Bis(trimethyl-silyl)trifluoroacetamide (BSTFA) (1:1 v/v) and heated for 1 h at 60°C.

Silylated polar fractions and ketone fractions were run on the gas chromatography-flame ionization detector (GC-FID), gas chromatography-mass spectrometry (GC-MS), and gas chromatography isotope-ratio mass spectrometry (GC-irMS). On the GC-FID, ketone fractions were run on a CP-Sil 5 column (50 m x 0.32 mm; df 0.12 μm) with a starting oven temperature of 70°C ramped to 200ºC at 20ºC/min and then to 320ºC at 3ºC/min for 25 min. The silylated polar fractions were run on a CP-Sil 5 column (25 m x 0.32 mm; df 0.12 μm) with a starting oven of 70ºC ramped to 130ºC at 20ºC/min and then to 320ºC at 4ºC/min for 10 min. Both fractions were run on GC-MS and irMS using the same column and oven ramping program as the GC-FID method used for the polar fractions. An in-house GC standard mix of *n*-alkanes and fatty acids were used for all three instruments to check GC performance. The performance of the GC-irMS was tested using additional standards of completely deuterated (99.1%) C_{20} (-32.7‰) and C_{24} (-27.0‰), which were co-injected with the

daily GC standard, as well as each sample, to check reproducibility of the carbon isotope values (within 0.5‰). The GC-irMS Isolink II combustion reactor was daily oxidized for 15 min, He backflushed for 10 min, and purged for 5 min. 2 min sequences were used for post-sample seed oxidation and 1 h oxidation sequences were used once week. Silylated phytol was corrected for three additional C in the trimethylsilyl group by using the known $\delta^{13}C$ value of BSTFA (-32.2‰).

4.3 Results and Discussion

4.3.1 Estimating PCO$_2$ from the $\delta^{13}C$ of phytol and alkenones

Multiple samples from each of the four sapropels (S1, S3, S4, and S5) all yielded enough material for carbon isotope analysis of phytol and alkenones. All were run in at least duplicate on the GC-irMS. Phytol yielded an overall range of $\delta^{13}C$ values from -22.3 to -27.7‰ (Fig. 4.1A; Table S1). The $\delta^{13}C$ of phytol ranged within sapropel S1 from -26.4 to -26.9‰, within S3 from -22.3 to -24.5‰, within S4 from -22.9 to -27.7‰ and within S5 from -23.5 to -25.0‰. $C_{37:3}$, $C_{37:2}$, $C_{38:3}$, and $C_{38:2}$ alkenones were detected in the ketone fractions and we report here the integrated isotope value of the $C_{37:3}$ and $C_{37:2}$ alkenones, which ranged overall from -24.5 to -27.0‰ (Fig. 4.1A; Table S1), a smaller range than observed for phytol. The $\delta^{13}C$ of alkenones ranged within sapropel S1 from -25.5 to -25.9‰, within S3 from -24.5 to -25.1‰, within S4 at -25.2 to -27.0‰, and within S5 from -24.8 to -26.2‰. The larger range in $\delta^{13}C$ of phytol is mainly due to the much larger variability observed in sapropel S4 compared to other sapropels; although not as extreme, there is also a larger range of values in S4 for the $\delta^{13}C$ of alkenones. The reason for this larger variability in S4 is unclear.

ε_p is calculated from the $\delta^{13}C$ of organic matter (δ_p) and the $\delta^{13}C$ value of dissolved CO$_2$ in the photic zone (δ_d) using Eq. 1. δ_p is calculated from the $\delta^{13}C$ value of each biomarker corrected for its offset from the $\delta^{13}C$ of biomass, which is the average offset of 3.5‰ ± 1.3 s.d. for phytol, based on twenty-three laboratory cultured species (Witkowski et al., 2018), and an average offset of 4.2‰ ± 0.9 s.d. for alkenones, based on the average of five laboratory culture species (Jasper and Hayes, 1990; Laws et al., 2001; Schouten et al., 1998; van Dongen et al., 2002) and commonly used in alkenone-based PCO$_2$ reconstructions (e.g. (Bijl et al., 2010; Pagani et al., 1999a; Pagani et al., 2005; Seki et al., 2010). The δ_d is derived from the high-resolution record of $\delta^{13}C$ of the surface-dwelling planktic foraminifera *Globigerinoides ruber* from the same core. When not precisely the same age, values

4

were interpolated. δ_d was corrected for temperature-dependent carbon isotopic fractionation of dissolved CO_2 with respect to HCO_3^- using the equation (Mook, 1974; Weiss, 1974):

$$\delta_d = \delta^{13}C_{carbonate} - 1 + (24.12 - 9866 / T^oK) \qquad [3]$$

For temperature, we used $U^{k'}_{37}$-based sea surface temperature (SST) estimates (Muller et al., 1998) derived from alkenones present in the same sapropel sediments (Table S2). The $U^{k'}_{37}$-based temperatures ranged from 17.7 to 23.5°C and are in agreement with those previously reported for sapropels (Emeis et al., 2003).

The culmination of each individual parameter with its associated uncertainty was calculated using Monte Carlo simulations, as described by Witkowski et al. (2018) and are expressed as 1 s.d. (68%; Table S1 and S2). The uncertainties included the $\delta^{13}C$ of the biomarkers (0.5‰), the $\delta^{13}C$ of the carbonates (0.1‰), SST (2°C), and the offset between the $\delta^{13}C$ of biomass from each biomarker (3.5‰ for phytol; 4.2‰ for alkenones), resulting in an uncertainty in ε_p values of ca. $\pm$ 1.4 ‰ for phytol and for alkenones. ε_p derived from phytol ranges from 9.0 to 15.0‰ over all sapropels (Fig. 4.1B; Table S1), ranging from 13.4 to 13.7‰ in S1, 9.0 to 11.5‰ in S3, 10.5 to 15.0‰ in S4, and 9.8 to 11.1‰ in S5. ε_p derived from alkenones ranges from 10.4 to 13.2‰ over all sapropels (Fig. 4.1B; Table S1), ranging from 11.3 to 12.4‰ in S1, 10.9 to 11.3‰ in S3, 12.2 to 13.2‰ in S4, and 10.4 to 11.6‰ in S5. We compare the individual ε_p values calculated from the $\delta^{13}C$ of phytol (derived from the whole phytoplankton community) and the individual ε_p values calculated from the $\delta^{13}C$ of alkenones (derived from specific producers) in the same sediments and thus time periods, along with associated error in uncertainty. There is a striking similarity between these two proxies, which yield statistically similar estimations (P-value = 0.005, Pearson's r-value = 0.645). This suggests that fractionation is similar between Haptophyte algae and other phytoplankton.

To reconstruct PCO$_2$ from ε_p, Eq. 2 was used. A b value of 168 ± 43 ‰ kg μM^{-1} has been used for phytol based on the $\delta^{13}C$ values of modern surface sediment organic matter and a study on phytol in the equatorial Pacific Ocean (Witkowski et al., 2018) as well as values of 170‰ kg μM^{-1} applied in previous studies that have estimated PCO$_2$ from phytol's diagenetic product phytane (Bice et al., 2006; Sinninghe Damsté et al., 2008; van Bentum et al., 2012; Witkowski et al., 2018). For alkenones, values used have ranged from ca. 55 to 400 with an average of 165 ± 53 ‰ kg μM^{-1} based on a compilation of modern alkenone-based environmental studies (Pagani, 2014). Given the similar values and large uncertainties in b-values for both phytol and C$_{37}$

alkenones, here we use $b = 170 \pm 50$ ‰ kg μM^{-1} for both. For ε_f, we use an average of 26.5‰ ($\pm$ 1.5‰ uniform uncertainty) for both phytol and alkenones to reflect the ε_f of 25-28‰ observed for laboratory cultures for a multitude of algal and cyanobacterial species (Goericke et al., 1994). Finally, K_0 is calculated from temperature and salinity (Weiss, 1974), in which SST is derived from the alkenone-based $U^{k'}_{37}$ temperature proxy measured in the same sapropel sample (Table S2), while sea surface salinity (SSS) is based on the average Mediterranean values for this region, i.e. ca. 39‰ (van der Meer et al., 2007). Regarding SSS, it has been shown that the onset of the period of sapropel deposition was associated with a large freshwater input from the North African continent, including the Nile (Lourens et al., 1996; Rohling and De Rijk, 1999) which has been shown to decrease SSS as low as 33‰ (van der Meer et al., 2007), suggesting SSS may have varied between 33 and 39‰. However, the impact of this salinity change is relatively minor on PCO$_2$ estimates (Fig. S1).

The resulting estimates for PCO$_2$ range from ca. 300 to 450 μatm for phytol and from ca. 330 to 390 μatm for alkenones for all sapropel time intervals (Fig. 4.1C; Table S1 and S2). Uncertainties in the estimates were calculated from Monte Carlo simulations, which consider the sum effect of each individual parameter on the final estimations for PCO$_2$ as described above. For individual sapropels (Fig. 4.1C), phytol-based PCO$_2$ estimates for S1 range from ca. 390 to 415 μatm with uncertainty estimations of ca. -90/+105 μatm, for S3 from ca. 300 to 330 μatm (ca. -65/+75 μatm s.d.), for S4 from ca. 325 to 450 μatm (uncertainty ca. -85/+100 μatm s.d.), and for S5 from 325 to 355 μatm (uncertainty ca. -70/+80 μatm s.d.). Alkenone-based PCO$_2$ estimates in S1 range from ca. 340 to 375 μatm (ca. -75/+85 μatm s.d.), in S3 from ca. 330 to 345 μatm (ca. -70/+80 μatm s.d.), in S4 from ca. 355 to 395 μatm (ca. -80/+95 μatm s.d.), and for S5 from 345 to 370 μatm (ca. -75/+85 μatm s.d.). When correlating individual data points at the same ages over the course of the record, phytol- and alkenone-based PCO$_2$ estimations are still statistically similar, though slightly less so after these calculations (now P-value = 0.020, Pearson's r-value = 0.559), but with similar uncertainties ($\pm$ 80 μatm) suggesting that these two biomarkers yield comparable estimates of past PCO$_2$.
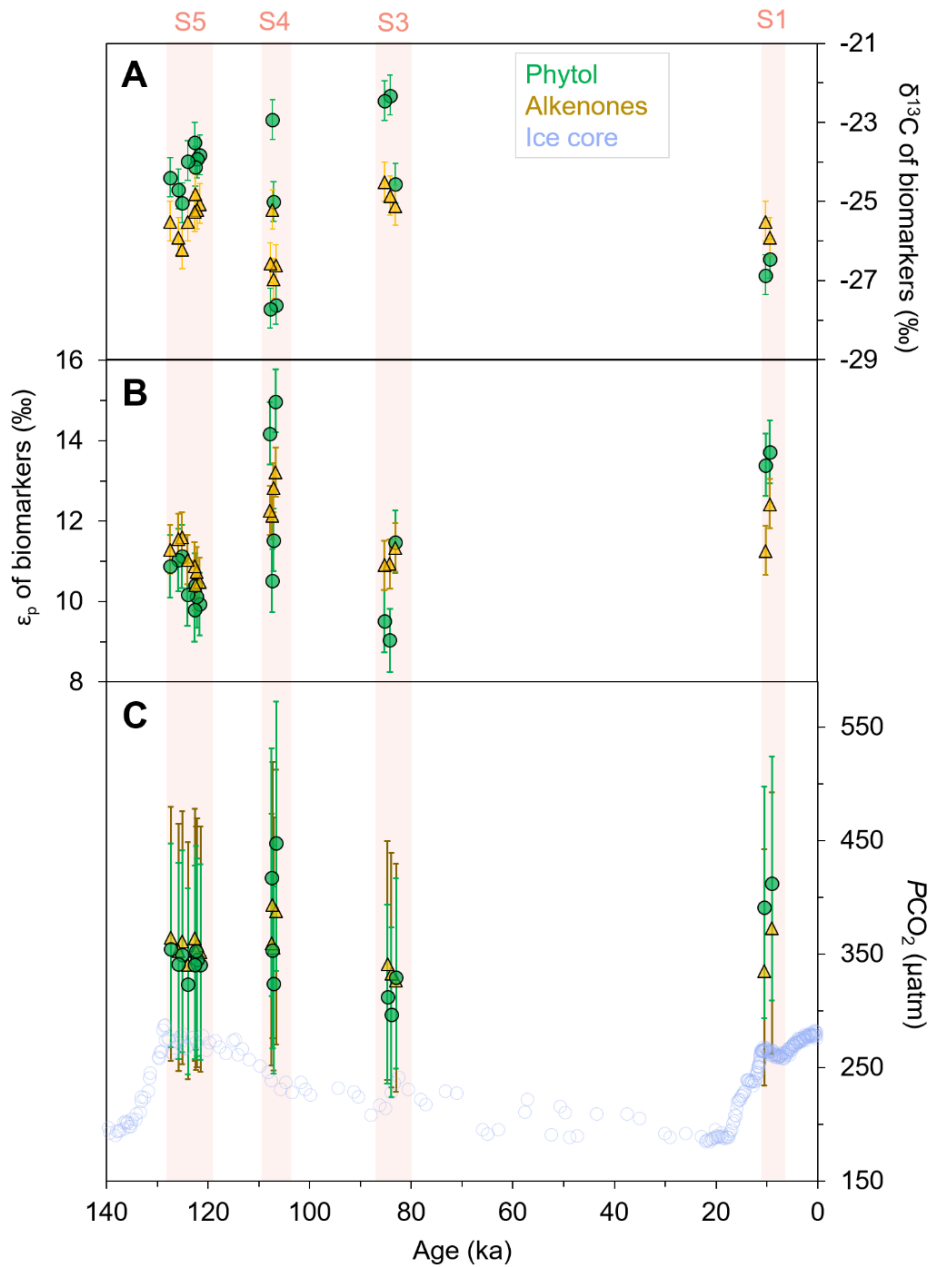
4

Fig. 4.1. *P*CO₂ estimated from the δ¹³C of algal biomarkers. A) $\delta^{13}C$ values, B) calculated ϵ_p, and C) estimated PCO₂ from the $\delta^{13}C$ of phytol (green circles) and alkenones (golden triangles) in four sapropels deposited over the past 140 ka. Sapropels are shown in light red bands. Open purple circles show direct *P*CO₂ measurements from ice cores (Monnin et al., 2001; Petit et al., 1999; Pepin et al., 2001; Raynaud et al., 2005).

4.3.2 Comparison of reconstructed $P\text{CO}_2$

Comparison with past global atmospheric $P\text{CO}_2$ recorded in ice core gas bubbles (Pepin et al., 2001; Petit et al., 1999; Raynaud, 2005) shows that our proxy estimations are within error of the ice core data but are offset by ca. 100 μatm (Fig. 4.1C; Fig. 4.2; Table S3). This offset may be due to the disequilibrium of the Mediterranean Sea with atmospheric $P\text{CO}_2$ due to the relatively high alkalinity in the Mediterranean Sea (Rivaro et al., 2010) which has been observed to have the equivalent $\text{CO}_{2[\text{aq}]}$ of ca. 100 μatm above the global average of $P\text{CO}_2$ (Bégovic and Copin-Montégut, 2002). Given this disequilibrium, the average values for the ice core $P\text{CO}_2$ and the average values for the ε_p-based $P\text{CO}_2$ are very similar, as seen by the ice core data (blue circles) and the ice core data plus the proposed 100 μatm offset (open circles) in Fig. 4.2, which overlaps with the reconstructed values shown here. Given this offset, both proxies based on ε_p (phytol as a general biomarker and the more commonly used alkenones as a species-specific biomarker), seem to yield reasonable $P\text{CO}_2$ estimations in the late Pleistocene to Holocene.

A detailed examination shows that the individual $P\text{CO}_2$ estimations based on alkenone- and phytol-derived ε_p do not covary with the individual ice core $P\text{CO}_2$ data (for phytol: P-value = 0.780, Pearson's r-value = 0.073; for alkenones: P-value = 0.784, Pearson's r-value = 0.072). There are several explanations for the lack of correlation between the individual data over the span of the record between our reconstructed Mediterranean Sea values with that of the ice core, likely either from local influences or from the mechanics of the proxy.

Firstly, local variability may differ from the global homogenized average seen in the ice core data. The different parameters used these equations, each with their own uncertainties, may lead to the deviations in the $P\text{CO}_2$ proxy reconstructions from the variability in the ice core $P\text{CO}_2$ during these time windows, as the range in ice core $P\text{CO}_2$ is small (from 1.4 to 11.2 μatm) relative to the calculated uncertainties. For example, dissolved CO_2 concentrations are more likely to vary locally over time as compared with the global atmospheric $P\text{CO}_2$, especially in a semi-enclosed Mediterranean Sea. This is supported by the notably high variability within S4, clearly seen in the larger error bars for this sapropel in Fig. 4.2, where the standard deviation for the individual $P\text{CO}_2$ estimations are 56.8 μatm. When this S4 data is removed from the overall dataset, an improved correlation between the biomarker $P\text{CO}_2$ reconstructions with the ice core data can already be seen (for phytol: P-value = 0.075, Pearson's r-value = 0.509; for alkenones: P-value = 0.028, Pearson's r-value = 0.606). These local offsets may be caused by different factors that may
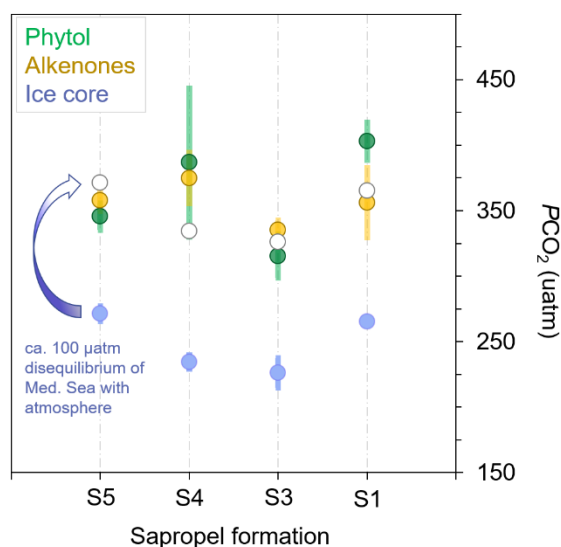
4

Fig. 4.2. PCO_2 averages for ice core and biomarker estimations. Averaged for the time period of each individual sapropel, estimates for PCO_2 from phytol (green circles) and alkenones (golden triangles) with standard deviations showing variability of estimations within each sapropel. Direct PCO_2 measurements from ice cores (purple; Monnin et al., 2001; Petit et al., 1999; Pepin et al., 2001; Raynaud et al., 2005) and offset of 100 µatm (open circle) to account for the disequilibrium of the Mediterranean Sea with the global average of PCO_2 (Bégovic and Copin-Montégut, 2002).

influence $CO_{2[aq]}$ in the Mediterranean Sea, such as the cyclic influence of freshwater input from the Nile that may change alkalinity, temperature, nutrient availability, and other seawater components. Local changes could affect the $\delta^{13}C$ of the CO_2 via periodic deep-water convection (Melki et al., 2010), causing the mixing of ^{13}C-depleted CO_2 from below the chemocline (Küspert, 1982) in the otherwise-stratified Mediterranean water column during sapropel formation. This effect on the $\delta^{13}C$ of CO_2 used by phytoplankton is not observed in the planktic foraminifera signal (Table S2). However, in contrast to shallow water dwelling foraminifera, OM production may also have taken place in deeper waters of the photic zone, i.e. in the deep chlorophyll maximum (Rohling and Gieskes, 1989). Given the common presence of isorenieratene or its diagenetic products in sapropels, anoxic conditions prevailed at the base of the photic zone (Menzel et al., 2002; Passier et al., 1999) and the steep heterogeneous isotopic composition throughout the water column may have occurred in a shallow oxycline (van Breugel et al., 2006).

Secondly, potential issues may arise from the proxy itself, especially with 1) the catch-all term b and/or 2) the possibility of carbon concentrating mechanisms. 1) The b value is derived in Eq. 2 based on parameter-by-parameter uncertainty analysis which uses the global average of 170 ± 50 ‰ kg μM^{-1} for all phytoplankton (Witkowski et al., 2018), a reasonable approach when the lack of data for the accurate estimation of b in paleoreconstructions, but nonetheless making this an intrinsically difficult parameter to estimate. During these unusual sapropel-forming events, b could be affected by enhanced productivity as a result of the freshwater input of the Nile River coupled with enhanced upward advection of nutrients to the base of the photic zone, fueling a productive deep chlorophyll maximum or a starved surface layer (Grelaud et al., 2012). As the b factor has been shown to be a mutable variable (Zhang et al., 2019), any major changes to the b value during sapropel deposition or among the four different sapropels may explain the lack of correlation with the ice core data. 2) Carbon concentrating mechanisms (CCMs), in which algae may actively pump bicarbonate into their cells under low PCO$_2$ conditions, may be a concern, as these mechanisms have been observed in many phytoplankton (Giordano et al., 2005). Here, we use a diffusive model (Eq. 1, Eq. 2) based on the assumption that dissolved CO$_{2[aq]}$ passively enters the algal cell, a concept upheld in laboratory cultures where CO$_2$ availability is high relative to cellular carbon demand (e.g. (Francois et al., 1993; Rau et al., 1996). However, cell membrane permeability is variable (e.g. (Cassar et al., 2006; Hopkinson et al., 2011) in order to supplementary CO$_2$ (via HCO$_3^-$ transport) via CCMs at the active site of Rubisco under insufficient levels of CO$_2$ (Kottmeier et al., 2016; Raven and Beardall, 2014). Active uptake is a concern given the substantial δ^{13}C difference between bicarbonate (0‰) and CO$_2$ (−8‰) (Mook, 1974), as well as very few experimental data to explain the effect of CCMs on the δ^{13}C of algae. Based on the results of a statistical multilinear regression model that quantitatively considering factors that influence ϵ_p in cultures using alkenone-producing algae, it has been suggested that there is lower sensitivity of ϵ_p to PCO$_2$ than proposed by the diffusive model (Stoll et al., 2019). Indeed, at Ocean Drilling Program Site 999 in the Caribbean, CCMs have been invoked to explain the muted response observed of the δ^{13}C of alkenones-reconstructed PCO$_2$ as compared with the δ^{11}B of foraminifer shell-reconstructed PCO$_2$, as well ice core PCO$_2$ data (Badger et al., 2019). This recent literature suggests that ϵ_p from alkenones may have a lessened relationship with PCO$_2$ as many algal species actively acquire CO$_2$ from other sources than diffusive uptake. However, here, we observe greater variability in PCO$_2$ estimations based on alkenone- and phytol-derived ϵ_p than the ice core PCO$_2$, which may suggest that one of the other aforementioned factors are instead at play.

4

4.4   Conclusion

The $\delta^{13}C$ of phytol and alkenones from Quaternary Mediterranean Sea sapropels were used to calculate photosynthetic isotopic fractionation (ε_p) and estimate PCO_2. Phytol- and alkenone-based PCO_2 yielded similar estimations, i.e. 300 to 450 µatm for phytol and ca. 330 to 390 µatm for alkenones. These values overestimate global atmospheric PCO_2 by ca. 100 μatm, which fits the enhanced dissolved CO_2 concentrations in the Mediterranean Sea due to its high alkalinity. Thus, given this consideration, the ε_p proxy for reconstructing PCO_2 seems to reflect CO_2 concentrations during Quaternary sapropel formation in the Mediterranean. Although these results are favorable, there is a lack of correlation between changes in the individual reconstructed PCO_2 values from the two biomarkers and those individual PCO_2 values from ice core, most notably in S4. Importantly, the calculated uncertainties for the phytol- and alkenone-based PCO_2 are much larger than the range observed in the ice core PCO_2 values, which largely explains this lack of covariation. This lack of correlation is likely due to local variability in the semi-enclosed Mediterranean, particularly influencing dissolved CO_2, and thus suggesting that open marine settings with more homogenized and stable conditions may be more suitable for ε_p-based PCO_2 reconstructions. Alternatively, there may be proxy limitations, such as variable growth-rates (b) and the operation of carbon concentration mechanisms. Nevertheless, our results show that ε_p-based PCO_2 estimates derived from general algal biomarkers may be as useful as those of alkenones and provide equally reasonable estimates.

Acknowledgements

4

Supplement

Table S1. All data and uncertainties used to estimate $P\mathrm{CO_2}$ from the $\delta^{13}\mathrm{C}$ of phytol and of alkenones.

Table S2. Peak abundances and equations used to calculate Uk'37-based sea surface temperatures.

Table S3. Composite of $P\mathrm{CO_2}$ in ice cores used for comparison in this study.
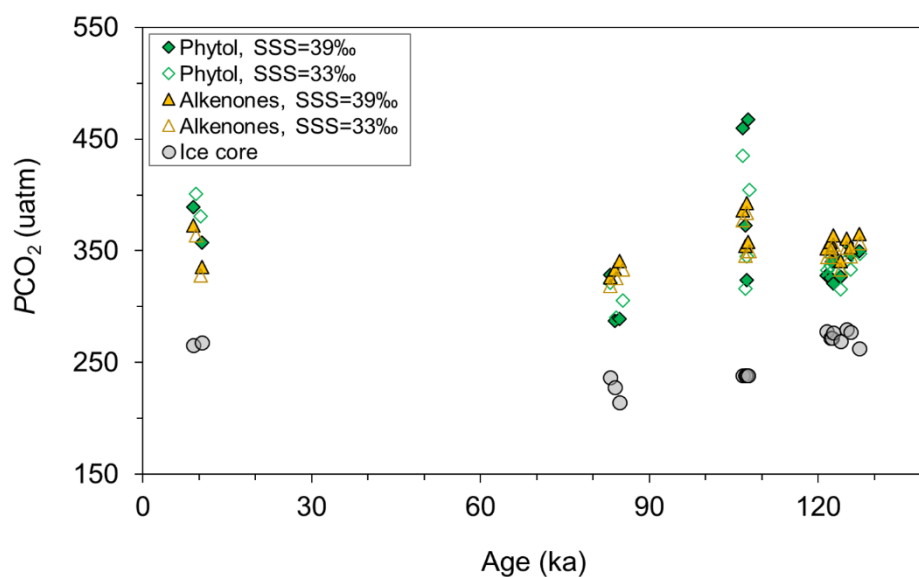
Fig. S1. Effect of salinity changes on reconstructed PCO$_2$ from algal biomarkers. Estimated values for PCO$_2$ based on different sea surface salinity of 39 (closed symbols) and 33 (open symbols) for algal biomarkers phytol (diamonds) and alkenones (triangles) over the past 140 ka. Direct PCO$_2$ measurements from ice cores (gray circles).

4

Chapter 5

Decline of PCO_2 from the Miocene based on the stable carbon isotopic composition of algal biomarkers

Caitlyn R Witkowski[1], Marcel TJ van der Meer[1], Jaap S Sinninghe Damsté[1,2],
Stefan Schouten[1,2]

[1] Department of Marine Microbiology and Biogeochemistry, Royal Netherlands Institute
for Sea Research, and Utrecht University, The Netherlands
[2] Department of Geosciences, Utrecht University, The Netherlands

Abstract

The concentration of atmospheric carbon dioxide (PCO$_2$) has risen to unprecedented rates within the past two centuries along with rising global temperatures. Past analogues of likely near-future climate conditions may help us better understand these changes, such as the relatively warmer Middle Miocene Climatic Optimum between 17 and 15 Ma. Although temperatures are well-constrained during this time, the evolution of Middle Miocene PCO$_2$ remains highly uncertain; different proxies yield different trends and values. In order to reconstruct PCO$_2$, we used the stable carbon isotopic composition of several algal biomarkers, i.e. steranes, phytane, and C_{37} alkenones, from sediments off the coast of California covering the past 16.4 Ma. The sterane- and phytane-based reconstructions show PCO$_2$ starting at ca. 500-580 μatm from 16.4 Ma and steadily declining to ca. 300 μatm by 0.1 Ma. The alkenone-based PCO$_2$ record is limited in this sedimentary sequence, covering only the final 4 Ma, but has remarkably similar PCO$_2$ estimations as the general phytoplankton biomarkers. The steadily declining trend in PCO$_2$ shown here mirror global temperature reconstructions, suggesting that PCO$_2$ and temperature were coupled during this time period.

5.1 Introduction

Greenhouse gas abundances are crucial in identifying climate sensitivities and potential tipping points (Lenton et al., 2008). The atmospheric concentration of carbon dioxide (expressed in partial pressure, PCO$_2$) has risen to 400 μatm over the past 170 years (Petit et al., 1999), nearly twice that observed in ice core records over the past one million years (Lüthi et al., 2008). Because the speed of these changes is unprecedented, reconstructions of past PCO$_2$ are attempted to gain critical context for understanding current environmental changes and for modeling future climate trends.

As a base of comparison for our prospective changing planet, the most recent greenhouse earth was the Miocene from ca. 23 to 5.3 million years ago (Ma), marked by relatively high global temperatures that steadily declined towards today (Zachos et al., 2008). In particular, the Middle Miocene Climatic Optimum (MMCO) from 17 to 15 Ma may be a close analogue for our near-future climate (You et al., 2009). As compared with today's global annual temperatures of 14.5°C (Hansen et al., 2010), this period experienced that of approximately 18.4°C (You et al., 2009) with mid-latitude estimates around 20.5°C (Flower and Kennett, 1993), suggesting a

smaller equator-to-pole temperature gradient than present day. In order to sustain these high temperatures, coupled models suggest that PCO_2 may have been between 460-580 μatm (You et al., 2009), concentrations that will be rapidly approached within decades.

However, proxy records for the MMCO show great discrepancies with the model values. Reconstructions using the $\delta^{13}C$ of pedogenic minerals, based on the difference between the $\delta^{13}C$ of calcium carbonate and organic matter preserved in paleosols, suggest a higher PCO_2 than these model estimations, suggesting PCO_2 of 700 μatm (Cerling, 1991) or possibly as high as 850 μatm (Retallack, 2009). PCO_2 estimates from stomatal indices, based on the negative relationship between the density of leaf stomata with PCO_2, are in better agreement with the model estimates and suggest between 400-500 μatm for the MMCO (Kurschner et al., 2008). Contrary, some proxies show considerably lower PCO_2 values. For example, the $\delta^{13}C$ of alkenones, based on the positive relationship between carbon isotopic fractionation during CO_2-fixation in alkenone-producing Haptophytes with PCO_2, suggest MMCO PCO_2 values ranging from 180-290 μatm (Pagani et al., 1999b, 2000; Pagani et al., 2005). Likewise, the $\delta^{11}B$ of marine carbonates, based on the boron isotopic fractionation between boric acid and borate with pH, reconstruct values between 140-300 μatm (Pearson and Palmer, 2000).

However, these latter two proxies have recently been reevaluated. Alkenone-producing Haptophytes may implement active uptake of bicarbonate based on their cell-size and on CO_2 availability (Bolton et al., 2016; Henderiks and Pagani, 2007), a concern when calculating isotopic fractionation given the considerable $\delta^{13}C$ difference between bicarbonate at ca. 0‰ and CO_2 at ca. -8‰ (Mook, 1974). These considerations may bring these estimations for PCO_2 up to 400 μatm (Zhang et al., 2013) or reach as high as 1500 μatm (Bolton et al., 2016; Stoll et al., 2019) in the MMCO. The $\delta^{11}B$ method based on foraminifera must consider the size of the measured specimen (Honisch and Hemming, 2004; Ni et al., 2007), and if done, result in an average PCO_2 estimate of 400 μatm for the MMCO (Foster et al., 2012). Furthermore, in a recent recalculation of $\delta^{11}B$-based reconstructions using a revised total alkalinity record has even suggested estimates similar to model of ca. 500-650 μatm (Sosdian et al., 2018; Boudreau et al., 2019). Despite this progress in understanding proxy mechanisms, the absolute PCO_2 for understanding climate sensitivity over this period nevertheless remains unclear and large gaps in the PCO_2 record make it difficult to constrain climate sensitivity.

Here we reconstruct the *P*CO$_2$ record from the MMCO towards present day using a different approach to the proxy using the stable carbon isotopic fractionation that occurs during photosynthetic fixation of CO$_2$ into biomass (ε$_p$). ε$_p$ occurs when the ^{12}C-preferring Rubisco enzyme in photoautotrophs becomes increasingly isotopically lighter with increasing *P*CO$_2$ (Farquhar et al., 1989; Hayes et al., 1990; Popp et al., 1989). In paleoreconstructions, ε$_p$ (and consequently *P*CO$_2$) can be calculated using the δ^{13}C of organic matter corrected for the δ^{13}C of CO$_2$. Nearly all studies have used the δ^{13}C of the select Haptophyte-produced alkenone compounds as the organic matter, but here we suggest expanding the source to the δ^{13}C of general phytoplankton biomarkers. General phytoplanktonic biomarkers, compounds produced by a large number of species, have the additional benefit of greater spatial and temporal distribution throughout the record (Freeman and Hayes, 1992; Popp et al., 1989; Witkowski et al., 2018) and the potential to curb species-specific concerns and environmental effects by averaging the whole phytoplankton community.

Here, we use 5α-cholestane, 24-ethyl-5α-cholestane, 24-methyl-5α-cholestane, and phytane in sediments off the coast of California during the Deep Sea Drilling Project (Site 467). We explore the record from the mid-Miocene towards the present (16.4 to 0.1 Ma), with an emphasis on the MMCO. Using ε$_p$ derived from these biomarkers, we estimate *P*CO$_2$ for the Miocene and compare these with the more traditionally used alkenone proxy estimations. *P*CO$_2$ estimated from the general phytoplanktonic biomarkers are compared with other proxy estimations during this time interval, as well as with temperature reconstructions.

5

5.2   Materials and Methods

5.2.1   DSDP Site 467

Site 467 (33º50.97'N, 120º45.47'W) was collected by Deep Sea Drilling Project Leg 63 at the San Miguel Gap off the coast of California, USA. The present-day oceanic regime of this region comprises of the California Current, a part of the North Pacific subtropical gyre which carries cold, fresher surface water from the North Pacific into the warmer, more saline surface water of the subtropical regions (Lyle et al., 2000). Over long timescale, orbital forces impact the latitudinal changes, strength, and mean transport of the California Current flow.

The sediment core spans the Quaternary through lower mid-Miocene. The core has the best preserved organic matter of Leg 63 (Elrod and Katz, 1982), likely due to incorporation of abiotic sulfur species into labile functionalized lipids, a process

which occurs rapidly during very early diagenesis (Damste et al., 1988; Kohnen et al., 1993). The most complete core of this leg, there are two small hiatuses based on the microfossils, ca. 600 ka in the early Quaternary and ca. 1 Ma in the Pliocene. The age model is based off diatom, coccolith, and radiolarian events (Initial Reports of the Deep Sea Drilling Project, Volume 63). For more details on the drilling site, we refer to the initial cruise report (Initial Reports of the Deep Sea Drilling Project, Volume 63).

5.2.2 Analytical Methodology

Thirty-five marine sediments, depths ranging from 9 to 1038 mbsf, were sampled approximately every 30 m from the Site 467 core (Dataset S1). 15-20 g of pulverized sediments were extracted on a Dionex 250 accelerated solvent extractor (ASE) at 100°C, 7.6×10^6 Pa, using dichloromethane (DCM): MeOH (9:1 v/v) and the extracts were dried over Na_2SO_4. The extracts were eluted over an alumina packed column and separated into an apolar (hexane: DCM, 9:1 v/v), ketone (DCM), and a polar fraction (DCM: MeOH, 1:1 v/v). Polar fractions were desulfurized using Raney-nickel, eluted over an alumina packed column into an apolar fraction (hexane: DCM, 9:1 v/v) and hydrogenated using acetic acid and platinum oxide (Damste and Leeuw, 1990; Damste et al., 1988). These were left over night and then cleaned over a small column of magnesium sulfate and sodium carbonate with DCM. To obtain baseline separation of the targeted biomarkers, *n*-alkanes were removed using vacuum-oven prepped 5Å molecular sieve added to the samples, dissolved in cyclohexane, and left overnight; the supernatant was then removed and analyzed.

An Agilent 7890A gas chromatograph-mass spectrometer (GC-MS) was used to identify compounds in the resulting apolar fraction from the desulfurized polar fraction, as well as the ketone fractions. An Agilent 7890B GC with flame ion detector (FID) was used to determine compound quantities prior to injection on a Thermo Trace 1310 GC-isotope ratio mass spectrometer (IRMS). GC-MS, GC-FID, and GC-IRMS measurements were conducted on a CP-Sil 5 column (25 m x 0.32 mm; d_f 0.12 μm). GC-MS and GC-FID used constant pressure and IRMS used constant flow of He carrier gas. All three instruments used the same GC program with starting oven temperatures of 70ºC ramped at 20ºC/min to 130ºC and then ramped at 4ºC/min to 320ºC for 10 min. For IRMS measurements, a standard with per-deuterated n-alkanes (C_{20} and C_{24}) with known isotopic values (-32.7 and -27.0‰, respectively) was run at the start of each day and then co-injected with samples to monitor the integrity of the instrument (within 0.5 ‰). At the start of each

day, the IRMS underwent an oxidation sequence for 10 min, He backflush after oxidation for 5 min, and purge conditioning line for 5 min; a shorter version of this sequence is conducted in a post-sample seed oxidation, which includes 2 min oxidation, 2 min He backflush, and 2 min purge conditioning line.

5.3 Results

Because the organic matter from DSDP Site 467 is organic sulfur rich (Katz and Elrod, 1983), the polar fractions were desulfurized to release apolar biomarkers bound by sulfur. These organic sulfur compounds (OSC) are formed by the reaction of labile functionalized lipids with abiotic sulfur species during very early stages of diagenesis (Sinninghe Damsté *et al.*, 1989a; Kohnen *et al.*, 1990a). OSC are particularly attractive for paleoreconstructions because the sulfur-incorporation preserves the original biological carbon skeleton and offers greater stability against mineralization and (bio)transformation (Kohnen et al., 1990; Schouten et al., 1997; Sinninghe Damsté et al., 1998a). The desulfurized polar fractions yielded the apolar biomarkers: pristane, phytane, C$_{25}$ highly branched isoprenoids, tricyclicterpanes, steranes, perhydro β carotene, and hopanes. In particular, 5α-cholestane, 24-methyl-5α-cholestane, 24-ethyl-5α-cholestane, 22R-17β,21β(H)-pentakishomohopane (C$_{35}$ hopane), phytane, and the C$_{25}$ highly branched isoprenoid were most abundant. Alkenones were only detected in the ketone fraction for the shallowest part of the core, covering the last 4 Ma, and consisted of C$_{37:3}$, C$_{37:2}$, C$_{38:3}$, and C$_{38:2}$ alkenones.

Because C$_{37:3}$ and C$_{37:2}$ did not always have a clear baseline separation for isotope analysis, we integrated these as one peak throughout the record. Isotopic analysis shows a wide variety of compositions of these biomarkers (Fig. 5.1A, Dataset S1). The different steranes share a similar overall trend throughout the record, though with a relatively consistent isotopic offset: 5α-cholestane ranges from -27.6 to -23.3‰, 24-ethyl-5α-cholestane from -28.5 to -23.8‰, and 24-methyl-5α-cholestane from -28.7 to -24.8‰. C$_{35}$ hopane ranges from -26.4 to -23.1‰. Phytane has the smallest variance over the core, ranging from -26.8 to -23.7‰, while the C$_{25}$ HBIs show variations in δ^{13}C values, which are more extreme than the other compounds, ranging from -34.1 to -21.5‰.
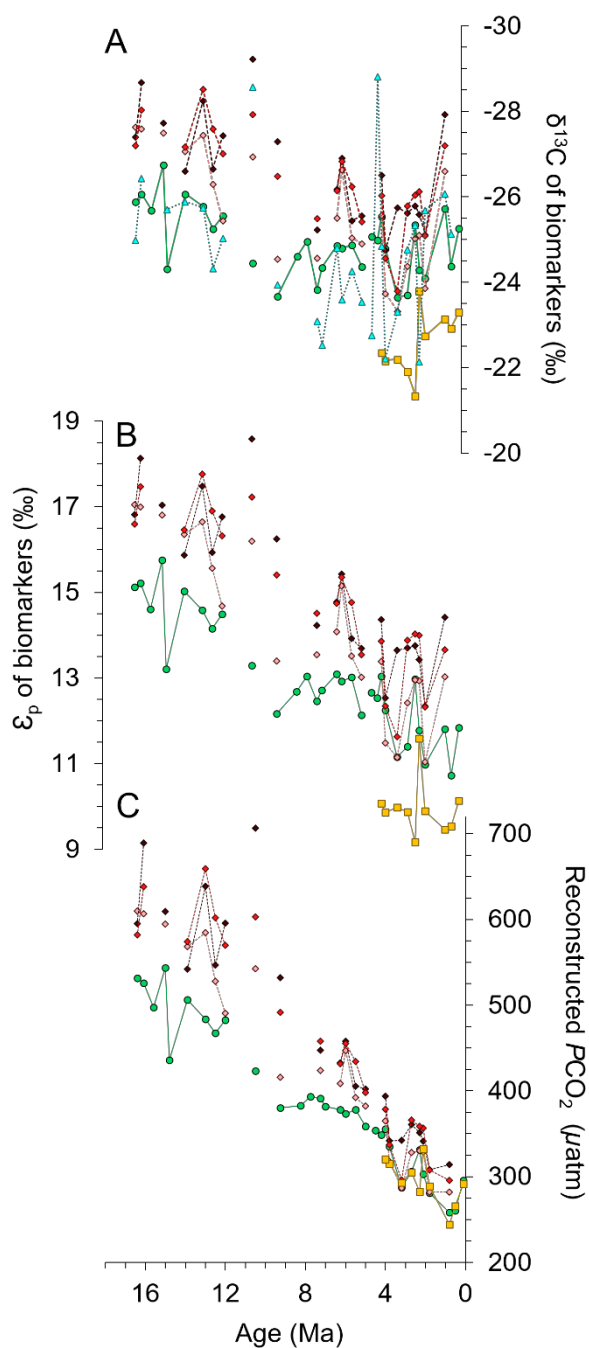
Fig. 5.1. Proxy records from at DSDP Site 467 (A) $\delta^{13}C$, (B) ϵ_p, and (C) PCO_2 derived from biomarkers: phytane (green circle), 5α-cholestane (light diamond), 24-methyl-5α-cholestane (dark diamond), 24-ethyl-5α-cholestane (red diamond), C_{35} hopane (cyan triangle), and C_{37} alkenones (yellow square).

5.4   Discussion

5.4.1   Sources of biomarkers

The δ^{13}C of the biomarkers show similar trends throughout the record with the exception of the large variances in isotopic signature observed in the C$_{25}$ HBI (ranging from -34.1 to -21.5‰). The similar trends for the three major steranes (5α-cholestane, 24-methyl-5α-cholestane, 24-ethyl-5α-cholestane), are supported by Pearson correlation (Fig. S1), showing strong *r* values ranging between 0.80 to 0.91 for the three steranes. The δ^{13}C of steranes also correlate significantly with that of phytane ($r = 0.52$ to 0.79; $p < 0.05$) and of the C$_{35}$ hopane ($r = 0.60$ to 0.64; at least $p < 0.05$). Similarly, the δ^{13}C of phytane and the C$_{35}$ hopane significantly correlate ($r = 0.76$; $p < 0.0001$). In contrast, the δ^{13}C of the C$_{25}$ HBI alkane shows no significant correlation with the δ^{13}C of other biomarkers. The δ^{13}C of alkenones also has no significant correlation with the δ^{13}C of any of the other biomarkers.

The strong correlation among the general phytoplankton biomarkers suggests that they may have a similar source, either from the same microbes or from different microbes with similar physiology and/or habitat. S-bound cholestane is an early diagenetic product of cholesterol (Kok et al., 2000), a sterol that all eukaryotes synthesize or modify from ingested sterols without large isotopic fractionation (Grice et al., 1996). Thus, cholestane likely reflects phytoplankton in the upper part of the water column in these Pacific coastal waters (Schoell et al., 1994). S-bound phytane is an early diagenetic product of phytol (Kohnen et al., 1993), the sidechain of the essential photoautotrophic pigment chlorophyll-a, and likely also reflects contributions from all phytoplankton (see Witkowski et al., 2018 for a detailed discussion). S-bound C$_{35}$ hopane is exclusively derived from bacteriohopanepolyol derivatives (Koster et al., 1997), which are produced by bacteria, including cyanobacteria (Welander et al., 2010), which are also photoautotrophic.

The weaker correlations between the δ^{13}C of the C$_{25}$ HBI alkane and the general phytoplankton biomarkers may be explained by different source organisms. The C$_{25}$ HBIs are considered biomarkers for specific groups of diatoms (Damste et al., 2004) and can become rapidly sulfurized in sediments (Damste et al., 2007; Kohnen et al., 1990). Diatoms are the most significant algal groups today and were omnipresent in Pacific waters during the Miocene, as seen by the deposition of silica rich sediments (Isaacs et al., 2001) and the presence of diatom shells throughout Leg 63 sediments (Initial Reports of the Deep Sea Drilling Project, Volume 63). As compared with other biomarkers within the same core, the widely fluctuating δ^{13}C values among C$_{25}$ HBI alkanes has also been observed in sediments of the Arabian Sea (Schouten et

5

al., 2000), the Veno del Gesso basin (Kohnen et al., 1990), and Monterey Formation (Schouten et al., 1995b). It has been interpreted to be due to changes in the diatom populations (e.g. Schouten et al., 1998), changes in biosynthetic pathways in the formation of these HBIs (Massé et al., 2004), and/or the proclivity for active bicarbonate uptake by certain diatom species (Tortell et al., 1997). Because our estimation of PCO$_2$ is based on isotopic fractionation of CO$_2$ through passive diffusion (Popp et al., 1989), the C$_{25}$ HBIs will not be further discussed.

In contrast to the situation with the C$_{25}$ HBI alkane, the lack of correlation between the δ^{13}C values of alkenones and those of general biomarkers (cholestanes and phytane, in particular) is likely due to the limited number of data points over a restricted time interval (Fig. 5.1). Unlike the general biomarkers, which are consistently detected throughout the record, alkenones span only the final 4 Ma of the 16.4 Ma record. Furthermore, the range in δ^{13}C of alkenones is relatively small (-21.3 to -23.8‰) compared to that of the general phytoplankton biomarkers.

The δ^{13}C of the general phytoplankton biomarkers (steranes, hopane, and phytane) are compared with those of the nearby age-equivalent Monterey Formation outcropping at Naples Beach in the Santa Barbara basin (Schoell et al., 1994; Schouten et al., 1995b) and Shell Beach in the Pismo basin (Schouten et al., 1997). The δ^{13}C of the steranes are comparable during the overlapping time periods, suggesting similar producers were present at all three sites (Fig. S2). Phytane also shows similar δ^{13}C values among the three sites, likewise suggesting similar sources and isotopic behavior on a regional scale. In contrast, the δ^{13}C values of the C$_{35}$ hopane among the three sites were very different to one another, where the DSDP 467 site shows an δ^{13}C difference of 2-4‰ from Shell Beach (15-11 Ma) and of 3-7‰ from Naples Beach (14-7 Ma), possibly because of regionally different sources. Because of this large discrepancy between among sites, we will not use the C$_{35}$ hopane to estimate PCO$_2$.

5.4.2   ε$_p$ derived from the δ^{13}C of algal biomarkers

The isotopic fractionation of phytoplanktonic biomass, ε$_p$, was calculated for the three cholestanes and phytane using the equation:

$$\varepsilon_p = 1000 \cdot [\ (\delta_d+1000) / (\delta_p+1000) – 1] \qquad [1]$$

where δ_p is the $\delta^{13}C$ of primary photosynthate calculated from the stable carbon isotopic offset between biomarker and biomass and where δ_d is the $\delta^{13}C$ of aqueous carbon dioxide ($CO_{2[aq]}$) in the photic zone.

Determining the $\delta^{13}C$ of photosynthetic biomass (δ_p) is challenging for general biomarkers because there are different isotopic offsets between biomass and biomarker per species (Popp et al., 1989; Witkowski et al., 2018). Here, we used the average offset reported for laboratory cultures (Table S1). The δ_p for steranes is 4.5‰ ± 3.0 standard deviation based on the offset between their precursor sterols and biomass reported for eight algal species (Schouten et al., 1998). For the δ_p of phytane, the average isotopic offset between its precursor phytol and biomass is 3.5‰ ± 1.3 standard deviation based on the average of twenty-three species (Witkowski et al., 2018). Finally, the δ_p for alkenones is 3.9 ‰ ± 0.4 standard deviation based on the laboratory cultures of *Isochrysis galbana* and *Emiliania huxleyi* (Laws et al., 2001; Schouten et al., 1998).

The same δ_d was applied to all of the biomarkers and calculated from:

$$\delta_d = \delta^{13}C_{carbonate} - 1 + \varepsilon_{b(a)} \qquad [2]$$

Here, the $\delta^{13}C$ of carbonate is estimated from a global compilation of $\delta^{13}C$ of planktonic foraminiferal shells (Tipple *et al.*, 2010) and corrected for the temperature-dependent carbon isotopic fractionation of $CO_{2[aq]}$ with respect to HCO_3^- ($\varepsilon_{b(a)}$), where $\varepsilon_{b(a)} = 24.12 - 9866/T$ (Mook et al., 1974). Sea surface temperatures are estimated from $U^{k'}_{37}$ values at Site 1010 (30ºN, 118ºW) in the subtropical east Pacific (LaRiviere et al., 2012) corrected for latitudinal temperature difference of 2.3ºC between the modern mean annual SST at the two locations.

All the biomarker-derived ε_p show a steady decline with time, starting with the highest values shown during the MMCO (Fig. 5.1B). The steranes all display similar values with a small offset between each, as aforementioned with the $\delta^{13}C$ values. The ε_p of 5α-cholestane declines from 16.5 to 13.5‰, of 24-ethyl-5α-cholestane from ca. 17 to 14‰, and of 24-methyl-5α-cholestane from ca. 17.5 to 14.5‰. The sterane trends closely track each other with exception of two periods of large ε_p differences: at 10.5 Ma where they respectively show 15.8, 16.8, and 18.2‰ and again at 9.5 Ma where they are 13, 15, and 16‰, respectively (Fig. 5.1B). Like the cholestanes, ε_p derived from phytane also declines with time but with an overall less steep trend, ranging from ca. 15‰ at 15 Ma to ca. 11‰ at 0.5 Ma. Alkenones show no distinguishable trend, with all ε_p values falling within a ca. 1‰ range (between 9.3 to 10.4‰) except for the ε_p of 11.6‰ at 2.1 Ma.

5.4.3 Estimating PCO_2

To estimate PCO_2 from ε_p values, we use the relationship first derived for higher plants (Farquhar et al., 1989; Farquhar et al., 1982), modified for algae (Jasper and Hayes, 1990; Popp et al., 1989):

$$PCO_2 = [\, b / (\varepsilon_f - \varepsilon_p) \,] / K_0 \qquad\qquad [3]$$

where b considers species-specific factors or essentially the species carbon demand per supply (Jasper et al., 1994), ε_f is the species-specific maximum isotopic fractionation due to photosynthesis, and the constant K_0 converts $CO_{2[aq]}$ to PCO_2 via Henry's law, which considers temperature and salinity (Weiss, 1974). Temperatures were obtained as described above. ε_f for phytoplankton species range from 25 to 28‰ in laboratory cultures (Goericke and Fry, 1994); we use an average 26.5‰ with an uncertainty of 1.5‰ uniformly distributed (Witkowski et al., 2018). ε_f for alkenones is set at 25‰, based on laboratory cultures (Hinga et al., 1994; Popp et al., 1998) and the value used in paleo PCO_2 reconstructions (Pagani et al., 1999; Pagani et al., 2000; Pagani et al., 2005).

The b factor, accounting for all factors which may influence ε_p such as growth rate, cell carbon allocation, and bicarbonate uptake, has been extensively and nearly exclusively studied in alkenone-producing *Emiliania huxleyi*, though the exact mechanics behind this term remain elusive (Bidigare et al., 1997; Riebesell et al., 2000). Measured alkenone-based b in environmental samples range from 70-240 ‰ kg μM^{-1} with a mean of 165 ‰ kg μM^{-1} ± 53 standard deviation (Bidigare et al., 1997; Eek et al., 1999; Laws et al., 2001; Popp et al., 1998b); this average has been applied to the alkenone-based PCO_2 reconstructions here. The b factor for the vast majority of contributors to the phytoplankton pool have not been established (Hoins et al., 2015; Laws et al., 1997; Popp et al., 1998b; Wilkes et al., 2017). Previous studies using the $\delta^{13}C$ of phytane as a PCO_2 proxy (Bice et al., 2006; Naafs et al., 2016; Sinninghe Damsté et al., 2008; van Bentum et al., 2012) have used a mean value of 170 ‰ kg μM^{-1}, similar to the alkenone mean. This value is supported by the b-value obtained from the ε_p of phytol in the equatorial Pacific Ocean (Bidigare et al., 1997) and compares well with a compilation of the $\delta^{13}C$ of organic matter in modern surface sediment which yields an average mean b of 168 ± 43 ‰ kg μM^{-1} (Witkowski et al., 2018). Considering the increased uncertainty over longer timescales, we expand the uncertainty to ± 60 kg μM^{-1} standard deviation, using this value for all of the general biomarkers.

The PCO$_2$ reconstructions show a consistent declining trend over the course of this 16.4 Ma record (Fig. 5.1C). The MMCO at the beginning of the record shows a larger spread of estimations, e.g. sterane-based PCO$_2$ estimates are ca. 580-680 μatm, whereas phytane-based estimates are ca. 500 μatm. With time, these records begin to converge by ca. 7.4 Ma, where cholestane-based estimates are ca. 425-450 μatm and the phytane-based estimate is 390 μatm. By the final 4 Ma, the PCO$_2$ estimated from all four general phytoplanktonic biomarkers converge even further to 340 μatm until the shallowest sediment (0.1 Ma) with a PCO$_2$ of ca. 290 μatm. The alkenone record in the last 4 Ma also yields similar PCO$_2$ estimates as the general biomarkers, nearly identical to phytane, further supporting the use of general biomarkers for PCO$_2$ estimations.

5.4.4   Comparison of PCO$_2$ proxies

Because the four general phytoplankton biomarkers, as well as alkenones, show similar trends and values for PCO$_2$ reconstructions throughout this 16.4 Ma core, we focus further comparative discussion using phytane, which has the most consistent record and has yielded secular trends in PCO$_2$ comparable to other proxies over the Phanerozoic (Witkowski et al., 2018). The error associated with phytane-based PCO$_2$ estimates is based on Monte Carlo simulations and considers each equation parameter, including: δ^{13}C of phytane (0.5‰), the δ^{13}C of carbonate (0.2‰), the offset from biomass to calculate δ_p (1.5‰), and uncertainty in SST (3.0ºC). SST is considered twice in the equations, once for calculating ε_p and again when converting CO$_{2[aq]}$ to PCO$_2$. These uncertainties are discussed in detail in Witkowski *et al.* (2018).

Here, we put our PCO$_2$ estimates in the context of estimations in the literature, comparing to models and proxy-data over the Miocene with an emphasis on the widely-debated MMCO. Based on modern environmental trends and ice core data, temperature and PCO$_2$ are considered to be linked, a relationship used in developing models. Based on this relationship, specifically on the temperature estimates for the MMCO, the coupled model from National Center for Atmospheric Research Community Atmosphere Model CAM3.1 and Land Model CLM3.0 suggest that PCO$_2$ may have been between 460-580 μatm (You et al., 2009). This range precisely corresponds with the phytane-based MMCO estimates of ca. 480-530 μatm.

We also compare our DSDP Site 467 record with two different sets of proxy-based PCO$_2$ estimations (Fig. 5.2). First, the PCO$_2$ reconstructions from phytane are

5

compared with a compilation comprising of four PCO_2 proxies during this time period: stomatal densities and indices in plants, $\delta^{13}C$ of pedogenic minerals, $\delta^{13}C$ of alkenones, and $\delta^{11}B$ of marine carbonate (Foster et al., 2017). Mimicking the methods in the paper, these proxy estimates are interpolated every half-million years, resampled using Monte Carlo, and smoothed with a LOESS fit (Foster et al., 2017). Many of the individual estimates from the compilation overlap with phytane-derived estimations but the ultimate trend does not. The most notable difference between these two records is during the MMCO, where our values are substantially higher. Whereas the average PCO_2 estimations in the Foster *et al.* compilation remains relatively constant over the Miocene, declining slightly from ca. 310 μatm during the MMCO to 275 μatm by 0.5 Ma, our phytane-based record, in contrast, suggests that PCO_2 steadily declined from ca. 500 μatm in the MMCO to 280 μatm by 0.1 Ma.

Second, we compare our estimates with PCO_2 reconstructions based on diatom frustules from a sediment core at ODP Site 846 in the Eastern Equatorial Pacific over the past 13 Ma (Mejia et al., 2017). In this paper, the influence of different parameters on diatom frustule to PCO_2 estimations are explored, including constant *b*, indicators of past productivity and growth rate (i.e. opal content, alkenone concentration, and coccolith Sr/Ca), and different active uptake rates. This pennate diatom-based PCO_2 record shows a different trend from our phytane-based record and the Foster et al. (2017) compilation, starting with much lower values ca. 12.9 Ma, increasing dramatically between 10.9 to 7.7 Ma, and declining rapidly again to very low values between 5.8 to 4.0 Ma. Starting with 12.9 Ma, Mejia et al. (2017) estimations are notably lower (ranging from 130 to 320 μatm) than the phytane-based estimations at ca. 480 μatm but in line with the Foster et al. (2017) estimations of ca. 300 μatm. Although this oldest measurement in the Mejia et al. (2017) record follows the MMCO, the values are noticeably lower than either our phytane-based record or the climate model simulation estimations. For the interval between 10.9 to 7.7 Ma, the Mejia *et al.* estimates based on a constant *b* and on past productivity and growth rate have similar absolute values (ranging from 480 to 340 μatm) to our record (480-380 μatm) but are much higher than the Foster et al. compilation of 300 μatm. During the same 10.9 to 7.7 Ma interval, Mejia et al. (2017) estimates using different active uptake rates, on the other hand, show much higher estimations, ranging from ca. 1080 to 425 μatm. For the final three samples at 5.8 Ma (310-230 μatm), 4.0 Ma (255-200 μatm), and 0.8 Ma (ca. 230 μatm), Mejia et al. estimations are lower than both the phytane-based estimations (ca. 375, 355, 260 μatm, respectively) and the Foster et al. estimations (320, 300, 285 μatm, respectively).
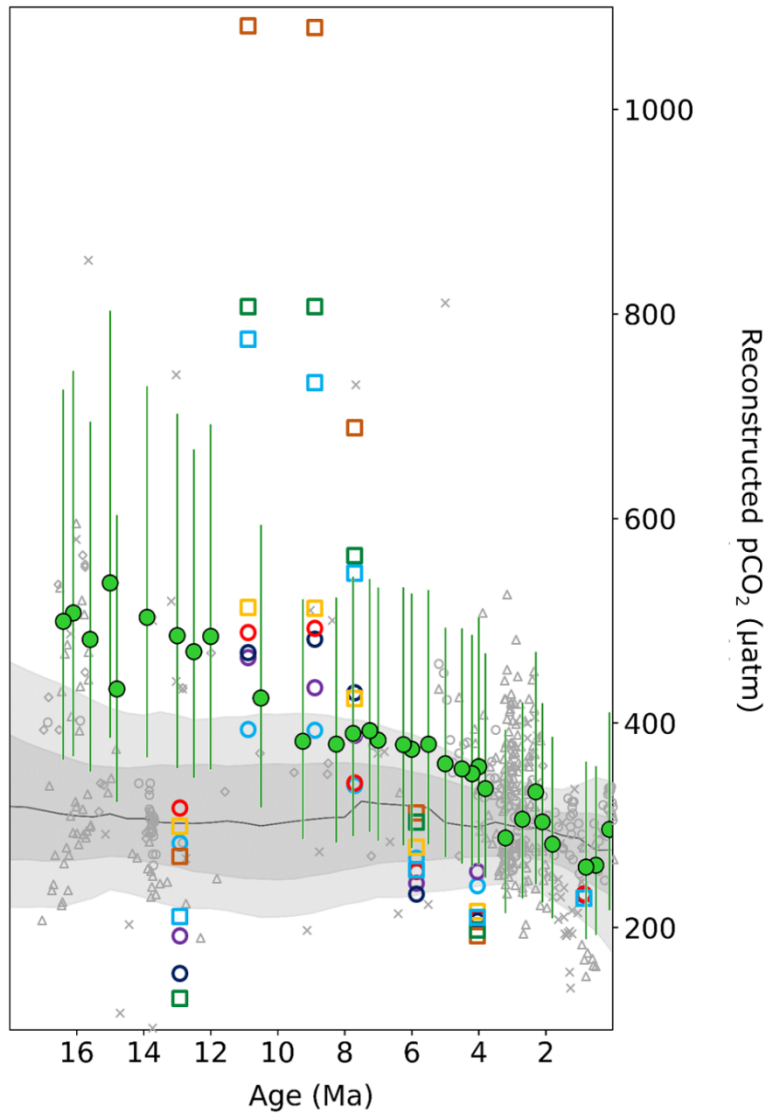
Fig. 5.2. Comparison of phytane-based PCO$_2$ estimates of DSDP Site 467 record (green circles) to published PCO$_2$ estimations. Error bars indicate 1 SD (68%) based on Monte Carlo simulations, combining uncertainty as shown in Fig. 5.1. Foster *et al.* (2017) compilation in gray open symbols: pedogenic minerals (x), alkenones (circles), stomata indices (diamond), and boron (triangle) and averaged with LOESS fitting (68% confidence interval dark gray, 95% light gray) and Mejía *et al.* (2017) compilation of ε_p-based pCO$_2$ calculated using: constant b (blue circle), opal content (magenta circle), alkenone concentration (purple circle), coccolith Sr/Ca (red circle), and active uptake of HCO$_3^-$ where μ=1.7 d^{-1} (orange square), μ=1 d^{-1} (green square), μ=0.5d^{-1} (yellow square), μ=0.5-0.85 d^{-1} (blue square).

5

There may be several reasons for the discrepancies between our phytane-based PCO_2 record and the other two PCO_2 proxy records (Foster et al., 2017; Mejia et al., 2017). One possible influence may be upwelling at our site. The California coastline experienced a sharp increase from a "generally weaker" to "generally stronger" upwelling during the interval 12.3 to 9.9 Ma, as indicated by diatom assemblages (Barron and Keller, 1983; Domack, 1986), likely due to global cooling trends, which altered shallow ocean circulation of an eastern boundary current flowing southward along the coast (Ingle and Keller, 1980) to a stronger (though still low-to-moderate) advection of cooler northern waters, resulting in upwelling, the transport of nutrients, and increased productivity (Bernal and McGowan, 1981; Eppley and Holm-Hansen, 1986). In theory, the signal from PCO_2 in the atmosphere may be masked by the response of phytoplankton to upwelling (Pancost et al., 1997), which brings more ^{13}C-depleted $CO_{2[aq]}$ and nutrients in cold bottom waters to the surface, as seen in e.g. the Arabian sea over the past 29 ka (Palmer et al., 2010). However, it is difficult to determine the effect of upwelling-related productivity variations on regions farther removed from upwelling centers (White et al., 1992), such as the DSDP site used here. There are only two data points (at 12.0 and 10.5 Ma) which fall within this 12.3 to 9.9 Ma upwelling timeframe; however, these two points do not deviate from the overall downward trend for the entire core.

Another limitation of our approach is the factor b, here based on the global compilation of total organic matter in modern marine surface sediments worldwide (Witkowski et al., 2018). Sensitivity tests, however, demonstrate that a 1% change in b results in only a 1% change in PCO_2 estimation (Witkowski et al., 2018), which is too small to account for the consistent decline over the studied time interval. Furthermore, the overlap between alkenone-based PCO_2 estimates, for which much more research has been conducted on the b-value (e.g. Bidigare et al., 1997; Popp et al., 1999; Laws et al., 2001), and the phytane-based PCO_2 estimates suggests that our estimates for the b-value of general phytoplankton are not unreasonable.

Finally, it should be noted that there are also large uncertainties with the other PCO_2 records for this time period. In the earlier part of the record, the Foster *et al.* compilation has fewer data with larger scatter in estimates, some of which seem unrealistic e.g. 80 μatm. The large scatter occurs not only among different proxies, but also within the same proxy during the same time period. Mejía *et al.* data also has large uncertainties based on the given assumptions in the calculations. At 8.86 Ma, for example, a diffusive model with constant b yields 393 μatm whereas an active uptake model yield 1081 μatm. Therefore, the discrepancies with current PCO_2 records a do not necessarily invalidate our phytane-based PCO_2 estimations.

4.5 Coupling of Miocene temperature and *P*CO$_2$

We compare our *P*CO$_2$ estimates based on δ^{13}C of phytane with compilations of Miocene sea surface temperature (SST) reconstructions based on U$^{k'}_{37}$ (Herbert et al., 2016) and bottom water temperatures based on the δ^{18}O of benthic foraminifera (Zachos et al., 2008). Herbert *et al.* compiled Miocene SST records for northern hemisphere high-latitudes (ODP Sites 883, 907, 982, 983), northern hemisphere mid-latitudes (ODP Sites 1010, 1021, 1208), southern hemisphere mid-latitudes (ODP Sites 594, 1085, 1088, 1125), and tropics (ODP Sites 722, 846, 850, 1241, U1338).
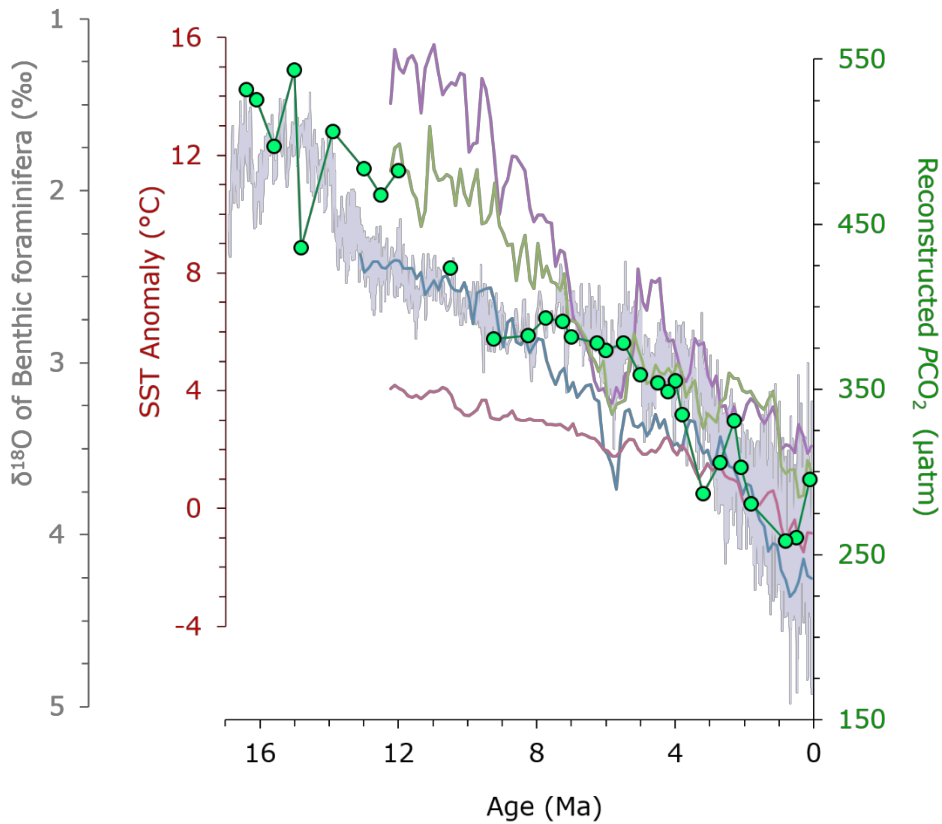

Fig. 5.3. Comparison of DSDP 467 record (represented by phytane, green circles with one standard deviation error bars) to two different temperature estimation compilations: U$^{k'}_{37}$ alkenone-based proxy compiled in Herbert *et al.*, 2016 (NH high latitudes: purple line; NH mid latitudes: blue line; SH mid latitudes: green line; tropics stack: red line) and δ^{18}O of benthic foraminifera stack compiled in Zachos *et al.*, 2001; 2008 (lavender line).

Each of these temperature records decline over time, though the magnitude differs from region to region, clearly seen in the difference between the tropics and northern hemisphere high-latitude sites (Fig. 5.3). The global compilation of the $\delta^{18}O$ derived from benthic foraminifera (Zachos et al., 2008), which reflects bottom water temperatures, shows a similarly declining trend over the past 16.4 Ma (Fig. 5.3). The phytane-based $P\text{CO}_2$ record shows a nearly identical declining trend to these five temperature compilations based on two different temperature proxies (Fig. 5.3), suggesting a strong link between temperature and $P\text{CO}_2$. A possible caveat is that temperature is used twice in our $P\text{CO}_2$ calculations: once when calculating ε_p and again when calculating $P\text{CO}_2$ from $\text{CO}_{2[aq]}$. In other words, if temperature significantly impacts the calculations, then the $P\text{CO}_2$ estimations may simply be the result of its temperature input. Sensitivity tests show temperature negligibly effects ε_p by $\pm$ 0.50 ‰. However, when calculating $P\text{CO}_2$ from $\text{CO}_{2[aq]}$, temperature may potentially effect $P\text{CO}_2$ estimations up to $\pm$ 50 μatm. Although a sizeable error, this potential $\pm$ 50 μatm is too small to suggest temperature alone is driving the declining trend we observe in our record. Thus, the remarkably similar trends of our $P\text{CO}_2$ estimates to independent temperature records over the Miocene into the Quaternary suggest that $P\text{CO}_2$ and temperature are in fact linked.

5.5   Conclusion

$P\text{CO}_2$ reconstructions for the Miocene, particularly the MMCO, show large variations and have therefore been widely discussed. To better clarify paleoclimate reconstructions for this period, general phytoplankton biomarkers were explored as potential proxies for $P\text{CO}_2$ reconstructions. $P\text{CO}_2$ reconstructions from steranes and phytane showed similar trends, declining from 500-600 μatm at 16.4 Ma to 290 μatm at 0.1 Ma. Comparison to other $P\text{CO}_2$ proxy records described in the literature (Foster et al., 2017; Mejia et al., 2017) showed some overlapping results but overall with a stronger declining trend than the literature. Comparison of the phytane-based $P\text{CO}_2$ reconstruction with SST and bottom water temperatures show a remarkably similar declining trend, suggesting that these two climate parameters were coupled over the past 16.4 Ma as currently observed in modern environments and ice core records. Compound-specific stable carbon isotope analysis of general phytoplankton biomarkers offers a refreshed approach to reconstructing $P\text{CO}_2$ from ε_p, particularly over longer timescales where other existing proxies are lacking, and thus warrants further investigation.

Acknowledgements

Supplement

Data S1. Spreadsheet of all data used. (Excel)

Table S1. Isotopic offset between biomass and biomarker. Phytane, steranes, and alkenones; $\Delta = \delta^{13}$C offset between bulk biomass and biomarker for each individual laboratory cultured species; Genus refers to the cultured phytoplankton.
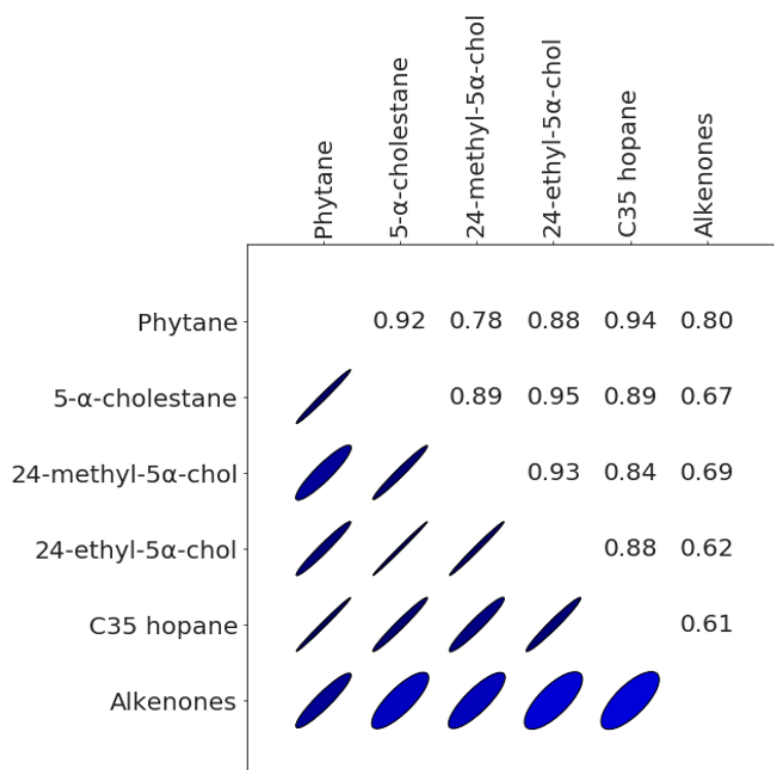
5

Fig. S1. Cross-correlation plot of the $\delta^{13}C$ for the examined biomarkers: 5α-cholestane, 24-methyl-5α-cholestane, 24-ethyl-5α-cholestane, 22R-17β,21β(H)-pentakishomo-hopane (C_{35} hopane), phytane, and the C_{25} highly branched isoprenoid (2,6,10,14-tetramethyl-7-(3'methylpentyl)pentadecane)), as well as alkenones. Asterisks indicate $p<0.5$ (*), $p<0.01$ (**), and $p<0.001$ (***).
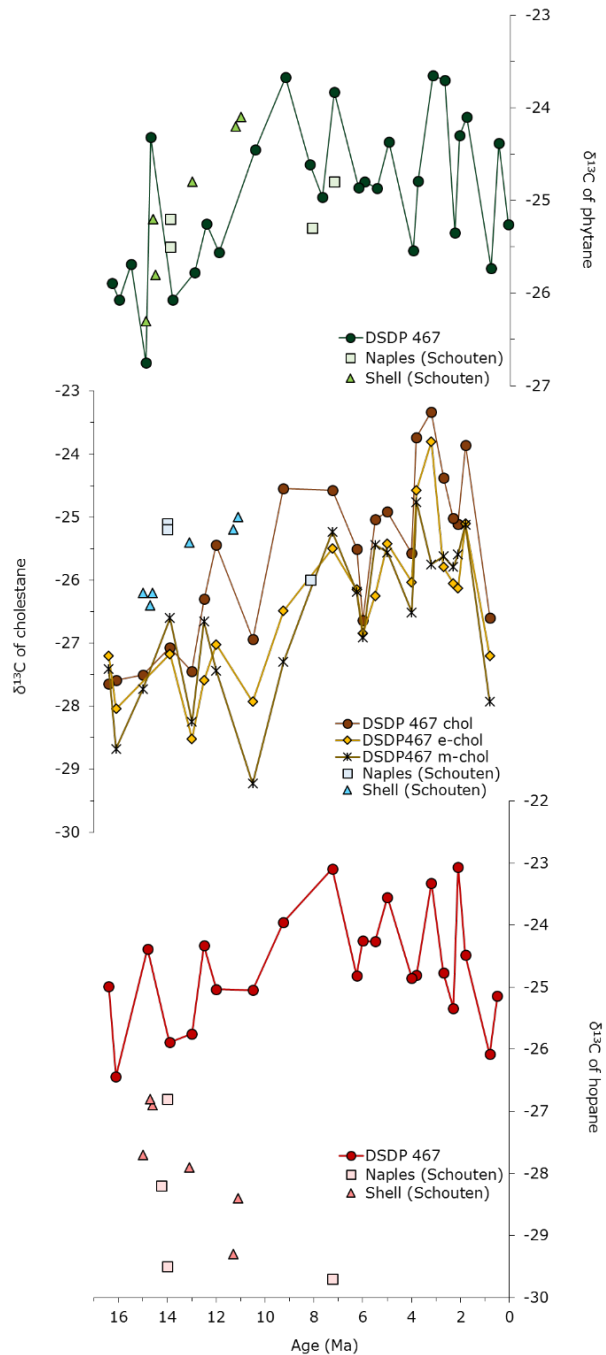
Fig. S2. Comparison of δ^{13}C of general biomarkers at DSDP Site 467 with the age-equivalent and nearby Monterey Formation outcropping at Naples Beach in the Santa Barbara basin (Schouten *et al.*, 1995) and Shell Beach in the Pismo basin (Schouten *et al.*, 1997).

Chapter 6

Molecular fossils from phytoplankton reveal secular PCO_2 trend over the Phanerozoic

Caitlyn R Witkowski[1], Johan WH Weijers[2], Brian Blais[3,4], Stefan Schouten[1,5], Jaap S Sinninghe Damsté[1,5]

[1] Department of Marine Microbiology and Biogeochemistry, NIOZ Royal Netherlands Institute for Sea Research, and Utrecht University, The Netherlands
[2] Shell Global Solutions International B.V., The Netherlands
[3] Department of Science and Technology, Bryant University, USA
[4] Institute for Brain and Neural Systems, Brown University, USA
[5] Department of Geosciences, Utrecht University, The Netherlands

Abstract

Past changes in the atmospheric concentration of carbon dioxide ($P\mathrm{CO}_2$) have had a major impact on earth system dynamics yet reconstructing secular trends of past $P\mathrm{CO}_2$ remains a prevalent challenge in paleoclimate studies. The current long-term $P\mathrm{CO}_2$ reconstructions rely largely on the compilation of many different proxies, often with discrepancies among proxies, particularly for periods older than 100 Ma. Here we reconstructed Phanerozoic $P\mathrm{CO}_2$ from a single proxy: the stable carbon isotopic fractionation associated with photosynthesis (ε_p) which increases as $P\mathrm{CO}_2$ increases. This concept has been widely applied to alkenones, but here we expand this concept both spatially and temporally by applying it to all marine phytoplankton via a diagenetic product of chlorophyll, phytane. We obtained data from 306 marine sediments and oils, which showed that ε_p ranges from 11–24‰, agreeing with the observed range of maximum fractionation of Rubisco (i.e. 25-28‰). The observed secular $P\mathrm{CO}_2$ trend derived from phytane-based ε_p mirrors the available compilations of $P\mathrm{CO}_2$ over the past 420 Ma, except for two periods in which our higher estimates agree with the warm climate during those time periods. Our record provides currently the longest secular trend in $P\mathrm{CO}_2$ based on a single marine proxy, covering the last 500 million years of Earth history.

6.1 Introduction

Carbon dioxide shapes climate, breathes life into the biosphere, and turns the cogs of the carbon cycle, both in the present as well as in the past. The past atmospheric concentrations of carbon dioxide (expressed in partial pressure; $P\mathrm{CO}_2$) are reconstructed from indirect measurements, i.e. proxies, such as stomatal densities and indices in plant fossils, the boron isotopic composition of marine carbonate, and the stable carbon isotopic composition ($\delta^{13}C$) of marine phytoplankton, paleosols, and liverworts e.g. (Foster et al., 2017). Each proxy has strengths and limitations, such as its timespan of application, associated estimation error, and sensitivity to specific $P\mathrm{CO}_2$ levels (Royer, 2014). The reconstruction of secular trends of $P\mathrm{CO}_2$ over long timescales (>10 My) often relies on compiling many different proxies in order to generate a continuous record (Foster et al., 2017). Thus, a single well-constrained proxy that spans the Phanerozoic may strengthen and support our understanding of $P\mathrm{CO}_2$.

6

The stable carbon isotopic fractionation associated with oxygenic photosynthesis (ε_p) is a proxy with potential to span the Phanerozoic. Isotopic fractionation occurs when the CO_2-fixing enzyme Rubisco (ribulose 1,5-biphosphate carboxylase oxygenase) favors ^{12}C over ^{13}C during inorganic carbon fixation, making the photosynthates' isotopic composition ($\delta^{13}C$) depleted in ^{13}C compared to its surrounding environmental CO_2 (Hayes et al., 1989). Higher CO_2 concentrations lead to greater fractionation and *vice versa*, resulting in a dynamic $\delta^{13}C$ of photoautotrophic biomass (Farquhar et al., 1989; Hayes et al., 1990). This concept is reverse-engineered to reconstruct past PCO_2 by calculating ε_p from the $\delta^{13}C$ of organic matter (OM) derived from photoautotrophic biomass and the $\delta^{13}C$ of CO_2 derived from fossilized carbonates e.g. planktonic foraminifera (Freeman and Hayes, 1992).

ε_p has been extensively tested as a PCO_2 proxy since it was first estimated using the $\delta^{13}C$ of geoporphyrins (Popp et al., 1989) and later using the $\delta^{13}C$ of bulk organic matter (Hayes et al., 1999). In subsequent studies, factors that influence ε_p other than CO_2 concentrations have been explored in laboratory cultures, e.g. growth rate (Laws et al., 1995) and cell-size (Popp et al., 1998b), and environmental conditions, such as seasonality, light, and temperature (Sackett et al., 1965). In addition, brought to the forefront in more recent studies, alkenones (and theoretically other phytoplankton) may underestimated PCO_2 due to other factors such as cell-size and carbon acquisition strategies (Bolton et al., 2016; Bolton and Stoll, 2013; Mejia et al., 2017). The impact of some factors remains difficult to constrain, such as the assumption that the primary source of carbon is passively-diffused $CO_{2[aq]}$ into the cell; under low CO_2 conditions, many phytoplankton implement active uptake of bicarbonate (Badger et al., 1998), a potential concern given the substantial $\delta^{13}C$ difference between bicarbonate (0‰) and CO_2 (-8‰) (Mook et al., 1974) and even further complicated by active uptake elevating CO_2 at the site of carboxylation.

The $\delta^{13}C$ of total organic carbon (TOC) to calculate ε_p, in principle, provides a long-term record for PCO_2 (Hayes et al., 1999). Using TOC does raise concerns regarding isotopic heterogeneity in different organisms due to kinetic isotope effects and Rayleigh distillation effects with branching points in biosynthetic pathways leading to distinct $\delta^{13}C$ values for e.g. carbohydrates, proteins, and lipids (Hayes, 1993). These $\delta^{13}C$ differences among biosynthetic products can be further influenced by diagenetic conditions, such as carbohydrate sulfurization (Sinninghe Damsté et al., 1998b), and mixing with terrestrial OM. Abating concerns of using TOC, compound-specific isotope analysis (CSIA) is used on shorter timescales, primarily relying on alkenone biomarkers, the long-chain unsaturated methyl and ethyl *n*-ketones produced by a select group of Haptophytes. However, ε_p of alkenones only

reconstructs PCO$_2$ during the evolutionary history of alkenone-producing Haptophytes, which are not common in the geologic record until the mid-Miocene (Zhang et al., 2013).

To extend the PCO$_2$ reconstruction over the Phanerozoic, ε_p is estimated here using the general phytoplanktonic molecular fossil phytane. Phytane is derived from chlorophyll-a, the omnipresent photoautotrophic pigment that absorbs and transfers light into chemical energy during oxygenic photosynthesis and which has been present for at least the past 2.15 Ga (Rasmussen et al., 2008). Indeed, phytane has been found in similarly ancient rocks and petroleum (Li et al., 2003). Furthermore, all photosynthetic phytoplankton will contribute to this general biomarker, thereby averaging the ε_p of the phytoplankton community at the time of synthesis. The ε_p calculated from phytane has been previously explored as a proxy for PCO$_2$ at selected sites during specific time periods (Bice et al., 2006; Damste et al., 2008; Naafs et al., 2016; van Bentum et al., 2012) and has been shown to mimic PCO$_2$ trends. Here, we explore its potential for reconstructing secular trends of PCO$_2$ over the Phanerozoic.

6.2   Materials and Methods

The isotopic composition of phytane was measured in seventy marine sediments and oils derived from marine source rocks. Marine oils were processed at Shell Global Solutions International B.V., The Netherlands. Crude oil was eluted over a AgNO$_3$-impregnated silica gel column using three column volumes of cyclohexane to yield saturated hydrocarbon fractions. To remove n-alkanes, the saturated fractions remained in cyclohexane when two layers of 0.5Å molecular sieve were added to the samples and saturated overnight. The remaining branched/cyclic fractions were injected splitless on GC-FID at 35ºC for 5 min, ramped to 325ºC at 4ºC/min for 15 min and hold isothermal for another 15 min. A silica capillary column (Ultra-1, 50 m x 0.22 mm; d$_f$ 0.11 μm) was used with helium as a carrier gas at a constant flow of 25 cm/s. GC-IRMS was conducted using a DB-1ms column (60 m x 0.32 mm; d$_f$ 0.25 μm). The samples were injected at 220ºC into a 70ºC oven for 1 min, ramped to 250ºC at a rate of 4ºC/min and then to 300ºC at a rate of 20ºC/min for 20 min at a flow rate of 30 cm/s using Helium as a carrier gas. The reference gas was normal CO$_2$ with a pre-determined isotopic composition.

Twenty-nine marine sediments from DSDP Site 467 offshore of southern California from the Middle Miocene to Lower Pliocene (Elrod and Katz, 1982) were processed

at NIOZ Royal Netherlands Institute for Sea Research, The Netherlands. Powdered sediments (15-20 g) were extracted with dichloromethane (DCM): MeOH (9:1 v/v) on a Dionex 250 accelerated solvent extractor (ASE) at 100°C, 7.6×10^6 Pa. Extracts were eluted over Na_2SO_4 to remove excess water and then over an alumina packed column to separate polar fractions (DCM: MeOH, 1:1 v/v). Polar fractions were desulfurized using Raney-nickel (Sinninghe Damsté et al., 1990), eluted over alumina oxide into an apolar fraction (hexane: DCM, 9:1 v/v), and hydrogenated. Desulfurized apolar fractions were injected on a GC-MS to identify the presence of phytane and on a GC-FID to determine quantity prior to injection on IRMS for the isotopic composition of phytane. GC-FID, GC-MS, and GC-IRMS all had a starting oven temperature of 70ºC ramped to 130ºC at 20ºC/min and then ramped to 320ºC for 10 min at 4ºC/min. GC-IRMS was conducted using a CP-Sil 5 column (25 m x 0.32 mm; d_f 0.12 μm) using a constant flow of He carrier gas.

6.3 Results

We generated $\delta^{13}C$ values of phytane ($\delta^{13}C_{phytane}$) from 41 oils and 29 sediments. Furthermore, we compiled $\delta^{13}C_{phytane}$ values from the literature. New and compiled data yielded 308 data points in total (Table S1). Only marine sediments and oils were used for our compilation in order to constrain the $\delta^{13}C_{phytane}$ to marine phytoplankton in a more stable and homogenous environment, avoiding the potential decoupling of PCO_2 that may occur in local carbon cycles of terrestrial and lacustrine settings. By using only marine settings, this also excludes the additional confounding influence of C_3 and C_4 higher plants; chlorophyll breaks down relatively quickly, eliminating effective transport of terrestrial phytol to the ocean. Immature oils lacking signs of biodegradation were selected based on the confidence in source rock identification to constrain age. Furthermore, these oils were selected based on the lack of terrestrial biomarkers (e.g. oleanane, taraxastane, bicadinanes) and the lack of local environmental irregularities (e.g. high salinity) in order to minimize spurious influences on the overall baseline signal for PCO_2 (see Supplementary text). In order to attain the general baseline trend for the $\delta^{13}C_{phytane}$ from marine phytoplankton over the Phanerozoic, short-term isotope anomalies were excluded e.g. carbon isotope excursion events (CIEs) with isotopic spikes of $\geq 2‰$ in less than 100 ka, such as the negative CIE of the Paleocene/Eocene boundary e.g. Koch et al. (1992). Data before and after CIEs (when the excursion has a clear endpoint) are included in this compilation.

In our dataset, most $\delta^{13}C_{phytane}$ is from extractable free phytane. Sulfur-bound phytane, i.e. phytane released from sulfur-bound moieties present in sediments that were deposited in anoxic environments, is also included. Sulfur-bound phytane is different than free phytane in that during early diagenesis, inorganic reduced sulfur species selectively react with labile functionalized lipids such as phytol or phytadienes (de Graaf et al., 1992). In other words, sulfur-bound phytane is an excellent addition to this record: it may more accurately reflect the $\delta^{13}C$ of the original phytol, whereas free phytane may have small influences by fluctuating inputs of terrestrial OM or archaeal derived ether lipids (Koopmans et al., 1999; van Bentum et al., 2012).
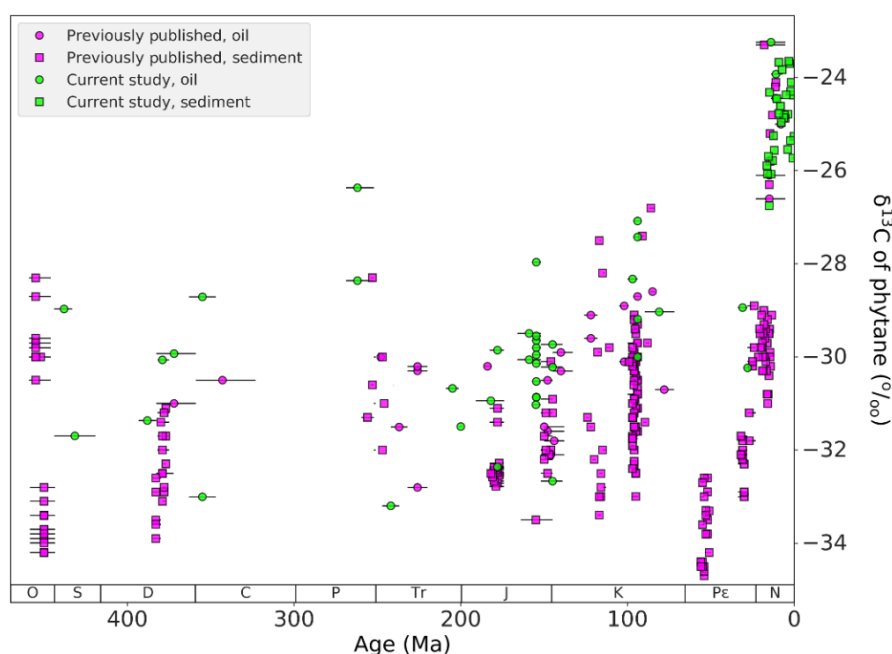

Fig. 6.1. δ^{13}C of phytane. Phanerozoic compilation of the δ^{13}C of phytane from literature (pink) and data from this study (blue), and from sediment (square) and oil (circle). Age uncertainties are shown in the horizontal error bars.

Our compilation shows that over the Phanerozoic, values for the $\delta^{13}C_{phytane}$ range from -34.7 to -23.2‰ (Fig. 6.1). During the Late Ordovician (455-450 Ma), there is a drastic negative shift from -28.3 to -34.2‰, followed by a data-scarce Silurian. A gradual positive trend during the Devonian is observed from -33.9‰ at ca. 380 Ma to -28.7‰ by ca. 355 Ma. The Carboniferous into the Early Permian lacks substantial data from which to describe a trend. There is a large decrease from the Permian through the Triassic, from -26.4‰ ca. 261 Ma to -33.2‰ by ca. 242 Ma. Then, a

smaller increase in the Jurassic $\delta^{13}C_{phytane}$, fluctuating between ca. -33 and -30‰, is observed through to the Cretaceous. A decrease and rapid increase is observed in the Late Cretaceous, from -33.0 to -26.8‰ between ca. 98 to 93 Ma. The Paleogene shows a similar decrease followed by increase from -34.7 to -32.6‰. There is a data gap between 52 and 30 Ma, after which the overall trend continues positive from -33.0‰ finally to -25.3‰ at 0.1 Ma, the most positive value in the record of -23.2‰ at 14 Ma.

6.4   Discussion

6.4.1 Phytane-derived Ɛ_p

To calculate ε_p, the $\delta^{13}C$ of the photosynthetic biomass (δ_p) and the $\delta^{13}C$ of dissolved CO_2 (δ_d) has to be estimated. δ_p is derived from the $\delta^{13}C_{phytane}$, correcting for the isotopic offset between phytol and biomass. The latter factor was estimated by compiling culture studies from twenty-two phytoplankton species, yielding an average of 3.3 ± 1.3‰ standard deviation (Fig. S1; SI text). δ_d is estimated from $\delta^{13}C$ of carbonate, correcting for the carbon isotopic fractionation between dissolved CO_2 with respect to HCO_3^- (Mook et al., 1974). Where available (Dataset S1), the $\delta^{13}C$ of carbonate is derived from planktonic foraminifera at the same (or nearby) site as the $\delta^{13}C_{phytane}$. Where unavailable, the average $\delta^{13}C$ of carbonate is obtained from the global compiled average of $\delta^{13}C$ of marine planktonic foraminiferal carbonate at the time of deposition (Barral et al., 2017; Hayes et al., 1999). Uncertainty for marine carbonate was assigned $\pm$ 0.4 ‰ with uniform distribution. The correction for the isotopic fractionation between dissolved CO_2 with respect to HCO_3^- requires sea surface temperature (SST). This information was obtained from SST proxies (preferably $\delta^{18}O$ from planktonic foraminifera, but otherwise from other proxies such as $U^{k'}_{37}$ or TEX_{86}) measured from each site or nearby site (Dataset S1) and assigned a $\pm$ 4ºC standard deviation of uncertainty. Where SST data is unavailable, temperature was estimated by adjusting the modern site for its paleolatitude (using www.paleolatitude.org), finding the SST at that location (e.g. seatemperature.org), and then correcting the present-day SST for global temporal SST anomalies i.e. 0-56 Ma (Friedrich et al., 2012; Hansen et al., 2013); 65-455 Ma (Royer et al., 2004). For further details on the calculations and uncertainty in each parameter on calculated ε_p, see SI text.
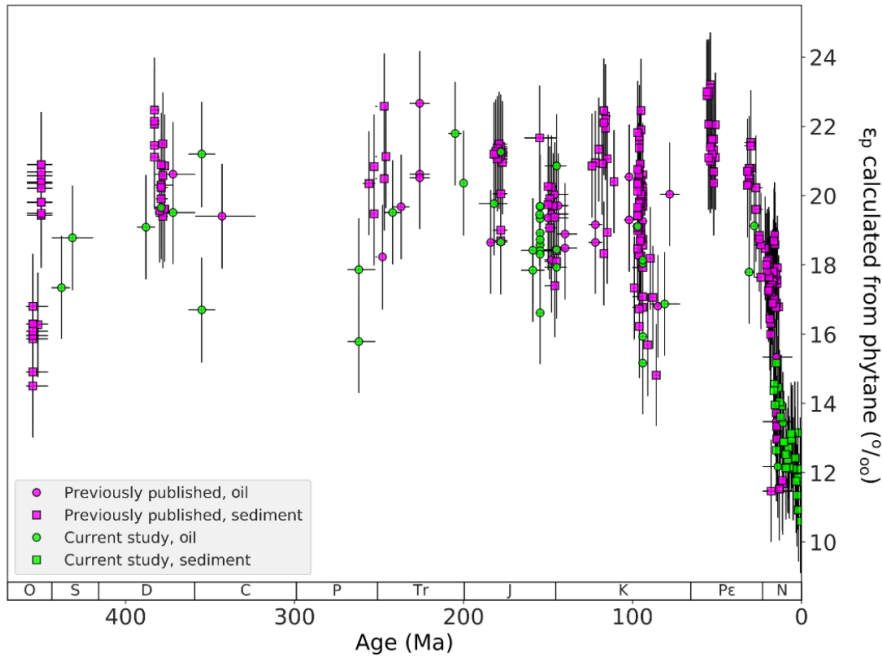
Fig. 6.2. Ɛ$_p$ calculated from phytane. Phanerozoic Ɛ$_p$ calculated from the δ^{13}C of phytane and δ^{13}C of dissolved CO$_2$ estimated from δ^{13}C of foraminifera from literature (pink) and data from this study (blue), and from sediment (square) and oil (circle). Horizontal error bars indicate dating uncertainty in sample age. Vertical error bars indicate one standard deviation (68%) uncertainty in Ɛ$_p$ estimation based on Monte Carlo simulations, culminating the uncertainty in δ^{13}C of the photosynthetic biomass (based on uncertainty in δ^{13}C of phytane ± 0.5 ‰ uniform distribution and the uncertainty in offset between biomass and phytane of 1.3‰ standard deviation) and the δ^{13}C of dissolved CO$_2$ (based on uncertainty in δ^{13}C of planktonic foraminifera ± 0.4 ‰ uniform distribution and uncertainty in SST ± 4ºC standard deviation).

Fig. 6.2 shows that calculated Ɛ$_p$ ranges from ca. 11–24‰. The vertical error bars indicate Monte Carlo simulations of uncertainty to one standard deviation (68%), the culmination of the aforementioned uncertainties within each calculation parameter. The calculated Ɛ$_p$ shows similar trends to the δ^{13}C$_{phytane}$ in Fig. 6.1 (side-by-side trends in Fig. S2) due to the relatively minor variations in the estimated δ^{13}C of dissolved CO$_2$. In this Phanerozoic record, Ɛ$_p$ does not surpass 25‰. This observation matches the theoretical assumption (Goericke et al., 1994) and culture-based observations (Hoins et al., 2016; Laws et al., 1995; Popp et al., 1998a; Wilkes et al., 2017) that maximum fractionation (Ɛ$_f$) for phytoplankton is 25-28‰. Because

our ε_p is derived from a common phytoplankton biomarker, this 25‰ limit suggests that ε_f is relatively similar among the major taxa. Furthermore, this limit suggests that ε_f has not significantly changed over the course of the Phanerozoic, despite that ε_f of Rubisco when measured in vitro has found to be substantially lower, e.g. 11‰ in *Emiliania huxleyi* (Boller et al., 2011). Young *et al.* (Young et al., 2012) show the positive selection of the chloroplast gene which encodes large Rubisco subunits appearing in the evolutionary lineage of ecologically important species (e.g. Chromista, Haptophyta, and Bacillariophyta), likely due to environmental stressors, i.e. during periods of dramatic PCO_2 declines. Considering our observed ε_p does not surpass 25‰ over the Phanerozoic, these evolutionary changes to Rubisco may not have made noticeably large changes to ε_f.

6.4.2 Estimates of PCO_2 based on phytane-derived ε_p

To estimate the dissolved carbon dioxide ($CO_{2[aq]}$) from ε_p, we use

$$CO_{2[aq]} = b / (\varepsilon_f - \varepsilon_p) \qquad\qquad [1]$$

a relationship developed by Hayes (Hayes, 1993) and Francois *et al.* (Francois et al., 1993) and which is a modification of the relationship developed for higher plants from Farquhar *et al.* (Farquhar et al., 1982). This concept has been successfully tested in laboratory cultures for $CO_{2[aq]}$ ranging over 0.4-79 µmol kg^{-1}, covering CO_2 concentrations lower than the glacial cycles to CO_2 much higher than inferred from the past e.g. (Laws et al., 2001; Popp et al., 1998b; Wilkes et al., 2017).

The term b accounts for all species-specific factors that may influence isotopic fractionation, in particular cell carbon allocation and bicarbonate uptake, as well as cell geometry and growth rate (Laws et al., 1995), and influencers of growth rate such as nutrient availability, e.g. b was found be empirically related to phosphate concentrations (Bidigare et al., 1997). The factor b has almost exclusively been studied in laboratory cultures of Haptophyte algae via alkenones, a relationship then extended into the modern environment (Bidigare et al., 1997). In marine surface sediments and suspended matter containing alkenones, b ranges from approximately 70-240 ‰ kg µM^{-1} with a mean of 165 ± 53 (Bidigare et al., 1997). Given that phytane is a general biomarker averaging the entire phytoplankton community, as opposed to the select group of Haptophytes for alkenones, we calculated b from the $\delta^{13}C$ of total organic matter in diverse modern marine surface sediments (SI text, Table S2, and references therein). Over these nineteen study sites, the average for b

is 168 ± 43 ‰ kg µM^{-1}, consistent with the alkenone studies and consistent with the b value used in previous phytane-based PCO_2 estimations (Bice et al., 2006; Damste et al., 2008). A mean value of 170 ‰ kg µM^{-1} with an assigned standard deviation of ± 60 is used throughout the record. Sensitivity plots (Fig. S3A) show that a 1% change in b results in a 1% change in PCO_2 estimation. For details on these calculations and uncertainty estimations, please see the SI text.

ϵ_f is the maximum isotopic fractionation associated with photosynthetic carbon fixation, generally ranging from 25–28‰ for algae in modern oceans and laboratory experiments (Pagani et al., 1999a; Seki et al., 2010). Given that phytane is a general phytoplankton biomarker, the exact percentages of each species in the phytoplankton composition contributing to the phytane pool is needed to estimate the value ϵ_f; something which cannot be practically achieved for ancient sediments. Thus, we use the average of the laboratory culture ϵ_f range (26.5 ± 1.5 ‰ uniform distribution) for the entire phytane-based reconstruction of PCO_2 Sensitivity tests are conducted in the SI text and shown in Fig. S3B.

To estimate the atmospheric concentration of carbon dioxide from the $CO_{2[aq]}$ we use:

$$PCO_2 = [CO_{2(aq)}] / K_0 \qquad\qquad\qquad [2]$$

based on Henry's Law, where the solubility constant K_0, expressed in M/atm, is:

$$\ln K_0 = A_1 + A_2(100/T) + A_3 \ln(T/100) + S‰ [B_1 + B_2(T/100) + B_3(T/100)^2] \quad [3]$$

where A and B are constants, T is the temperature in Kelvin, and S‰ is salinity in ‰ (Weiss, 1974). The constants used here are A_{1-3} (-58.0931, 90.5069, 22.2940) and B_{1-3} (0.02777,-0.02589, 0.00506), respectively (Weiss and Cohen, 1974). Temperatures are obtained as described above. Salinity is estimated to be 34 ‰ and assigned a ± 2 ‰ standard deviation uncertainty. Fig. 6.3 shows the consideration of these factors in the error bars of these PCO_2 estimations. The vertical error bars show one standard deviation (68%) uncertainty in PCO_2 estimation based on Monte Carlo simulations, culminating the uncertainty in b (± 60 ‰ kg µM-1 standard deviation), ϵ_f (± 1.5‰), and ϵ_p (combined uncertainties of $\delta^{13}C$ of phytane ± 0.5 ‰ uniform distribution, the offset between biomass and phytane of ± 1.3‰ standard deviation, $\delta^{13}C$ of planktonic foraminifera ± 0.4 ‰ uniform distribution, and SST ± 4ºC standard deviation). The impact of uncertainties in these parameters on the final estimated PCO_2 is discussed in the SI text and shown in Fig. S3C.

The resulting PCO_2 values based on $\delta^{13}C_{phytane}$ range from ca. 250 to 1700 µatm (Fig. 3). The estimated PCO_2 shows similar trends as $\delta^{13}C_{phytane}$ and ϵ_p; side-by-side trends in Fig. S2 show the similarity of these three different trend lines over the Phanerozoic. For further context we included the glaciation paleolatitude as determined by glaciogenic detritus compiled in Cather *et al.* (Cather et al., 2009) as an indicator of climate (Fig. 6.3). Finally, Fig. 6.3 includes context for the phytane record by incorporating the compilation of Foster *et al.* (Foster et al., 2017) which averages the
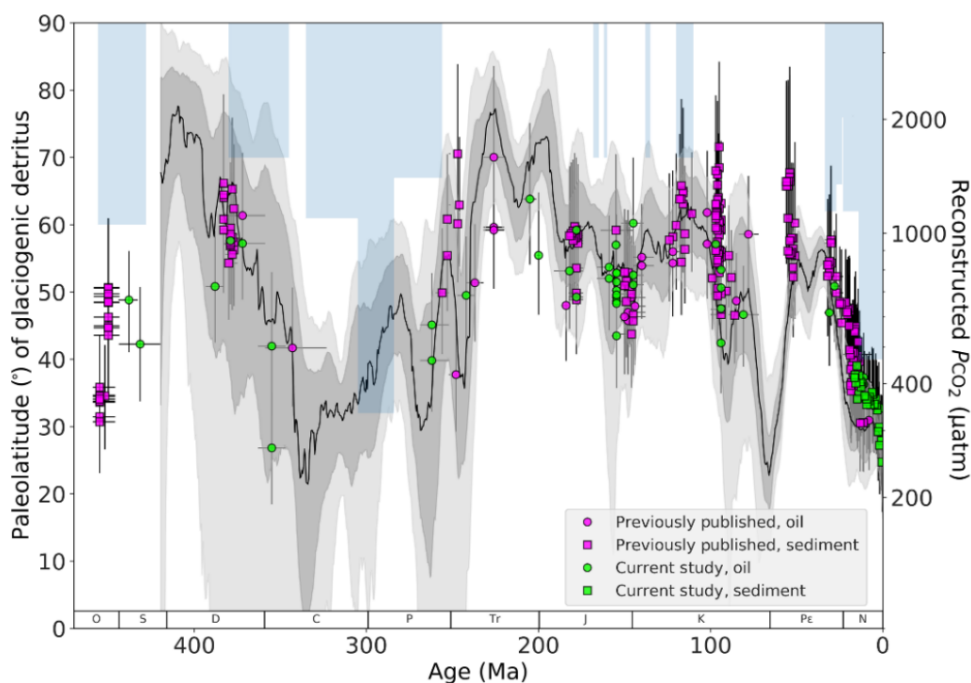

Fig. 6.3. Phanerozoic PCO_2 from phytane. Estimated Phanerozoic PCO_2 (on a log-scale) from literature (pink) and data from this study (blue), and from sediment (square) and oil (circle). Horizontal error bars indicate uncertainty in age. Vertical error bars indicate one standard deviation (68%) uncertainty in PCO_2 estimation based on Monte Carlo simulations, culminating the uncertainty in b (± 60 ‰ kg µM^{-1} standard deviation), ϵ_f (± 1.5‰ uniform distribution), and ϵ_p (combined uncertainty in $\delta^{13}C$ of phytane ± 0.5 ‰ uniform distribution, the offset between biomass and phytane ± 1.3‰ standard deviation, $\delta^{13}C$ of planktonic foraminifera ± 0.4 ‰ uniform distribution, and SST ± 4°C standard deviation). Plotted for comparison, Foster *et al.* compilation shows the Monte Carlo resampling and LOESS fit of ca. 1500 data points from the five most robust PCO_2 proxies: $\delta^{13}C$ of long-chain alkenones, $\delta^{11}B$ of marine carbonate, $\delta^{13}C$ of paleosols, stomatal densities and indices in plants, and the $\delta^{13}C$ of liverworts. 68 and 95% confidence intervals are shown in gray and light gray, respectively. The light blue bars represent glacial paleolatitude as determined by the literature compilation of glaciogenic detritus (Cather et al., 2009).

five most robust $P\text{CO}_2$ proxies in current literature: $\delta^{13}\text{C}$ of long-chain alkenones, $\delta^{11}\text{B}$ of marine carbonate, $\delta^{13}\text{C}$ of paleosols, stomatal densities and indices in plants, and the $\delta^{13}\text{C}$ of liverworts. A comparison between the phytane-based record and the Foster *et al.* compilation is also shown by timeframe (Neogene, Paleogene, Cretaceous, and Phanerozoic) in Fig. S4. The phytane-based record here contains ca. 310 estimations, fewer than the ca. 1500 data in the five-proxy Foster et al. compilation, though it does extend more than 50 Ma beyond the current record and has the potential to extend further.

The phytane-based proxy and the Foster et al. compilation show very similar values throughout the entire Phanerozoic. During the Late Ordovician (ca. 460-440 Ma), the phytane-based record jumps from ca. 450 to 700 µatm, a more dramatic shift than seen in the $\delta^{13}\text{C}_{\text{phytane}}$ and E_p trends mostly due to the low estimates for temperatures in the Ordovician (ca. 10ºC) relative to the estimates for the Devonian (ca. 23ºC). The glaciation paleolatitude for this time interval extends to 60° (Cather et al., 2009) suggesting a cold climate, which agrees with the relatively low $P\text{CO}_2$. From the Devonian into the Early Carboniferous, $P\text{CO}_2$ drops from 1400 to 300 µatm, amplified from the trend seen in phytane-based E_p but a trend that is similar to the Foster *et al.* estimations. This significant drop in $P\text{CO}_2$ is further supported by the glaciation paleolatitude, where this significantly drops to 60° at the start of the Carboniferous and moves up to 30° by the end of the Carboniferous into the early Permian (Cather et al., 2009). Then, $P\text{CO}_2$ increases from the Late Permian at 450 µatm through to the Triassic at 1600 µatm. The Jurassic exhibits a gradually decreases from 1000 µatm during the Toarcian to a low of 600 µatm in the Tithonian. From the Late Jurassic to the mid-Cretaceous, there is a gradually increase to a high of 1300 µatm. The Cenomanian starts at 1500 µatm, the highest $P\text{CO}_2$ values for the $\delta^{13}\text{C}_{\text{phytane}}$-based Phanerozoic record, which then rapidly drops to 600 µatm from ca. 98 to 85 Ma. Interestingly, the high values during the Cenomanian are much higher than those based on the Foster *et al.* compilation. This may also be attributed to the important role that temperature has when converting raw $\delta^{13}\text{C}$ values from biomarkers to $P\text{CO}_2$ (see SI text and Fig. S3). However, considering that this period is marked with extremely high sea surface temperatures (O'Brien et al., 2017), the high phytane-based $P\text{CO}_2$ estimations may be appropriate. A second increase and second drop in the record then occurs in the early Paleogene from ca. 56-54 Ma, dropping from 1400 µatm to 7500 µatm. Here, our $P\text{CO}_2$ estimates are much higher than those of Foster *et al.* Our high estimates agree with the high sea surface temperatures record during this time e.g. (Frieling et al., 2017). Finally, a decrease in $P\text{CO}_2$ from ca. 1000 to 250 µatm is observed from the late Paleogene towards the Holocene (ca. 30 Ma to 0.1 Ma), the lowest estimate for the Phanerozoic. This

6

lowering of CO_2 is supported by the glaciation paleolatitude which extended as far as 40° (Cather et al., 2009), and in agreement with the overall cooling observed in bottom water temperatures and the descent in the so-called icehouse world (Zachos et al., 2008).

6.5   Conclusion

Our Phanerozoic PCO_2 record based on the $\delta^{13}C_{phytane}$ is, to the best of our knowledge, one of the longest reconstructions based on a single proxy, extending the known PCO_2 record. As a spatially and temporally ubiquitous compound, phytane is one of the most abundantly available phytoplanktonic biomarkers suitable for PCO_2 reconstructions, more so considering that both sediments and oils can be used. Among marine-based proxies, this phytane record is the longest reconstruction for PCO_2. Phytane-based PCO_2 reconstruction yield similar estimates as compilations of PCO_2 proxies giving the potential to yield a more robust and consistent PCO_2record from a single biomarker.

Acknowledgments

Supplementary Materials

Materials and Methods

Supplementary Text

Table S1-S3

Code S1

Data S1

6
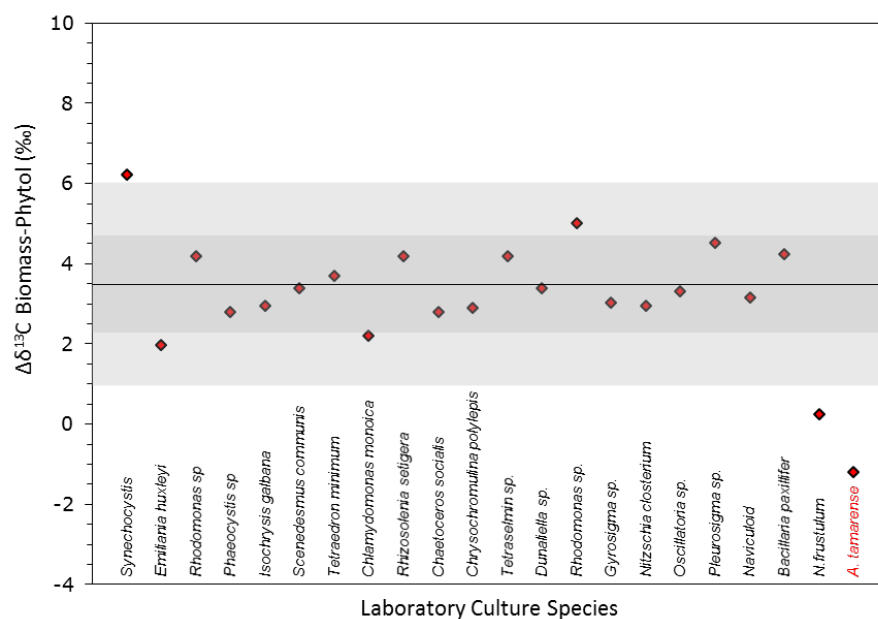
Fig. S1. Isotopic offset between biomass and phytol. On the x-axis are laboratory culture experiments from individual species of phytoplankton. The black line represents the mean, the dark band is the first standard deviation, and the light band is the second standard deviation for the entire set of phytoplankton. All references can be found in Table S1.
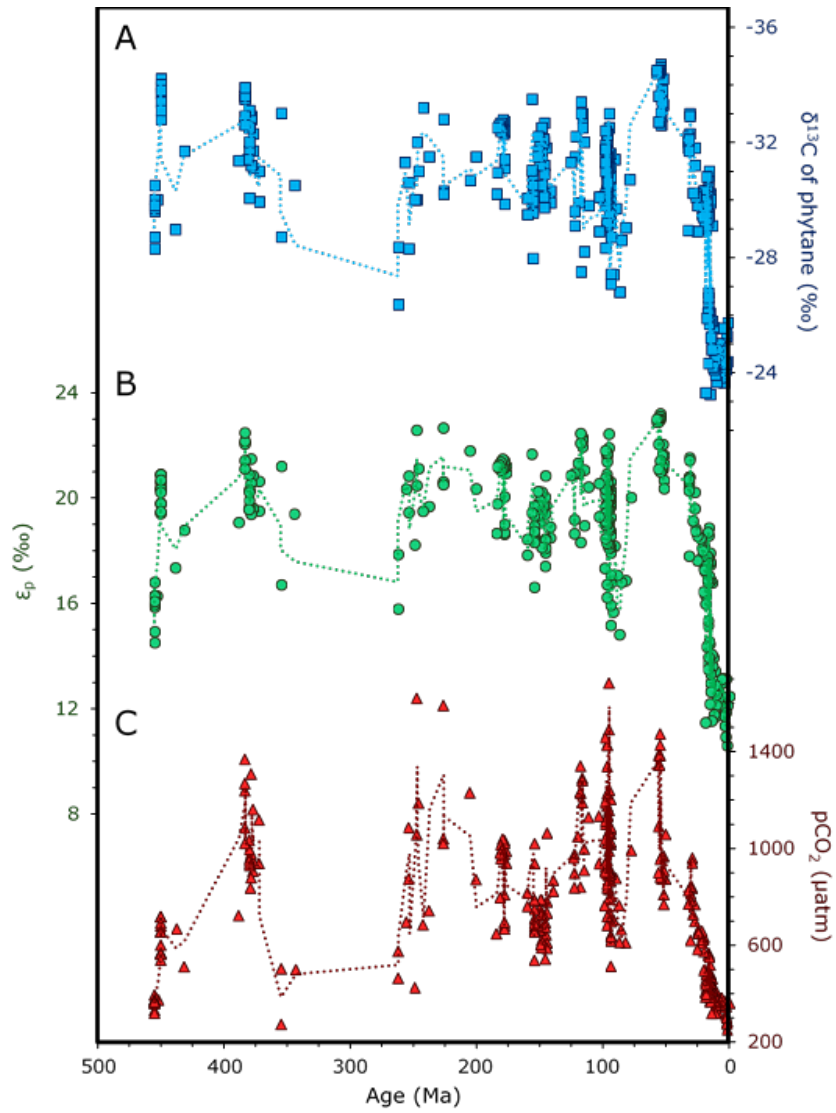
Fig. S2. Trends from reported δ^{13}C phytane data to PCO$_2$. Phytane data over the Phanerozoic for A) δ^{13}C, B) calculated ε_p, and C) estimated PCO$_2$.
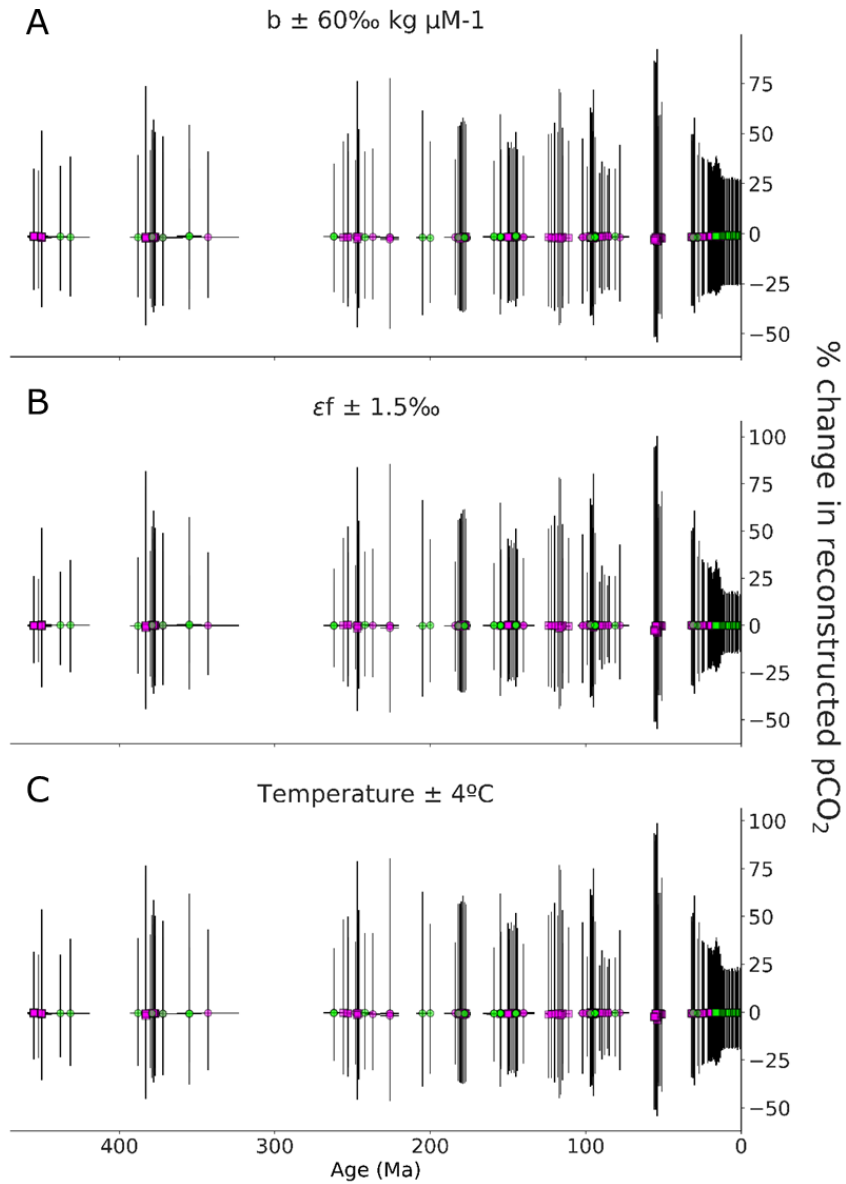
Fig. S3. Uncertainties associated with equation parameters. Percentage change in reconstructed $P\mathrm{CO}_2$ given the following uncertainties within each equation parameter, A) $b \pm 60$ ‰ kg μM^{-1} standard deviation, B) $\varepsilon_\mathrm{f} \pm 1.5$ ‰ uniform distribution, and C) temperature ± 4°C standard deviation.
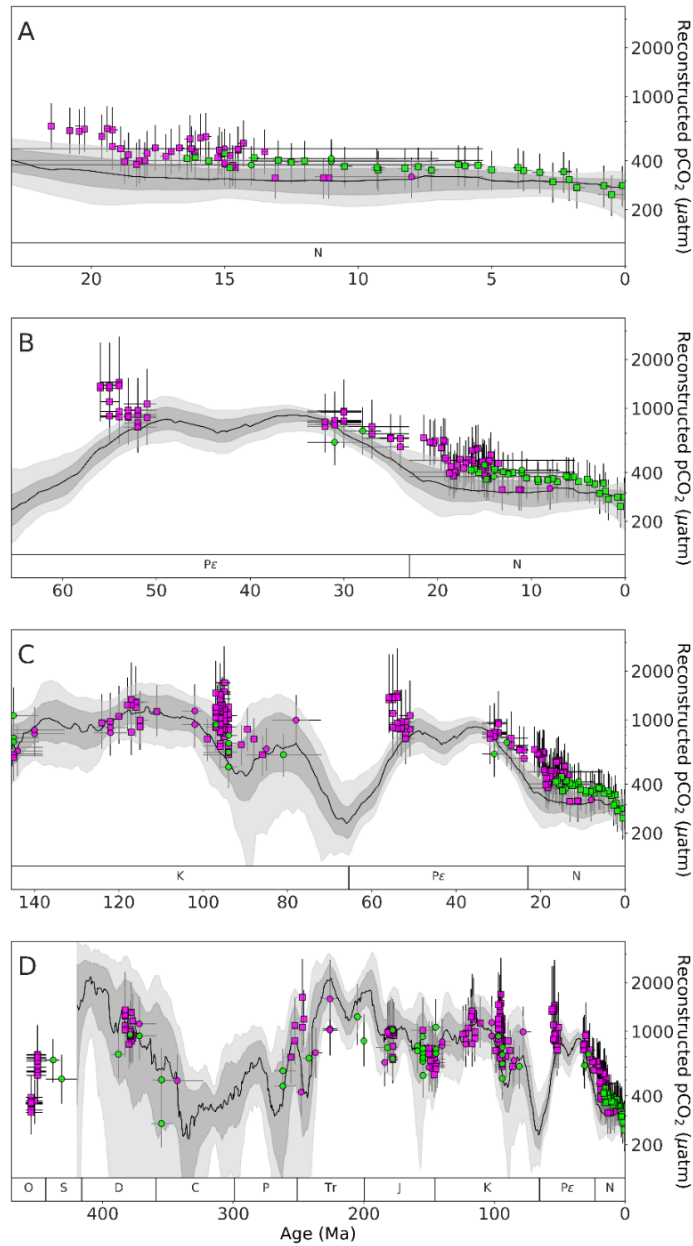
Fig. S4. *P*CO₂ from phytane over the Phanerozoic in time slices. Estimated *P*CO₂ (on a log-scale) from literature (pink) and new data (blue), by sediment (square) and oil (circle). Horizontal error bars indicate age uncertainty. Vertical error bars indicate uncertainty in estimation. Foster et al. compilation of *P*CO₂ proxies with LOESS fit (line) with 68 and 95% confidence intervals in gray and light gray plotted for comparison. A) Neogene, B) Paleogene, C) Cretaceous, and D) Phanerozoic.

Chapter 7

Synthesis

Here, new methods are developed and applied for reconstructing past atmospheric concentrations of PCO$_2$, reconstructions that are necessary to understand the fate of our near-future climate and to constrain climate sensitivity as current PCO$_2$ far surpasses historic trends (Lüthi et al., 2008; Petit et al., 1999). Although many PCO$_2$ proxies have been developed over the past several decades, there remain some substantial challenges in estimating past PCO$_2$; there are often large discrepancies among these proxies, including large uncertainties in estimation, bounds set by low or high PCO$_2$ values, and limitations in the age, location, and availability of the proxies (Hollis et al., 2019). Thus, a new approach to reconstructing PCO$_2$ may offer clarity to the current record, particularly beyond the Cenozoic.

This thesis explores the stable carbon isotopic composition (δ^{13}C) of algal biomarkers for the purpose of improving PCO$_2$ reconstructions. This is achieved through the measurement of the carbon isotopic fractionation associated with photosynthesis (ε_p), in which ^{12}C is more readily incorporated into biomass than ^{13}C by the CO$_2$-fixing enzyme Rubisco (Farquhar et al., 1989; Farquhar et al., 1982). As opposed to the traditional approach of investigating species-specific biomarkers (i.e. alkenones), general algal biomarkers were investigated, i.e. compounds which are derived from a multitude of species. Some early studies in ε_p utilized general biomarkers, such as the work done on chlorophyll-a diagenetic products, geoporphyrins (Freeman and Hayes, 1992; Popp et al., 1989). However, few subsequent studies have followed this broader approach to ε_p, with several exceptions of Cretaceous PCO$_2$ reconstructions from another chlorophyll-a diagenetic product, i.e. phytane (Bice et al., 2006; Naafs and Pancost, 2016; Sinninghe Damsté et al., 2008; van Bentum et al., 2012). In this thesis a comprehensive examination of this approach was done, using modern environmental samples over high PCO$_2$ gradients (Chapters 2-3) and through the application using ancient sediments over different timescales: 200 ka (Chapter 4), 16 Ma (Chapter 5), and 500 Ma (Chapter 6).

Because general algal biomarkers are intrinsically not representative of just a few species, laboratory cultures cannot be readily utilized. Instead, initial explorative efforts focused on environmental samples which contain natural phytoplankton communities. This was achieved by examining the isotopic composition of natural phytoplankton communities along a naturally occurring, high CO$_2$ gradient from a continually bubbling CO$_2$ seep towards ambient values within the same bay, first in Japan (Chapter 2) and then in Italy (Chapter 3). In both chapters, a targeted analysis of general algal biomarkers for diatoms (i.e. loliolide), eukaryotes (i.e. cholesterol), and photoautotrophs (i.e. phytol) were conducted, based on their omnipresence in

7

the collected sea surface sediments. At both sites, the $\delta^{13}C$ values of the three biomarkers decreased from the ambient PCO$_2$ site to the high PCO$_2$ site near the seep, suggesting that they were indeed influenced by CO$_2$ concentrations in the seawater. However, the Japan-based reconstructions in Chapter 2 underestimated absolute values. We considered the conspicuously different isotopic values between June and September sea surface sediments, which presumably should show the same long-term, integrated signal. A simple explanation is annual extreme weather events (i.e. typhoons) that likely mix the sediments of bay and dilute the high PCO$_2$ signal. At the CO$_2$ seep off the coast of Vulcano Island, Italy, loliolide showed large variability for much of the transect than other biomarkers. Light microscopy showed drastically different assemblages and abundances of diatoms at each site, particularly between centric and pennate diatoms, likely impacting isotopic fractionation because of the different cell geometries and morphologies (Popp et al., 1998) and carbon concentrating mechanisms (Hinga et al., 1994), as have been observed in diatom species (Burkhardt et al., 2001; Pancost et al., 1997). This limits the applicability of loliolide as a PCO$_2$ proxy. Phytol, on the other hand, did show a strong, consistent isotopic change over the transect like at Shikine Island, and was thus used to estimate dissolved CO$_2$ and PCO$_2$. As compared with literature values of measured dissolved CO$_2$, phytol-based reconstructions had remarkably close values. This confirms the hypothesis that extreme weather events in Japan (Chapter 2) were masking the CO$_2$ signal, in contrast to the site in Italy. This study also confirms that general algal biomarkers that consider the entire phytoplankton community (e.g. phytol instead of loliolide) can be used for ε_p-based PCO$_2$ reconstructions.

Applying the knowledge from Chapters 2 and 3, Chapter 4 then reconstructs PCO$_2$ from the $\delta^{13}C$ of phytol, along with the more conventionally-used alkenones, from sediments deposited during late Pleistocene sapropel formation in the Eastern Mediterranean, a time interval chosen for its overlap with known PCO$_2$ concentrations, i.e. from gas bubbles trapped in ice cores. The resulting estimates for PCO$_2$ range from ca. 300 to 450 μatm for phytol and from ca. 330 to 390 μatm for alkenones ($\pm$ 100 μatm s.d.), which is ca. 100 μatm higher than the ice core estimations. These results correspond with the disequilibrium of the Mediterranean Sea with atmospheric PCO$_2$ due to the relatively high alkalinity in the Mediterranean (Rivaro et al., 2010) and has been observed be ca. 100 μatm above the global average of PCO$_2$ (Bégovic and Copin-Montégut, 2002). This suggests that both proxies may yield robust PCO$_2$ estimations in the late Pleistocene. However, there is a lack of correlation between individual data from the sapropels and ice core values which may be due to the higher variability of change in CO$_2$ concentrations at a local site versus the global average, periodic deep-water convection (Melki et al., 2010), a

variable growth rate (Zhang et al., 2013), or the implementation of carbon concentrating mechanisms in some algae at lower CO_2 concentrations (Badger et al., 2019; Stoll et al., 2019).

The results in Chapters 2-4 suggest promise for general biomarkers as a PCO_2 proxy but also some issues, particularly the potential issue of carbon concentrating mechanisms that may mask the relationship between isotopic fractionation with CO_2 concentrations. The equations used throughout this thesis to estimate PCO_2 rely on the assumption of the diffusive model, i.e. that dissolved $CO_{2[aq]}$ passively enters the algal cell when CO_2 availability is high relative to cellular carbon demand, as supported by laboratory cultures and environmental experiments (e.g. Francois et al., 1993; Rau et al., 1996). However, carbon concentrating mechanisms may affect cell membrane permeability (e.g. Cassar et al., 2006; Hopkinson et al., 2011) and consequently provide additional internal CO_2 under insufficient levels of external CO_2 at the active site of Rubisco via HCO_3^- transport (Kottmeier et al., 2016; Raven and Beardall, 2014). Active uptake of HCO_3^- is a concern given the substantial difference between the $\delta^{13}C$ of HCO_3^- (0‰) and CO_2 (−8‰) (Mook, 1974), as well as the current lack of experimental data to explain the effect of carbon concentrating mechanisms on the $\delta^{13}C$ of algae (Stoll et al., 2019). Indeed, at Ocean Drilling Program Site 999, this mechanism has been invoked to explain the muted response observed of the $\delta^{13}C$ of alkenones-reconstructed PCO_2 as compared with the $\delta^{11}B$ of foraminifer shell-reconstructed PCO_2, as well ice core PCO_2 data (Badger et al., 2019). Lower sensitivity of ε_p to PCO_2 than proposed by the diffusive model has also been recently proposed, based on the results of a statistical multilinear regression model that quantitatively considering factors that influence ε_p in alkenone-producing algae based on laboratory culture studies (Stoll et al., 2019). This recent literature suggests that ε_p from alkenones (and probably also ε_p from phytol and likely other general algal biomarkers) may have a lessened relationship with PCO_2 at low PCO_2 concentrations as many algal species actively acquire CO_2 from other sources than passive CO_2 diffusion. For this reason, caution is recommended with the proxy during periods of PCO_2 stress, especially the Quaternary. Nevertheless, and keeping the considerations of Chapter 2-4 in mind, our results still show that PCO_2 estimates based on general algal biomarkers may be as useful as those of alkenones and provide broadly robust estimates over large PCO_2 ranges (up to 3x present day values; Chapter 6).

In Chapter 5 and 6, longer trends of PCO_2 from the $\delta^{13}C$ general algal biomarkers were reconstructed. In Chapter 5, the mid-Miocene Climatic Optimum (17-15 Ma) was the object of study, a particularly important time period for understanding

7

climate sensitivity given that 1) it is considered an analogue for modern PCO_2 and 2) it has highly disputed PCO_2 estimations. In Chapter 5, sediments from Deep Sea Drilling Project Site 467 off the coast of California span further back in time than the previous chapters; as such, the diagenetic products of phytol (now phytane) and cholesterol (now 5α-cholestane, 24-ethyl-5α-cholestane, and 24-methyl-5α-cholestane) are instead used to reconstruct PCO_2. The PCO_2 reconstructed from the isotopic composition of steranes and phytane all showed a steady declining trend starting at ca. 500-580 μatm from 16.4 Ma to ca. 300 μatm by 0.1 Ma, tracking with the PCO_2 reconstructions estimated from alkenones taken in the same core (though only spanning the final 4 Ma). This differs from the majority of other PCO_2 proxies from the literature which show an unmoving average value throughout this period, although it should be noted that the individual estimates show large scatter and some unrealistic estimations, e.g. 80 μatm (Foster et al., 2017). As compared with global sea surface temperatures, on the other hand, our reconstructed values from general algal biomarkers mirror the steady cooling trends, suggesting that PCO_2 and temperature were in fact coupled during this time period. This provides key information for understanding climate sensitivity and further suggests that the $\delta^{13}C$ of general algal biomarkers are promising for longer reconstructions.

Given the promising PCO_2 reconstructions in Chapter 5, secular trends in PCO_2 from phytane over the Phanerozoic were then reconstructed (Chapter 6). Marine sediments and oils from open ocean settings were used in order to constrain the source of phytane to phytoplankton and the data was screened for extreme environmental conditions, e.g. salinity crisis, which might significantly affect the overall signal. In the reconstructions of PCO_2 from the $\delta^{13}C$ of phytane, each parameter was thoroughly tested and estimated via Monte Carlo simulations in order to provide a comprehensive investigation on uncertainties in estimation. The PCO_2 reconstructed values range from ca. 250 to 1700 μatm and showed remarkably similar trends to those compiled of five other PCO_2 proxies (Foster et al., 2017). Overall, these findings show that the $\delta^{13}C$ of general algal biomarkers has great potential for reconstructing PCO_2 for much of Earth's history, offering the longest spanning and most ubiquitous proxy for reconstructing PCO_2. Nevertheless, despite this extensive record over the Phanerozoic with more than 300 data, some important time periods are missing. For example, understanding data-scarce time periods, e.g. Silurian or Devonian, may provide a fuller and more robust understanding of past PCO_2 and provide further insights into the effectiveness of the phytane-based proxy, as well as provide climate information on these less studied periods. Furthermore, although multiple general algal biomarkers were explored in Chapters 2, 3, and 5, the remaining work was focused on phytol and its diagenetic product phytane.

Expansion of this general algal biomarker investigation to other compounds, such as cholesterol and its diagenetic products, may be useful to reconstruct longer, more robust secular trends.

In addition to further application of general algal biomarkers for $P\text{CO}_2$ reconstructions, further investigation of the proxy's underpinnings is needed. For example, the isotopic fractionation as a theoretical concept requires further investigation, such as the role of active uptake for a proxy otherwise conceptually built on the assumption of passive diffusion. Furthermore, although the reconstructed $P\text{CO}_2$ values in this thesis fit mostly with other proxy data, the uncertainties on those values remain very large and future research should focus on reducing these uncertainties. Some ways to handle these uncertainties include the constraint of factors to fractionation other than CO_2, such as exploring the b-factor or investigating maximum fractionation due to CO_2-fixation (ε_f), both of which are primarily based on theory, as well as laboratory culture observations of alkenone-producing species, not entire phytoplankton communities. Furthermore, major reconsiderations of the proxy in Wilkes and Pearson (2019) suggests that isotopic differences in algae may not rely as heavily on kinetic isotopic fractionation as a whole, but rather on limitations of growth by photon and nutrient fluxes, which could lead to major ecological transitions and consequent change in producers in that given environment, each with their own unique fractionation factors.

In order to tackle these major uncertainties, the use of modern environmental studies and laboratory cultures may provide some answers. For example, the influence of growth rates and consequently on ε_p and the b-factor could be examined via a stationary sediment trap (far from the influences of terrestrial input) in which organic matter is collected throughout the year in order to observe isotopic changes in general biomarkers in concert with concentration fluctuations due to growth rate changes. Furthermore, the sediment trap data could be compared with nearby sea surface sediment in order to understand the how effects observed in the sediment trap are reflected in surface sediments. Another useful study would be a global core top calibration of ε_p. Exploring changes in isotopic fractionation on a global scale could illuminate how sensitive is the proxy to CO_2 versus other environmental parameters (i.e. productivity, temperature, salinity), constraining these parameters, and especially the b-value. In Fig. 1, pilot data shows the $\delta^{13}\text{C}$ of phytol in sea surface sediments of a Greenland-United Kingdom transect, an Africa-South America transect, and the Okhotsk Sea. The isotopic compositions range from -23 to -31 ‰ which is larger than can be expected based on differences in local CO_2 concentrations and suggest possible other factors that may play a role in fractionation. This requires

further investigation and is key to grasping the extent of uncertainties in paleoreconstructions of PCO$_2$. Finally, although laboratory cultures were not examined here as we examined general phytoplankton biomarkers, they can be useful in constraining e.g. maximum Rubisco fractionation and the offset between the isotopic composition if phytol and biomass.

Overall, modern environmental studies described in this thesis show the sensitivity of several general algal biomarkers to PCO$_2$ over a high CO$_2$ gradient. This thesis also demonstrates the ability of these general algal biomarkers to reconstruct PCO$_2$ similar to those reconstructed from other proxies. Although further investigation on this PCO$_2$ proxy is required, δ^{13}C of algal biomarkers show great promise for the reconstruction of PCO$_2$ over deep geological time.
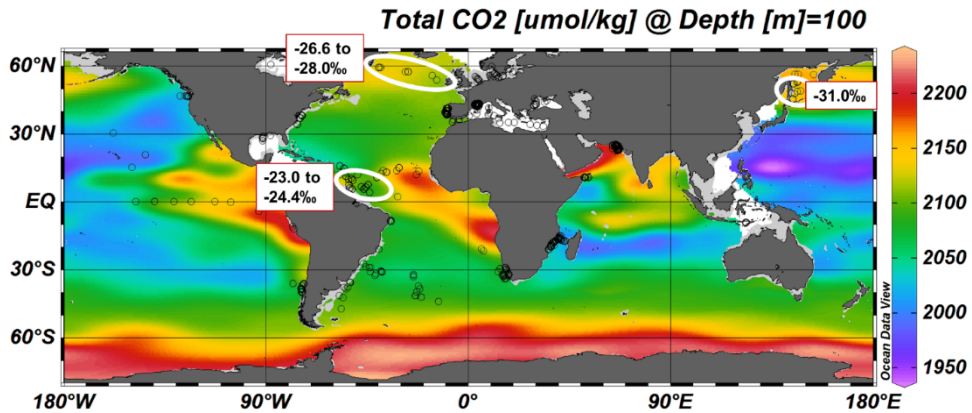

Fig. 1. Map of potential global core top calibration sites. The map shows potential sites (black circles), as well as some preliminary results from a pilot study. Each region has very different isotopic composition values, ranging from -23 to -31 ‰, a much larger range than expected.

Fieldwork at CO$_2$ seep in Vulcano Island, Italy

Fieldwork at CO$_2$ seep in Shikine Island, Japan

References

Agostini, S., Harvey, B., Wada, S., Kon, K., Milazzo, M., Inaba, K., Hall-Spencer, J.M., 2018. Ocean acidification drives community shifts towards simplified non-calcified habitats in a subtropical-temperate transition zone. Sci Rep-Uk 8.

Agostini, S., Wada, S., Kon, K., Omori, A., Kohtsuka, H., Fujimura, H., Tsuchiya, Y., Sato, T., Shinagawa, H., Yamada, Y., Inaba, K., 2015. Geochemistry of two shallow CO_2 seeps in Shikine Island (Japan) and their potential for ocean acidification research. Regional Studies in Marine Science 2, 45-53.

Badger, M.P.S., Chalk, T.B., Foster, G.L., Bown, P.R., Gibbs, S.J., Sexton, P.F., Schmidt, D.N., Pälike, H., Mackensen, A., Pancost, R.D., 2019. Insensitivity of alkenone carbon isotopes to atmospheric CO_2 at low to moderate CO_2 levels. Climate of the Past 15, 539-554.

Badger, M.P.S., Lear, C.H., Pancost, R.D., Foster, G.L., Bailey, T.R., Leng, M.J., Abels, H.A., 2013. CO_2 drawdown following the middle Miocene expansion of the Antarctic Ice Sheet. Paleoceanography 28.

Badger, M.R., Andrews, T.J., Whitney, S.M., Ludwig, M., Yellowlees, D.C., Leggat, W., Price, G.D., 1998. The diversity and coevolution of Rubisco, plastids, pyrenoids, and chloroplast-based CO_2-concentrating mechanisms in algae. Can J Bot 76, 1052-1071.

Barral, A., Gomez, B., Fourel, F., Daviero-Gomez, V., Lecuyer, C., 2017. CO_2 and temperature decoupling at the million-year scale during the Cretaceous Greenhouse. Sci Rep-Uk 7.

Barron, J.A., Keller, G., 1983. Paleotemperature Oscillations in the Middle and Late Miocene of the Northeastern Pacific. Micropaleontology 29, 150-&.

Beerling, D.J., Royer, D.L., 2011. Convergent Cenozoic CO_2 history. Nat Geosci 4, 418-420.

Bégovic, M., Copin-Montégut, C., 2002. Processes controlling annual variations in the partial pressure of CO_2 in surface waters of the central northwestern Mediterranean Sea (Dyfamed site). Deep-Sea Res Pt Ii 49, 2031-2047.

Benthien, A., Zondervan, I., Engel, A., Hefter, J., Terbruggen, A., Riebesell, U., 2007. Carbon isotopic fractionation during a mesocosm bloom experiment dominated by Emiliania huxleyi: Effects of CO_2 concentration and primary production. Geochim Cosmochim Ac 71, 1528-1541.

Bernacchi, C.J., VanLoocke, A., 2015. Terrestrial Ecosystems in a Changing Environment: A Dominant Role for Water. Annual Review of Plant Biology, Vol 66 66, 599-622.

Bernal, P.A., McGowan, J.A., 1981. Advection and upwelling in the California Current, in: Garrison, R.E., Douglas, R.G. (Eds.), The Monterey Formation and related siliceous rocks of California. Society of Economic Paleontologists and Mineralogists, Los Angeles, CA, pp. 1-14.

Betts, R.A., Jones, C.D., Knight, J.R., Keeling, R.F., Kennedy, J.J., 2016. El Nino and a record CO_2 rise. Nat Clim Change 6, 806-810.

Bice, K.L., Birgel, D., Meyers, P.A., Dahl, K.A., Hinrichs, K.U., Norris, R.D., 2006. A multiple proxy and model study of Cretaceous upper ocean temperatures and atmospheric CO_2 concentrations. Paleoceanography 21.

R

Bidigare, R.R., Fluegge, A., Freeman, K.H., Hanson, K.L., Hayes, J.M., Hollander, D., Jasper, J.P., King, L.L., Laws, E.A., Milder, J., Millero, F.J., Pancost, R., Popp, B.N., Steinberg, P.A., Wakeham, S.G., 1997. Consistent fractionation of C-13 in nature and in the laboratory: Growth-rate effects in some haptophyte algae. Global Biogeochem Cy 11, 279-292.

Bijl, P.K., Houben, A.J.P., Schouten, S., Bohaty, S.M., Sluijs, A., Reichart, G.J., Damste, J.S.S., Brinkhuis, H., 2010. Parallel trends in Middle Eocene temperatures and atmospheric carbon dioxide concentration? Geochim Cosmochim Ac 74, A90-A90.

Boatta, F., D'Alessandro, W., Gagliano, A.L., Liotta, M., Milazzo, M., Rodolfo-Metalpa, R., Hall-Spencer, J.M., Parello, F., 2013. Geochemical survey of Levante Bay, Vulcano Island (Italy), a natural laboratory for the study of ocean acidification. Mar Pollut Bull 73, 485-494.

Boller, A.J., Thomas, P.J., Cavanaugh, C.M., Scott, K.M., 2011. Low stable carbon isotope fractionation by coccolithophore RubisCO. Geochim Cosmochim Ac 75, 7200-7207.

Bolton, C.T., Hernandez-Sanchez, M.T., Fuertes, M.A., Gonzalez-Lemos, S., Abrevaya, L., Mendez-Vicente, A., Flores, J.A., Probert, I., Giosan, L., Johnson, J., Stoll, H.M., 2016. Decrease in coccolithophore calcification and CO_2 since the middle Miocene. Nat Commun 7.

Bolton, C.T., Stoll, H.M., 2013. Late Miocene threshold response of marine algae to carbon dioxide limitation. Nature 500, 558-562.

Boudreau, B.P., Middelburg, J.J., Sluijs, A., van der Ploeg, R., 2019. Secular variations in the carbonate chemistry of oceans over the Cenozoic. EPSL 512, 194-206.

Bowen, G.J., Beerling, D.J., 2004. An integrated model for soil organic carbon and CO_2: Implications for paleosol carbonate pCO_2 paleobarometry. Global Biogeochem Cy 18.

Brassell, S.C., 2014. Climatic influences on the Paleogene evolution of alkenones. Paleoceanography 29, 255-272.

Brassell, S.C., Eglinton, G., Marlowe, I.T., Pflaumann, U., Sarnthein, M., 1986. Molecular Stratigraphy - a New Tool for Climatic Assessment. Nature 320, 129-133.

Breecker, D.O., Sharp, Z.D., McFadden, L.D., 2010. Atmospheric CO_2 concentrations during ancient greenhouse climates were similar to those predicted for AD 2100. P Natl Acad Sci USA 107, 576-580.

Brinkman, T.J., Smith, A.M., 2015. Effect of climate change on crustose coralline algae at a temperate vent site, White Island, New Zealand. Mar Freshwater Res 66, 360-370.

Burkhardt, S., Amoroso, G., Riebesell, U., Sultemeyer, D., 2001. CO_2 and HCO_3- uptake in marine diatoms acclimated to different CO_2 concentrations. Limnol Oceanogr 46, 1378-1391.

Caillon, N., Severinghaus, J.P., Jouzel, J., Barnola, J.M., Kang, J.C., Lipenkov, V.Y., 2003. Timing of atmospheric CO_2 and Antarctic temperature changes across termination III. Science 299, 1728-1731.

Cassar, N., Laws, E.A., Popp, B.N., 2006. Carbon isotopic fractionation by the marine diatom Phaeodactylum tricornutum under nutrient- and light-limited growth conditions. Geochim Cosmochim Ac 70, 5323-5335.

Castaneda, I.S., Werne, J.P., Johnson, T.C., 2009. Influence of climate change on algal community structure and primary productivity of Lake Malawi (East Africa) from the Last Glacial Maximum to present. Limnol Oceanogr 54, 2431-2447.

Cather, S.M., Dunbar, N.W., McDowell, F.W., McIntosh, W.C., Scholle, P.A., 2009. Climate forcing by iron fertilization from repeated ignimbrite eruptions: The icehouse-silicic large igneous province (SLIP) hypothesis. Geosphere 5, 315-324.

Cerling, T.E., 1991. Carbon-Dioxide in the Atmosphere - Evidence from Cenozoic and Mesozoic Paleosols. Am J Sci 291, 377-400.

Chiodini, G., Cioni, R., Marini, L., 1993. Reactions Governing the Chemistry of Crater Fumaroles from Vulcano-Island, Italy, and Implications for Volcanic Surveillance. Appl Geochem 8, 357-371.

Cornwall, C.E., Revill, A.T., Hall-Spencer, J.M., Milazzo, M., Raven, J.A., Hurd, C.L., 2017. Inorganic carbon physiology underpins macroalgal responses to elevated CO_2. Sci Rep-Uk 7.

Cotton, J.M., Sheldon, N.D., 2012. New constraints on using paleosols to reconstruct atmospheric pCO_2. Geol Soc Am Bull 124, 1411-1423.

DaMatta, F.M., Godoy, A.G., Menezes-Silva, P.E., Martins, S.C.V., Sanglard, L.M.V.P., Morais, L.E., Torre-Neto, A., Ghini, R., 2016. Sustained enhancement of photosynthesis in coffee trees grown under free-air CO_2 enrichment conditions: disentangling the contributions of stomatal, mesophyll, and biochemical limitations. J Exp Bot 67, 341-352.

Dando, P.R., Stuben, D., Varnavas, S.P., 1999. Hydrothermalism in the Mediterranean Sea. Prog Oceanogr 44, 333-367.

de Graaf, W., Damste, J.S.S., Deleeuw, J.W., 1992. Laboratory Simulation of Natural Sulfurization .1. Formation of Monomeric and Oligomeric Isoprenoid Polysulfides by Low-Temperature Reactions of Inorganic Polysulfides with Phytol and Phytadienes. Geochim Cosmochim Ac 56, 4321-4328.

de Leeuw, J.W., Meer, F.W.V.D., Rijpstra, W.I.C., Schenck, P.A., 1980. On the occurrence and structural identification of long chain unsaturated ketones and hydrocarbons in sediments, in: Douglas, A.E., Maxwell, J.R. (Eds.), Advances in Organic Geochemistry. Pergamon, Oxford, pp. 211-217.

Degens, E.T., Guillard, R.R., Sackett, W.M., Hellebus.Ja, 1968. Metabolic Fractionation of Carbon Isotopes in Marine Plankton .I. Temperature and Respiration Experiments. Deep-Sea Res 15, 1-&.

Domack, C.R., 1986. Reconstruction of California Current at 5, 8, and 10 Ma Using Radiolarian Indicators. Aapg Bull 70, 467-467.

Eek, M.K., Whiticar, M.J., Bishop, J.K.B., Wong, C.S., 1999. Influence of nutrients on carbon isotope fractionation by natural populations of Prymnesiophyte algae in NE Pacific. Deep-Sea Res Pt Ii 46, 2863-2876.

Elrod, L.W., Katz, B.J., 1982. Organic Geochemistry of Dsdp Site-467, Middle Miocene to Lower Pliocene Strata. Abstr Pap Am Chem S 183, 57-Geoc.

Emeis, K.-C., Schulz, H., Struck, U., Rossignol-Strick, M., Erlenkeuser, H., Howell, M.W., Kroon, D., Mackensen, A., Ishizuka, S., Oba, T., Sakamoto, T., Koizumi, I., 2003. Eastern Mediterranean surface water temperatures and δ18O composition during deposition of sapropels in the late Quaternary. Paleoceanography 18.

Eppley, R.W., Holm-Hansen, O., 1986. Primary production in the Southern California Bight, in: Eppley, R.W. (Ed.), Plankton dynamics of the Southern California Bigh. Sprigner-Verlag, New York, pp. 176-215.

Erez, J., Luz, B., 1983. Experimental Paleotemperature Equation for Planktonic-Foraminifera. Geochim Cosmochim Ac 47, 1025-1031.

R

Fabricius, K.E., Langdon, C., Uthicke, S., Humphrey, C., Noonan, S., De'ath, G., Okazaki, R., Muehllehner, N., Glas, M.S., Lough, J.M., 2011. Losers and winners in coral reefs acclimatized to elevated carbon dioxide concentrations. Nat Clim Change 1, 165-169.

Farquhar, G.D., Ehleringer, J.R., Hubick, K.T., 1989. Carbon Isotope Discrimination and Photosynthesis. Annu Rev Plant Phys 40, 503-537.

Farquhar, G.D., Oleary, M.H., Berry, J.A., 1982. On the Relationship between Carbon Isotope Discrimination and the Inter-Cellular Carbon-Dioxide Concentration in Leaves. Aust J Plant Physiol 9, 121-137.

Flower, B.P., Kennett, J.P., 1993. Middle Miocene Ocean-Climate Transition - High-Resolution Oxygen and Carbon Isotopic Records from Deep-Sea Drilling Project Site 588a, Southwest Pacific. Paleoceanography 8, 811-843.

Forster, P., Ramaswamy, V., Artaxo, P., Berntsen, T., Betts, R., Fahey, D.W., Haywood, J., Lean, J., Lowe, D.C., Myhre, G., Nganga, J., Prinn, R., Raga, G., Schulz, M., Van Dorland, R., 2007. Contribution of Working Group I to the Fourth Assessment Report of the Intergovernmental Panel on Climate Change, in: Solomon, S., Qin, D., Manning, M., Chen, Z., Marquis, M., Averyt, K.B., Tignor, M., Miller, H.L. (Eds.), Climate Change 2007: The Physical Science Basis. Cambridge University Press, Cambridge, United Kingdom, pp. 131-217.

Foster, G.L., Lear, C.H., Rae, J.W.B., 2012. The evolution of pCO(2), ice volume and climate during the middle Miocene. Earth and Planetary Science Letters 341, 243-254.

Foster, G.L., Royer, D.L., Lunt, D.J., 2017. Future climate forcing potentially without precedent in the last 420 million years. Nat Commun 8.

Francois, R., Altabet, M.A., Goericke, R., Mccorkle, D.C., Brunet, C., Poisson, A., 1993. Changes in the Delta-C-13 of Surface-Water Particulate Organic-Matter across the Subtropical Convergence in the Sw Indian-Ocean. Global Biogeochem Cy 7, 627-644.

Franks, P.J., Royer, D.L., Beerling, D.J., Van de Water, P.K., Cantrill, D.J., Barbour, M.M., Berry, J.A., 2014. New constraints on atmospheric CO_2 concentration for the Phanerozoic. Geophys Res Lett 41, 4685-4694.

Frazzetta, G., La Volpe, L., Sheridan, M.F., 1984. Evolution of the Fossa cone, Vulcano. Journal of Volcanology and Geothermal Research 17, 139-360.

Freeman, K.H., Hayes, J.M., 1992. Fractionation of Carbon Isotopes by Phytoplankton and Estimates of Ancient CO_2 Levels. Global Biogeochem Cy 6, 185-198.

Friedrich, O., Norris, R.D., Erbacher, J., 2012. Evolution of middle to Late Cretaceous oceans-A 55 m.y. record of Earth's temperature and carbon cycle. Geology 40, 107-110.

Frieling, J., Gebhardt, H., Huber, M., Adekeye, O.A., Akande, S.O., Reichart, G.J., Middelburg, J.J., Schouten, S., Sluijs, A., 2017. Extreme warmth and heat-stressed plankton in the tropics during the Paleocene-Eocene Thermal Maximum. Sci Adv 3.

Giordano, M., Beardall, J., Raven, J.A., 2005. CO_2 concentrating mechanisms in algae: Mechanisms, environmental modulation, and evolution. Annual Review of Plant Biology 56, 99-131.

Goericke, R., Fry, B., 1994. Variations of Marine Plankton Delta-C-13 with Latitude, Temperature, and Dissolved CO_2 in the World Ocean. Global Biogeochem Cy 8, 85-90.

Goericke, R., J.P, M., B., F., 1994. Physiology of isotope fractionation in algae and cyanobacteria, in: K, L., B, M. (Eds.), Stable Isotope in Ecology. Blackwell, Cambridge, pp. 187-221.

Grant, K.M., Grimm, R., Mikolajewicz, U., Marino, G., Ziegler, M., Rohling, E.J., 2016. The timing of Mediterranean sapropel deposition relative to insolation, sea-level and African monsoon changes. Quaternary Sci Rev 140, 125-141.

Grelaud, M., Marino, G., Ziveri, P., Rohling, E.J., 2012. Abrupt shoaling of the nutricline in response to massive freshwater flooding at the onset of the last interglacial sapropel event. Paleoceanography 27.

Grice, K., Breteler, W.C.M.K., Schouten, S., Grossi, V., de Leeuw, J.W., Damste, J.S.S., 1998. Effects of zooplankton herbivory on biomarker proxy records. Paleoceanography 13, 686-693.

Hall-Spencer, J.M., Rodolfo-Metalpa, R., Martin, S., Ransome, E., Fine, M., Turner, S.M., Rowley, S.J., Tedesco, D., Buia, M.C., 2008. Volcanic carbon dioxide vents show ecosystem effects of ocean acidification. Nature 454, 96-99.

Hansen, J., Ruedy, R., Sato, M., Lo, K., 2010. Global Surface Temperature Change. Rev Geophys 48.

Hansen, J., Sato, M., Russell, G., Kharecha, P., 2013. Climate sensitivity, sea level and atmospheric carbon dioxide. Philos T R Soc A 371.

Harvey, B.P., Agostini, S., Wada, S., Inaba, K., Hall-Spencer, J.M., 2018. Dissolution: The Achilles' Heel of the Triton Shell in an Acidifying Ocean. Front Mar Sci 5.

Haworth, M., Elliott-Kingston, C., McElwain, J.C., 2013. Co-ordination of physiological and morphological responses of stomata to elevated [CO_2] in vascular plants. Oecologia 171, 71-82.

Hayes, J.M., 1993. Factors Controlling C-13 Contents of Sedimentary Organic-Compounds - Principles and Evidence. Mar Geol 113, 111-125.

Hayes, J.M., Freeman, K.H., Popp, B.N., Hoham, C.H., 1990. Compound-Specific Isotopic Analyses - a Novel Tool for Reconstruction of Ancient Biogeochemical Processes. Org Geochem 16, 1115-1128.

Hayes, J.M., Popp, B.N., Takigiku, R., Johnson, M.W., 1989. An Isotopic Study of Biogeochemical Relationships between Carbonates and Organic-Carbon in the Greenhorn Formation. Geochim Cosmochim Ac 53, 2961-2972.

Hayes, J.M., Strauss, H., Kaufman, A.J., 1999. The abundance of C-13 in marine organic matter and isotopic fractionation in the global biogeochemical cycle of carbon during the past 800 Ma. Chem Geol 161, 103-125.

Hemming, N.G., Hanson, G.N., 1992. Boron Isotopic Composition and Concentration in Modern Marine Carbonates. Geochim Cosmochim Ac 56, 537-543.

Henderiks, J., Pagani, M., 2007. Refining ancient carbon dioxide estimates: Significance of coccolithophore cell size for alkenone-based pCO(2) records. Paleoceanography 22.

Herbert, T.D., Lawrence, K.T., Tzanova, A., Peterson, L.C., Caballero-Gill, R., Kelly, C.S., 2016. Late Miocene global cooling and the rise of modern ecosystems. Nat Geosci 9, 843-+.

Higgins, J.A., Kurbatov, A.V., Spaulding, N.E., Brook, E., Introne, D.S., Chimiak, L.M., Yan, Y.Z., Mayewski, P.A., Bender, M.L., 2015. Atmospheric composition 1 million years ago from blue ice in the Allan Hills, Antarctica. P Natl Acad Sci USA 112, 6887-6891.

R

Hinga, K.R., Arthur, M.A., Pilson, M.E.Q., Whitaker, D., 1994. Carbon-Isotope Fractionation by Marine-Phytoplankton in Culture - the Effects of CO_2 Concentration, Ph, Temperature, and Species. Global Biogeochem Cy 8, 91-102.

Hoins, M., Eberlein, T., Van de Waal, D.B., Sluijs, A., Reichart, G.J., Rost, B., 2016. CO_2-dependent carbon isotope fractionation in dinoflagellates relates to their inorganic carbon fluxes. J Exp Mar Biol Ecol 481, 9-14.

Hoins, M., Van de Waal, D.B., Eberlein, T., Reichart, G.J., Rost, B., Sluijs, A., 2015. Stable carbon isotope fractionation of organic cyst-forming dinoflagellates: Evaluating the potential for a CO_2 proxy. Geochim Cosmochim Ac 160, 267-276.

Hollis, C.J., Dunkley Jones, T., Anagnostou, E., Bijl, P.K., Cramwinckel, M.J., Cui, Y., Dickens, G.R., Edgar, K.M., Eley, Y., Evans, D., Foster, G.L., Frieling, J., Inglis, G.N., Kennedy, E.M., Kozdon, R., Lauretano, V., Lear, C.H., Littler, K., Lourens, L., Meckler, A.N., Naafs, B.D.A., Pälike, H., Pancost, R.D., Pearson, P.N., Röhl, U., Royer, D.A., Salzmann, U., Schubert, B.A., Seebeck, H., Sluijs, A., Speijer, R.P., Stassen, P., Tierney, J., Tripati, A., Wade, B., Westerhold, T., Witkowski, C.R., Zachos, J.C., Zhang, Y.G., Huber, M., Lunt, D.J., 2019. The DeepMIP contribution to PMIP4: methodologies for selection, compilation and analysis of latest Paleocene and early Eocene climate proxy data, incorporating version 0.1 of the DeepMIP database. Geoscientific Model Development 12, 3149-3206.

Holtz, L.M., Wolf-Gladrow, D., Thoms, S., 2015. Simulating the effects of light intensity and carbonate system composition on particulate organic and inorganic carbon production in Emiliania huxleyi. J Theor Biol 372, 192-204.

Honisch, B., Bijma, J., Russell, A.D., Spero, H.J., Palmer, M.R., Zeebe, R.E., Eisenhauer, A., 2003. The influence of symbiont photosynthesis on the boron isotopic composition of foraminifera shells. Mar Micropaleontol 49, 87-96.

Honisch, B., Hemming, N.G., 2004. Ground-truthing the boron isotope-paleo-pH proxy in planktonic foraminifera shells: Partial dissolution and shell size effects. Paleoceanography 19.

Honisch, B., Hemming, N.G., 2005. Surface ocean pH response to variations in pCO(2) through two full glacial cycles. Earth and Planetary Science Letters 236, 305-314.

Hopkinson, B.M., Dupont, C.L., Allen, A.E., Morel, F.M.M., 2011. Efficiency of the CO_2-concentrating mechanism of diatoms. P Natl Acad Sci USA 108, 3830-3837.

Horwitz, R., Borell, E.M., Yam, R., Shemesh, A., Fine, M., 2015a. Natural high PCO$_2$ increases autotrophy in Anemonia viridis (Anthozoa) as revealed from stable isotope (C, N) analysis. Sci Rep-Uk 5.

Horwitz, R., Borell, E.M., Yam, R., Shemesh, A., Fine, M., 2015b. Natural high pCO(2) increases autotrophy in Anemonia viridis (Anthozoa) as revealed from stable isotope (C, N) analysis. Sci Rep-Uk 5.

Ingle, J.C., Keller, G., 1980. Benthic Foraminiferal Biofacies of Eastern Pacific Margin between 32-Degrees-S and 32-Degrees-N. Aapg Bull 64, 444-444.

Inguaggiato, S., Mazot, A., Diliberto, I.S., Inguaggiato, C., Madonia, P., Rouwet, D., Vita, F., 2012. Total CO_2 output from Vulcano Island (Aeolian Islands, Italy) Geochem. Geophys. Geosyst. 13.

IPCC, 2013. The Physical Science Basis. Contribution of Working Group I to the Fifth Assessment Report of the Intergovernmental Panel on Climate Change, in: Stocker, T.F., Qin, D., Plattner, G.K., Tignor, M., Allen, S.K., Boschung, J., Nauels, A., Xia, Y.F., Bex, V., Midgley, P.M. (Eds.), Climate Change 2013, Cambridge, p. 1535.

Jasper, J.P., Hayes, J.M., 1990. A Carbon Isotope Record of CO_2 Levels during the Late Quaternary. Nature 347, 462-464.

Jasper, J.P., Hayes, J.M., Mix, A.C., Prahl, F.G., 1994. Photosynthetic Fractionation of C-13 and Concentrations of Dissolved CO_2 in the Central Equatorial Pacific during the Last 255,000 Years. Paleoceanography 9, 781-798.

Johnson, V.R., Brownlee, C., Rickaby, R.E.M., Graziano, M., Milazzo, M., Hall-Spencer, J., 2011a. Responses of marine benthic microalgae to elevated CO_2. Mar Biol.

Johnson, V.R., Brownlee, C., Rickaby, R.E.M., Graziano, M., Milazzo, M., Hall-Spencer, J.M., 2013. Responses of marine benthic microalgae to elevated CO_2. Mar Biol 160, 1813-1824.

Johnson, V.R., Brownless, C., Rickaby, R.E.M., Graziano, M., Milazzo, M., Hall-Spencer, J.M., 2011b. Responses of marine benthic microalgae to elevated CO_2. Marine Biology.

Keeling, R.F., Kortzinger, A., Gruber, N., 2010. Ocean Deoxygenation in a Warming World. Annu Rev Mar Sci 2, 199-229.

Klok, J., Cox, H.C., Deleeuw, J.W., Schenck, P.A., 1984. Loliolides and Dihydroactinidiolide in a Recent Marine Sediment Probably Indicate a Major Transformation Pathway of Carotenoids. Tetrahedron Lett 25, 5577-5580.

Koch, P.L., Zachos, J.C., Gingerich, P.D., 1992. Correlation between Isotope Records in Marine and Continental Carbon Reservoirs near the Paleocene Eocene Boundary. Nature 358, 319-322.

Kohnen, M.E.L., Damste, J.S.S., Baas, M., Kockvandalen, A.C., Deleeuw, J.W., 1993. Sulfur-Bound Steroid and Phytane Carbon Skeletons in Geomacromolecules - Implications for the Mechanism of Incorporation of Sulfur into Organic-Matter. Geochim Cosmochim Ac 57, 2515-2528.

Kohnen, M.E.L., Damste, J.S.S., Kockvandalen, A.C., Tenhaven, H.L., Rullkotter, J., Deleeuw, J.W., 1990. Origin and Diagenetic Transformations of C-25 and C-30 Highly Branched Isoprenoid Sulfur-Compounds - Further Evidence for the Formation of Organically Bound Sulfur during Early Diagenesis. Geochim Cosmochim Ac 54, 3053-3063.

Kok, M.D., Rijpstra, W.I.C., Robertson, L., Volkman, J.K., Damste, J.S.S., 2000. Early steroid sulfurisation in surface sediments of a permanently stratified lake (Ace Lake, Antarctica). Geochim Cosmochim Ac 64, 1425-1436.

Konrad, W., Roth-Nebelsick, A., Grein, M., 2008. Modelling of stomatal density response to atmospheric CO_2. J Theor Biol 253, 638-658.

Koopmans, M.P., Rijpstra, W.I.C., Klapwijk, M.M., de Leeuw, J.W., Lewan, M.D., Damste, J.S.S., 1999. A thermal and chemical degradation approach to decipher pristane and phytane precursors in sedimentary organic matter. Org Geochem 30, 1089-1104.

Koster, J., VanKaamPeters, H.M.E., Koopmans, M.P., DeLeeuw, J.W., Damste, J.S.S., 1997. Sulphurisation of homohopanoids: Effects on carbon number distribution, speciation, and 22S/22R epimer ratios. Geochim Cosmochim Ac 61, 2431-2452.

Kottmeier, D.M., Rokitta, S.D., Rost, B., 2016. Acidification, not carbonation, is the major regulator of carbon fluxes in the coccolithophore Emiliania huxleyi. New Phytol 211, 126-137.

Krumhardt, K.M., Lovenduski, N.S., Inglesias-Rodriguez, M.D., Kleypas, J.A., 2017. Coccolithophore growth and calcification in a changing ocean. Progress in Oceanography 159, 276-295.

R

Kurschner, W.M., Kvacek, Z., Dilcher, D.L., 2008. The impact of Miocene atmospheric carbon dioxide fluctuations on climate and the evolution of terrestrial ecosystems. P Natl Acad Sci USA 105, 449-453.

Küspert, W., 1982. Environmental change during oil shale deposition as deduced from stable isotope ratios, in: Einsele, S., Seilacher, A. (Eds.), Cyclic and Event Stratification. Springer, New York, pp. 482-501.

LaRiviere, J.P., Ravelo, A.C., Crimmins, A., Dekens, P.S., Ford, H.L., Lyle, M., Wara, M.W., 2012. Late Miocene decoupling of oceanic warmth and atmospheric carbon dioxide forcing. Nature 486, 97-100.

Laws, E.A., Bidigare, R.R., Popp, B.N., 1997. Effect of growth rate and CO_2 concentration on carbon isotopic fractionation by the marine diatom Phaeodactylum tricornutum. Limnol Oceanogr 42, 1552-1560.

Laws, E.A., Popp, B.N., Bidigare, R.R., Kennicutt, M.C., Macko, S.A., 1995. Dependence of Phytoplankton Carbon Isotopic Composition on Growth-Rate and $[CO_2](Aq)$ - Theoretical Considerations and Experimental Results. Geochim Cosmochim Ac 59, 1131-1138.

Laws, E.A., Popp, B.N., Bidigare, R.R., Riebesell, U., Burkhardt, S., 2001. Controls on the molecular distribution and carbon isotopic composition of alkenones in certain haptophyte algae. Geochem Geophy Geosy 2.

Laws, E.A., Thompson, P.A., Popp, B.N., Bidigare, R.R., 1998. Sources of inorganic carbon for marine microalgal photosynthesis: A reassessment of delta C-13 data from batch culture studies of Thalassiosira pseudonana and Emiliania huxleyi. Limnol Oceanogr 43, 136-142.

Lemarchand, E., Schott, J., Gaillardet, J., 2002. Isotopic fractionation related to boron sorption on humic acids. Geochim Cosmochim Ac 66, A446-A446.

Lenton, T.M., Held, H., Kriegler, E., Hall, J.W., Lucht, W., Rahmstorf, S., Schellnhuber, H.J., 2008. Tipping elements in the Earth's climate system. P Natl Acad Sci USA 105, 1786-1793.

Lewis, E., Wallace, D., 1998. Program developed for CO_2 system calculations. Oak Ridge National Laboaotry, Oak Ridge, Tennessee.

Li, C., Peng, P., Sheng, G.Y., Fu, J.M., Yan, Y.Z., 2003. A molecular and isotopic geochemical study of Meso- to Neoproterozoic (1.73-0.85 Ga) sediments from the Jixian section, Yanshan Basin, North China. Precambrian Res 125, 337-356.

Liaaen-Jensen, S., 1978. Marine carotenoids, in: Scheuer, P.J. (Ed.), Marine natural products, Academic Press.

Lourens, L.J., Hilgen, F.J., Raffi, I., VergnaudGrazzini, C., 1996. Early pleistocene chronology of the Vrica section (Calabria, Italy). Paleoceanography 11, 797-812.

Lüthi, D., Le Floch, M., Bereiter, B., Blunier, T., Barnola, J.M., Siegenthaler, U., Raynaud, D., Jouzel, J., Fischer, H., Kawamura, K., Stocker, T.F., 2008. High-resolution carbon dioxide concentration record 650,000-800,000 years before present. Nature 453, 379-382.

Ma, Q., Tipping, R.H., 1998. The distribution of density matrices over potential-energy surfaces: Application to the calculation of the far-wing line shapes for CO_2. J Chem Phys 108, 3386-3399.

Madigan, M.T., Takigiku, R., Lee, R.G., Gest, H., Hayes, J.M., 1989. Carbon Isotope Fractionation by Thermophilic Phototrophic Sulfur Bacteria - Evidence for Autotrophic Growth in Natural-Populations. Applied and Environmental Microbiology 55, 639-644.

Martin-Creuzburg, D., von Elert, E., 2009. Good food versus bad food: the role of sterols and polyunsaturated fatty acids in determining growth and reproduction of Daphnia magna. Aquat Ecol 43, 943-950.

Mccarthy, E.D., Calvin, M., 1967. Organic Geochemical Studies .I. Molecular Criteria for Hydrocarbon Genesis. Nature 216, 642-&.

Mejia, L.M., Mendez-Vicente, A., Abrevay, L., Lawrence, K.T., Ladlow, C., Bolton, C., Cacho, I., Stoll, H., 2017. A diatom record of CO_2 decline since the late Miocene. Earth and Planetary Science Letters 479, 18-33.

Melki, T., Kallel, N., Fontugne, M., 2010. The nature of transitions from dry to wet condition during sapropel events in the Eastern Mediterranean Sea. Palaeogeogr Palaeocl 291, 267-285.

Menzel, D., Hopmans, E.C., van Bergen, P.F., de Leeuw, J.W., Damste, J.S.S., 2002. Development of photic zone euxinia in the eastern Mediterranean Basin during deposition of Pliocene sapropels. Mar Geol 189, 215-226.

Monnin, E., Indermuhle, A., Dallenbach, A., Fluckiger, J., Stauffer, B., Stocker, T.F., Raynaud, D., Barnola, J.M., 2001. Atmospheric CO_2 concentrations over the last glacial termination. Science 291, 112-114.

Mook, W.G.B., J.C.; Staverman, W.H., 1974. Carbon isotope fractionation between dissolved bicarbonate and gaseous carbon dioxide. Earth Planet Sc Lett 22, 169-176.

Mouritsen, O.G., Zuckermann, M.J., 2004. What's so special about cholesterol? Lipids 39, 1101-1113.

Muller, P.J., Kirst, G., Ruhland, G., von Storch, I., Rosell-Mele, A., 1998. Calibration of the alkenone paleotemperature index U-37(K ') based on core-tops from the eastern South Atlantic and the global ocean (60 degrees N-60 degrees S). Geochim Cosmochim Ac 62, 1757-1772.

Naafs, B.D.A., Castro, J.M., De Gea, G.A., Quijano, M.L., Schmidt, D.N., Pancost, R.D., 2016. Gradual and sustained carbon dioxide release during Aptian Oceanic Anoxic Event 1a. Nat Geosci 9, 135-+.

Nes, W.D., Janssen, G.G., Crumley, F.G., Kalinowska, M., Akihisa, T., 1993. The Structural Requirements of Sterols for Membrane-Function in Saccharomyces-Cerevisiae. Archives of Biochemistry and Biophysics 300, 724-733.

Ni, Y.Y., Foster, G.L., Bailey, T., Elliott, T., Schmidt, D.N., Pearson, P., Haley, B., Coath, C., 2007. A core top assessment of proxies for the ocean carbonate system in surface-dwelling foraminifers. Paleoceanography 22.

Nimer, N.A., Merrett, M.J., 1993. Calcification Rate in Emiliania-Huxleyi Lohmann in Response to Light, Nitrate and Availability of Inorganic Carbon. New Phytol 123, 673-677.

O'Brien, C.L., Robinson, S.A., Pancost, R.D., Damste, J.S.S., Schouten, S., Lunt, D.J., Alsenz, H., Bomemann, A., Bottini, C., Brassell, S.C., Farnsworth, A., Forster, A., Huber, B.T., Inglis, G.N., Jenkyns, H.C., Linnert, C., Littler, K., Markwick, P., McAnena, A., Mutterlose, J., Naafs, B.D.A., Puttmann, W., Sluijs, A., van Helmond, N.A.G.M., Vellekoop, J., Wagner, T., Wrobel, N.E., 2017. Cretaceous sea-surface temperature evolution: Constraints from TEX86 and planktonic foraminiferal oxygen isotopes. Earth-Sci Rev 172, 224-247.

Pagani, M., 2002. The alkenone-CO_2 proxy and ancient atmospheric carbon dioxide. Philos T Roy Soc A 360, 609-632.

R

Pagani, M., 2014. Biomarker-Based Inferences of Past Climate: The Alkenone pCO$_2$ Proxy, in: Holland, H., Turekian, K. (Eds.), Treatise on Geochemistry. Elsevier, Oxford, pp. 361-378.

Pagani, M., Arthur, M.A., Freeman, K.H., 1999a. Miocene evolution of atmospheric carbon dioxide. Paleoceanography 14, 273-292.

Pagani, M., Freeman, K.H., Arthur, M.A., 1999b. Late Miocene atmospheric CO$_2$ concentrations and the expansion of C-4 grasses. Science 285, 876-879.

Pagani, M., Freeman, K.H., Arthur, M.A., 2000. Isotope analyses of molecular and total organic carbon from Miocene sediments. Geochim Cosmochim Ac 64, 37-49.

Pagani, M., Zachos, J.C., Freeman, K.H., Tipple, B., Bohaty, S., 2005. Marked decline in atmospheric carbon dioxide concentrations during the Paleogene. Science 309, 600-603.

Palmer, M.R., Brummer, G.J., Cooper, M.J., Elderfield, H., Greaves, M.J., Reichart, G.J., Schouten, S., Yu, J.M., 2010. Multi-proxy reconstruction of surface water pCO(2) in the northern Arabian Sea since 29 ka. Earth and Planetary Science Letters 295, 49-57.

Pancost, R.D., Freeman, K.H., Wakeham, S.G., Robertson, C.Y., 1997. Controls on carbon isotope fractionation by diatoms in the Peru upwelling region. Geochim Cosmochim Ac 61, 4983-4991.

Passier, H.F., Bosch, H.J., Nijenhuis, I.A., Lourens, L.J., Bottcher, M.E., Leenders, A., Damste, J.S.S., de Lange, G.J., de Leeuw, J.W., 1999. Sulphidic Mediterranean surface waters during Pliocene sapropel formation. Nature 397, 146-149.

Pearson, P.N., Palmer, M.R., 2000. Atmospheric carbon dioxide concentrations over the past 60 million years. Nature 406, 695-699.

Pepin, L., Raynaud, D., Barnola, J.M., Loutre, M.F., 2001. Hemispheric roles of climate forcings during glacial-interglacial transitions as deduced from the Vostok record and LLN-2D model experiments. J Geophys Res-Atmos 106, 31885-31892.

Petit, J.R., Jouzel, J., Raynaud, D., Barkov, N.I., Barnola, J.M., Basile, I., Bender, M., Chappellaz, J., Davis, M., Delaygue, G., Delmotte, M., Kotlyakov, V.M., Legrand, M., Lipenkov, V.Y., Lorius, C., Pepin, L., Ritz, C., Saltzman, E., Stievenard, M., 1999. Climate and atmospheric history of the past 420,000 years from the Vostok ice core, Antarctica. Nature 399, 429-436.

Popp, B.N., Bidigare, R.R., Deschenes, B., Laws, E.A., Prahl, F.G., Tanimoto, J.K., Wallsgrove, R.J., 2006. A new method for estimating growth rates of alkenone-producing haptophytes. Limnol Oceanogr-Meth 4, 114-129.

Popp, B.N., Kenig, F., Wakeham, S.G., Laws, E.A., Bidigare, R.R., 1998a. Does growth rate affect ketone unsaturation and intracellular carbon isotopic variability in Emiliania huxleyi? Paleoceanography 13, 35-41.

Popp, B.N., Laws, E.A., Bidigare, R.R., Dore, J.E., Hanson, K.L., Wakeham, S.G., 1998b. Effect of phytoplankton cell geometry on carbon isotopic fractionation. Geochim Cosmochim Ac 62, 69-77.

Popp, B.N., Takigiku, R., Hayes, J.M., Louda, J.W., Baker, E.W., 1989. The Post-Paleozoic Chronology and Mechanism of C-13 Depletion in Primary Marine Organic-Matter. Am J Sci 289, 436-454.

Quast, A., Hoefs, J., Paul, J., 2006. Pedogenic carbonates as a proxy for palaeo-CO$_2$ in the Palaeozoic atmosphere. Palaeogeogr Palaeocl 242, 110-125.

Rasmussen, B., Fletcher, I.R., Brocks, J.J., Kilburn, M.R., 2008. Reassessing the first appearance of eukaryotes and cyanobacteria. Nature 455, 1101-U1109.

Rau, G.H., Riebesell, U., WolfGladrow, D., 1996. A model of photosynthetic C-13 fractionation by marine phytoplankton based on diffusive molecular CO_2 uptake. Mar Ecol Prog Ser 133, 275-285.

Rau, G.H., Riebesell, U., WolfGladrow, D., 1997. CO_{2aq}-dependent photosynthetic C-13 fractionation in the ocean: A model versus measurements. Global Biogeochem Cy 11, 267-278.

Raven, J.A., Beardall, J., 2014. CO_2 concentrating mechanisms and environmental change. Aquat Bot 118, 24-37.

Raynaud, D., 2005. The Milankovitch signature of the paleo-gas record in ice cores. Sasa Dep Math Phys G 110, 141-144.

Repeta, D.J., 1989. Carotenoid Diagenesis in Recent Marine-Sediments .2. Degradation of Fucoxanthin to Loliolide. Geochim Cosmochim Ac 53, 699-707.

Retallack, G.J., 2009. Refining a pedogenic-carbonate CO_2 paleobarometer to quantify a middle Miocene greenhouse spike. Palaeogeogr Palaeocl 281, 57-65.

Riebesell, U., Revill, A.T., Holdsworth, D.G., Volkman, J.K., 2000. The effects of varying CO_2 concentration on lipid composition and carbon isotope fractionation in Emiliania huxleyi. Geochim Cosmochim Ac 64, 4179-4192.

Rivaro, P., Messa, R., Massolo, S., Frache, R., 2010. Distributions of carbonate properties along the water column in the Mediterranean Sea: Spatial and temporal variations. Marine Chemistry 121, 236-245.

Rohling, E.J., De Rijk, S., 1999. Holocene Climate Optimum and Last Glacial Maximum in the Mediterranean: the marine oxygen isotope record. Mar Geol 153, 57-75.

Rohling, E.J., Gieskes, W.W.C., 1989. Late Quaternary Changes in Mediterranean Intermediate Water Density and Formation Rate. Paleoceanography 4, 531-545.

Royer, D.L., 2014. Atmospheric CO_2 and O_2 During the Phanerozoic: Tools, Patterns,

and Impacts, in: Turekian, K., Holland, H. (Eds.), Treatise on Geochemistry 2nd Edition. Elsevier Science, pp. 251-267.

Royer, D.L., Berner, R.A., Montanez, I.P., Tabor, N.J., Beerling, D.J., 2004. CO_2 as a primary driver of Phanerozoic climate. GSA Today 14, 4-10.

Royer, D.L., Wing, S.L., Beerling, D.J., Jolley, D.W., Koch, P.L., Hickey, L.J., Berner, R.A., 2001. Paleobotanical evidence for near present-day levels of atmospheric CO_2 during part of the tertiary. Science 292, 2310-2313.

Sackett, W.M., Eckelmann, W.R., Bender, M.L., Be, A.W.H., 1965. Temperature Dependence of Carbon Isotope Composition in Marine Plankton and Sediments. Science 148, 235-+.

Schoell, M., Schouten, S., Damste, J.S.S., Deleeuw, J.W., Summons, R.E., 1994. A Molecular Organic-Carbon Isotope Record of Miocene Climate Changes. Science 263, 1122-1125.

Schouten, S., Breteler, W.C.M.K., Blokker, P., Schogt, N., Rijpstra, W.I.C., Grice, K., Baas, M., Sinninghe Damsté, J.S., 1998. Biosynthetic effects on the stable carbon isotopic compositions of algal lipids: Implications for deciphering the carbon isotopic biomarker record. Geochim Cosmochim Ac 62, 1397-1406.

Schouten, S., de Loureiro, M.R.B., Sinninghe Damsté, J.S., De Leeuw, J.W., 1995b. Molecular biogeochemistry of Monterey sediments (Naples Beach, USA). Distributions of hydrocarbons and organic sulfur-bound compounds, in: Isaacs, C.M., Rullkotter, J. (Eds.), The Monterey Formation: From Rocks to Molecules. Columbia University Press, New York, pp. 150-175.

R

Schouten, S., Hoefs, M.J.L., Damste, J.S.S., 2000. A molecular and stable carbon isotopic study of lipids in late Quaternary sediments from the Arabian Sea. Org Geochem 31, 509-521.

Schouten, S., Hopmans, E.C., Schefuss, E., Damste, J.S.S., 2002. Distributional variations in marine crenarchaeotal membrane lipids: a new tool for reconstructing ancient sea water temperatures? Earth and Planetary Science Letters 204, 265-274.

Schouten, S., Schoell, M., Rijpstra, W.I.C., Damste, J.S.S., deLeeuw, J.W., 1997. A molecular stable carbon isotope study of organic matter in immature Miocene Monterey sediments, Pismo basin. Geochim Cosmochim Ac 61, 2065-2082.

Seki, O., Foster, G.L., Schmidt, D.N., Mackensen, A., Kawamura, K., Pancost, R.D., 2010. Alkenone and boron-based Pliocene pCO(2) records. Earth Planet Sc Lett 292, 201-211.

Siegenthaler, U., Monnin, E., Kawamura, K., Spahni, R., Schwander, J., Stauffer, B., Stocker, T.F., Barnola, J.M., Fischer, H., 2005. Supporting evidence from the EPICA Dronning Maud Land ice core for atmospheric CO_2 changes during the past millennium. Tellus B 57, 51-57.

Sinninghe Damsté, J.S., Eglinton, T.I., Rijpstra, W.I.C., De Leeuw, J.W., 1990. Characterization of organically bound sulfur in high-molecular-weight sedimentary organic matter using flash pyrolysis and Raney Ni desulfurization, in: Orr, W.L., White, C.M. (Eds.), Geochemistry of Sulfur in Fossil Fuels. American Chemical Society, Washington, D.C., pp. 486-528.

Sinninghe Damsté, J.S., Kohnen, M.E.L., Horsfield, B., 1998a. Origin of low-molecular-weight alkylthiophenes in pyrolysates of sulphur-rich kerogens as revealed by micro-scale sealed vessel pyrolysis. Org Geochem 29, 1891-1903.

Sinninghe Damsté, J.S., Kok, M.D., Koster, J., Schouten, S., 1998b. Sulfurized carbohydrates: an important sedimentary sink for organic carbon? Earth Planet Sc Lett 164, 7-13.

Sinninghe Damsté, J.S., Kuypers, M.M.M., Pancost, R.D., Schouten, S., 2008. The carbon isotopic response of algae, (cyano)bacteria, archaea and higher plants to the late Cenomanian perturbation of the global carbon cycle: Insights from biomarkers in black shales from the Cape Verde Basin (DSDP Site 367). Org Geochem 39, 1703-1718.

Sinninghe Damsté, J.S., Leeuw, J.W., 1990. Analysis, Structure and Geochemical Significance of Organically-Bound Sulfur in the Geosphere - State-of-the-Art and Future-Research. Org Geochem 16, 1077-1101.

Sinninghe Damsté, J.S., Muyzer, G., Abbas, B., Rampen, S.W., Masse, G., Allard, W.G., Belt, S.T., Robert, J.M., Rowland, S.J., Moldowan, J.M., Barbanti, S.M., Fago, F.J., Denisevich, P., Dahl, J., Trindade, L.A.F., Schouten, S., 2004. The rise of the rhizosolenid diatoms. Science 304, 584-587.

Sinninghe Damsté, J.S., Rijpstra, W.I.C., Coolen, M.J.L., Schouten, S., Volkman, J.K., 2007. Rapid sulfurisation of highly branched isoprenoid (HBI) alkenes in sulfidic Holocene sediments from Ellis Fjord, Antarctica. Org Geochem 38, 128-139.

Sinninghe Damsté, J.S., Rijpstra, W.I.C., Deleeuw, I.W., Schenck, P.A., 1988. Origin of Organic Sulfur-Compounds and Sulfur-Containing High Molecular-Weight Substances in Sediments and Immature Crude Oils. Org Geochem 13, 593-606.

Smith, R.Y., Greenwood, D.R., Basinger, J.F., 2010. Estimating paleoatmospheric pCO_2 during the Early Eocene Climatic Optimum from stomatal frequency of Ginkgo, Okanagan Highlands, British Columbia, Canada. Palaeogeogr Palaeocl 293, 120-131.

Stoll, H.M., Guitian, J., Hernandez-Almeida, I., Mejia, L.M., Phelps, S., Polissar, P., Rosenthal, Y., Zhang, H.R., Ziveri, P., 2019. Upregulation of phytoplankton carbon concentrating mechanisms during low CO_2 glacial periods and implications for the phytoplankton PCO$_2$ proxy. Quaternary Sci Rev 208, 1-20.

Thomas, P.J., Boller, A.J., Satagopan, S., Tabita, F.R., Cavanaugh, C.M., Scott, K.M., 2018. Isotope discrimination by form IC RubisCO from *Ralstonia eutropha* and *Rhodobacter sphaeroides*, metabolically versatile members of 'Proteobacteria' from aquatic and soil habitats. Environmental Microbiology 21, 72-80.

Urbarova, I., Foret, S., Dahl, M., Emblem, A., Milazzo, M., Hall-Spencer, J.M., 2019. Ocean acidification at a coastal CO_2 vent induces expression of stress-related transcripts and transposable elements in the sea anemone Anemonia viridis (vol 14, e0210358, 2019). Plos One 14.

van Bentum, E.C., Reichart, G.J., Sinninghe Damsté, J.S., 2012. Organic matter provenance, palaeoproductivity and bottom water anoxia during the Cenomanian/Turonian oceanic anoxic event in the Newfoundland Basin (northern proto North Atlantic Ocean). Org Geochem 50, 11-18.

van Breugel, Y., Baas, M., Schouten, S., Mattioli, E., Sinninghe Damsté, J.S., 2006. Isorenieratane record in black shales from the Paris Basin, France: Constraints on recycling of respired CO_2 as a mechanism for negative carbon isotope shifts during the Toarcian oceanic anoxic event. Paleoceanography 21.

van der Meer, M.T.J., Baas, M., Rijpstra, W.I.C., Marino, G., Rohling, E.J., Sinninghe Damsté, J.S., Schouten, S., 2007. Hydrogen isotopic compositions of long-chain alkenones record freshwater flooding of the Eastern Mediterranean at the onset of sapropel deposition. Earth and Planetary Science Letters 262, 594-600.

van Dongen, B.E., Schouten, S., Damste, J.S.S., 2002. Carbon isotope variability in monosaccharides and lipids of aquatic algae and terrestrial plants. Mar Ecol Prog Ser 232, 83-92.

Volkman, J.K., 2003. Sterols in microorganisms. Appl Microbiol Biot 60, 495-506.

Volkman, J.K., Eglinton, G., Corner, E.D.S., Forsberg, T.E.V., 1980. Long-Chain Alkenes and Alkenones in the Marine Coccolithophorid Emiliania-Huxleyi. Phytochemistry 19, 2619-2622.

Ward, E.J., Bell, D.M., Clark, J.S., Oren, R., 2013. Hydraulic time constants for transpiration of loblolly pine at a free-air carbon dioxide enrichment site. Tree Physiol 33, 123-134.

Wei, J.H., Yin, X.C., Welander, P.V., 2016. Sterol Synthesis in Diverse Bacteria. Frontiers in Microbiology 7.

Weiss, H.R., Cohen, J.A., 1974. Effects of Low-Levels of Carbon-Monoxide on Rat-Brain and Muscle-Tissue P02. Environ Physiol Bioc 4, 31-39.

Weiss, R.F., 1974. Carbon dioxide in water and seawater: The solubility of a non-deal gas. Mar Chem 2, 203-215.

Welander, P.V., Coleman, M.L., Sessions, A.L., Summons, R.E., Newman, D.K., 2010. Identification of a methylase required for 2-methylhopanoid production and implications for the interpretation of sedimentary hopanes. P Natl Acad Sci USA 107, 8537-8542.

White, L.D., Garrison, R.E., Barron, J.A., 1992. Miocene intensification of upwelling along the California margin as recorded in siliceous facies of the Monterey Formation and offshore DSDP sites, in: Summerhayes, C.P., Prell, W.L., Emeis, K.C. (Eds.),

R

Upwelling Systems: Evolution since the Early Miocene. Goelogical Society Special Publication, Oxford, UK, pp. 429-442.

Wilkes, E.B., Carter, S.J., Pearson, A., 2017. CO_2-dependent carbon isotope fractionation in the dinoflagellate Alexandrium tamarense. Geochim Cosmochim Ac 212, 48-61.

Wilkes, E.B., Pearson, A., 2019. A general model for carbon isotopes in red-lineage phytoplankton: Interplay between unidirectional processes and fractionation by RubisCO. Geochim Cosmochim Ac 265, 163-181.

Witkowski, C.R., Agostini, S., Harvey, B.P., Van Der Meer, M.T.J., Sinninghe Damsté, J.S., Schouten, S., 2019. Validation of carbon isotope fractionation in algal lipids as a PCO2 proxy using a natural CO_2 seep (Shikine Island, Japan). Biogeosciences, in review.

Witkowski, C.R., Weijers, J.W.H., Blais, B., Schouten, S., Sinninghe Damsté, J.S., 2018. Molecular fossils from phytoplankton reveal secular PCO$_2$ trend over the Phanerozoic. Sci Adv 4, eaat4556.

Woodward, F.I., 1987. Stomatal Numbers Are Sensitive to Increases in Co2 from Preindustrial Levels. Nature 327, 617-618.

Xu, Z., Jiang, Y., Jia, B., Zhou, G., 2016. Elevated-CO_2 Response of Stomata and Its Dependence on Environmental Factors. Front Plant Sci 7.

You, Y., Huber, M., Muller, R.D., Poulsen, C.J., Ribbe, J., 2009. Simulation of the Middle Miocene Climate Optimum. Geophys Res Lett 36.

Young, J.N., Rickaby, R.E.M., Kapralov, M.V., Filatov, D.A., 2012. Adaptive signals in algal Rubisco reveal a history of ancient atmospheric carbon dioxide. Philos T R Soc B 367, 483-492.

Zachos, J.C., Dickens, G.R., Zeebe, R.E., 2008. An early Cenozoic perspective on greenhouse warming and carbon-cycle dynamics. Nature 451, 279-283.

Zhang, Y.G., Pagani, M., Liu, Z.H., Bohaty, S.M., DeConto, R., 2013. A 40-million-year history of atmospheric CO_2. Philos T R Soc A 371.

Zhang, Y.G., Pearson, A., Benthien, A., Dong, L., Huybers, P., Liu, X.Q., Pagani, M., 2019. Refining the alkenone-pCO(2) method I: Lessons from the Quaternary glacial cycles. Geochim Cosmochim Ac 260, 177-191.

Acknowledgements

This thesis would not have been possible without the extraordinary guidance from my promotors. Jaap, Stefan, and Marcel not only helped me finish a PhD but more importantly fostered a nurturing environment for me to ask questions, to think and act independently, to not take myself so seriously, and to ultimately grow both as a scientist (and as a person).

Jaap, I am sometimes in complete awe of you. It's a complete joy to witness your fierce pursuit of good science and to learn from your remarkable way of distilling complex ideas into simple clarity, your daring questions, and your good-natured, good-humored approach to life.

Stefan, I cannot imagine this thesis without you…. your guidance, your encouragement for independence and creativity, your devotion to problem-solving with me (dropping everything, sometimes for hours), and your unparalleled Zen-like wisdom. There are no words to describe just how grateful I am for your mentorship.

Marcel, thank you for always taking good care of me, not just answering questions or helping with analytical instrumentation but also just checking in on me. In this final year, thank you for stepping into role of copromotor and thus dealing with countless emails, manuscripts, translations, and my general existential-dread.

Thank you to the reading committee members for their assessment for this thesis, and the members of the sitting committee for the public defense.

Thank you to my colleagues at the NIOZ, especially in the MMB (formerly BGC) department. All the senior staff and technicians keep the department like a well-oiled machine and nearly all of you have helped me at some point. Thanks: Ellen for your general support, Alle Tjipke for making me feel welcomed in a new country, and Jort for limitless patience and willingness to teach me anything and everything with instrumentation. I miss the isotope lab (Jort, Ronald, Marcel, and Philip) – thanks for toasting my last sample!

I'd also like to thank the more indirect (but still great) influences on this thesis. Thank you to: Mr. Gessler for first sparking my love for science and Mr. Shelley and Mr. Kelly for their kindness, wisdom, and guidance; Hong, Qin, and Gaytha for providing me so many opportunities, including my first time ever leaving the US, my first conferences, my first of many things; Bryan for bringing me on my first

fieldwork which lead to my pursuit of science as a major; John for your kindness and for helping me through hard times; and Chris and Brian for teaching me so much in and out of the classroom. Brian, you've changed the way I think (and argue) and my admiration of you as a professor has steadily grown into admiration of you as a friend and colleague. You're always there for me, my Bayesian guardian angel.

To all the wonderful friends I've made along the way in this PhD, thanks for the good times. Shout out to Zeynep, the G&T chickies, the O.G. BGC chickies, the MMB babies, the Molenstraat girls, the knitting club, and the long-lasting friendships formed at USSP, the GRC, IMOG, and on fieldwork. To the wonderful friendships I made in NESSC, thank you all, especially Josh, Nadine, Emily, Allix, Robin, Shaun, Loes, Anne, Cindy, and Carolien. Josh, we've had more great memories and laughs than I can remember.

To my paranymphs, thank you! Sophie, I miss our weekend coffee breaks chatting about science and films and podcasts and obsessions. I love the way you think. Vittoria, you are a total force to be reckoned with and I love it. You've been such an incredible new friend, from our good times in China, helping me out in the lab, finding an apartment, to guiding me in the end of this PhD.

I'd like to thank my new Bristol gang for the smooth transition while still finishing this PhD. Thanks Rich, Paul, and David for being understanding of my unfinished business and really rooting for me. And cheers to my new crew – Vittoria, Antonio, Jerome, Leo, and Farid. You really made this last stretch of PhD possible.

Finally, I'd like to thank my family and friends from back home for being so supportive of my pursuits and for living so far away. Justin, you are the driving force behind my growing, evolving perspectives and I can never thank you enough for your influence on my life. Garrett and Ryan, thanks for being those wonderful friends with whom we can always pick up exactly where we left off. Bobby, you are and will always be my oldest, dearest friend. And finally, to my parents, my brothers (Pete, Brad, Bryn, Hunter, John) and their beautiful families, my Nana, and the rest of my family who have all been so supportive - I love you.

Curriculum Vitae

Caitlyn Rose Witkowski was born on the 31st of January, 1989 in New York, USA. From 2007-2011, she completed double Bachelors degrees in Environmental Science and in Global Studies, with a minor in Business Administration at Bryant University. During that time, she gained experience in the field and lab, including mentorships at M.I.T. in Roger Summons' group and at Yale University in Mark Pagani and Derek Briggs' groups. From 2011-2012, she worked and studied at the China University of Geosciences in Wuhan, China. She returned to the US as a laboratory manager on a NASA Rhode Island Space Grant while completing her Masters. Her thesis entitled "Mimicking early stages of diagenesis in modern *Metasequoia* leaves: Implications for plant fossil *Lagerstätten*" under supervision of Prof. Hong Yang was completed in 2014. She wrote for science textbooks before being offered a PhD position in 2015 under the guidance of Prof. Jaap Sinninghe Damsté and Prof. Stefan Schouten, and later also with Dr. Marcel van der Meer, at the Royal Netherlands Institute for Sea Research (NIOZ) on Texel, the Netherlands. She will continue her scientific career as a postdoctoral research associate at the University of Bristol in the group of Prof. Rich Pancost and Dr. David Naafs.
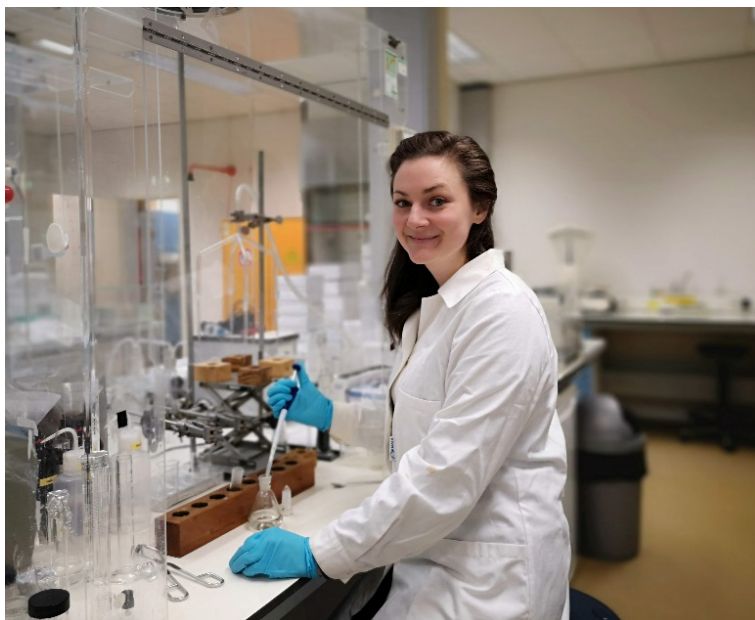
Publications

Witkowski CR, Weijers JWH, Blais B, Schouten S, Sinninghe Damsté JS. 2018. Molecular fossils from phytoplankton reveal secular pCO_2 trend over the Phanerozoic. _Science Advances_.

Hollis CJ, Dunkley Jones T…**Witkowski CR**… Lunt DJ. 2019. The DeepMIP contribution to PMIP4: methodologies for selection, compilation and analysis of latest Paleocene and early Eocene climate proxy data, incorporating version 0.1 of the DeepMIP database. _Geoscientific Model Development_.

Witkowski CR, Agostini S, Harvey BP, van der Meer MTJ, Schouten S, Sinninghe Damsté JS. 2019. Validation of carbon isotope fractionation in algal lipids as a PCO_2 proxy using a natural CO_2 seep (Shikine Island, Japan). _Biogeosciences_.

Witkowski CR, van der Meer MTJ, Smit NT, Schouten S, Sinninghe Damsté JS. 2019. Testing algal-based PCO_2 proxies at a modern CO_2 seep (Vulcano, Italy). In review at _Scientific Reports_.

Witkowski C, Gupta NS, Yang H, Leng Q, Williams CJ, Briggs DEG, Summons RE. 2012. Molecular preservation of Cenozoic conifer fossil _lagerstätten_ from Banks Island, the Canadian Arctic. _Palaois_.

Witkowski, CR. 2014. Masters Dissertation: Mimicking early stages of diagenesis in modern _Metasequoia_ leaves: Implications for plant fossil _lagerstätten_. _Digital Commons_ at Bryant University.

Witkowski C, Blais B. 2013. Bayesian Analysis of Epidemics - Zombies, Influenza, and other Diseases. _arXiv at Cornell University Library_.

Dietrich JW, **Witkowski C**. Obama's Human Rights Policy: Déjà vu with a Twist. 2011. _Human Rights Review_.

Laboratory Manuals:

Witkowski CR, Hubbard A, Patalano R, Davis R. 2014. Sustaining Air and Water (SAW) Laboratory Manual. Bryant University.

Witkowski CR, Hubbard A, Patalano R, Davis R. 2014. Human Impact on Land and Life (HILL) Laboratory Manual. Bryant University.

In preparation:

Witkowski CR, van der Meer MTJ, Blais B, Hennekam R, Reichart G-J, Sinninghe Damsté JS, Schouten S. Stable carbon isotopic fractionation of algal biomarkers as a proxy for PCO_2: Constraints from late Quaternary sapropels in the Eastern Mediterranean. In preparation for _Organic Geochemistry_.

Witkowski CR, van der Meer MTJ, von der Heydt AS, Schouten S, Sinninghe Damsté JS. Decline of PCO_2 from the Miocene based on the stable carbon isotopic composition of algal biomarkers. In preparation for _Nature Geoscience_.